Ion transport by viscous gas flow through capillaries and electrospray mass spectrometry of proteins
by Baiwei Lin

A thesis submitted in partial fulfillment of the requirements for the degree of Doctor of Philosophy in Chemistry
Montana State University

Abstract:
The efficiency of ion transport by viscous gas flow through narrow capillaries has been studied. The currents to the front end and to the walls of the capillary, as well as the currents passing through, were measured. A number of experimental parameters were varied, such as the dimensions and the material of the capillaries, the gas throughput, and the temperature. Both electrospray and corona ion sources were used. A transmitted current was measured even through the longest capillaries used, 50 ft (I.D. 2.1 mm).

A Monte Carlo method was used to simulate the radial diffusion of ions in the laminar gas flow. These simulations showed that the effect of the parabolic flow profile is to greatly increase the transmitted current through long capillaries. Indeed, all the data is consistent with ion loss by radial diffusion to the walls. In very long capillaries, higher mass ions can be effectively separated from lower mass ions due to the difference in diffusion constants.

A home-built electrospray ion source was installed on a VG-TRI02 quadruple and the experimental conditions were optimized for good signals. The performance of this source, particularly with regard to protein spectra, was evaluated.

Electrospray mass spectrometry was used to probe conformational changes of proteins. The effects of acids and organic solvents in the electrospray solution and in the gas phase of the ion source as well as the effect of temperature on the protein mass spectra and conformations were investigated. Acids or methanol in the electrospray solution strongly promotes the unfolding of the native myoglobin, while the addition of acids or methanol to the gas phase can well retain the native conformation of myoglobin and greatly increase the native ion intensities.

Electrospray mass spectrometry was used as an off-line HPLC detector for tryptic digests of cytochrome c, unlabeled and labeled with a fluorescent Cascade Blue ligand. Almost all of the tryptic peptides were observed in the ESI mass spectra. The additional dimension provided by ESI mass spectrometry makes the combined HPLC/ESI/MS an extremely powerful analytical method, particularly for modified proteins.

ION TRANSPORT BY VISCOUS GAS FLOW THROUGH CAPILLARIES AND ELECTROSPRAY MASS SPECTROMETRY OF PROTEINS

by

Baiwei Lin

A thesis submitted in partial fulfillment
of the requirements for the degree

of

Doctor of Philosophy

in

Chemistry

MONTANA STATE UNIVERSITY
Bozeman, Montana
November 1992

APPROVAL

of a thesis submitted by

Baiwei Lin

This thesis has been read by each member of the thesis committee and has been found to be satisfactory regarding content, English usage, format, citations, bibliographic style, and consistency, and is ready for submission to the College of Graduate Studies.

12/8/92
Date

Jan Sum
Chairperson, Graduate Committee

Approved for the Major Department

12/8/92
Date

John R Qumsiyeh
Head, Major Department

Approved for the College of Graduate Studies

12/14/92
Date

R L Brown
Graduate Dean

STATEMENT OF PERMISSION TO USE

In presenting this thesis in partial fulfillment of the requirements for a doctoral degree at Montana State University, I agree that the Library shall make it available to borrowers under rules of the Library. I further agree that copying of this thesis is allowable only for scholarly purposes, consistent with "fair use" as prescribed in the U.S. Copyright Law. Requests for extensive copying or reproduction of this thesis should be referred to University Microfilms International, 300 North Zeeb Road, Ann Arbor, Michigan 48106, to whom I have granted "the exclusive right to reproduce and distribute copies of the dissertation in and from microfilm and the right to reproduce and distribute by abstract in any format."

Signature Baiwei Li

Date 12/10/92

ACKNOWLEDGMENTS

I wish to thank Professor Jan Sunner for his guidance and instruction throughout my research and thesis preparation. The success of my graduate education was only possible because of his full support.

Thanks are extended to Dr. L. Joseph Sears for his advice in the instrumentation of mass spectrometry.

I also wish to thank Craig Johnson for his contribution to the work of HPLC.

The sample provided by Dr. A. Jesaitis and Dr. M. Quinn is greatly appreciated.

TABLE OF CONTENTS

TABLE OF CONTENTS (Cont)

TABLE OF CONTENTS (Cont)

LIST OF TABLES

LIST OF FIGURES

LIST OF FIGURES (Cont)

LIST OF FIGURES (Cont)

LIST OF FIGURES (Cont)

ABSTRACT

The efficiency of ion transport by viscous gas flow through narrow capillaries has been studied. The currents to the front end and to the walls of the capillary, as well as the currents passing through, were measured. A number of experimental parameters were varied, such as the dimensions and the material of the capillaries, the gas throughput, and the temperature. Both electrospray and corona ion sources were used. A transmitted current was measured even through the longest capillaries used, 50 ft (I.D. 2.1 mm).

A Monte Carlo method was used to simulate the radial diffusion of ions in the laminar gas flow. These simulations showed that the effect of the parabolic flow profile is to greatly increase the transmitted current through long capillaries. Indeed, all the data is consistent with ion loss by radial diffusion to the walls. In very long capillaries, higher mass ions can be effectively separated from lower mass ions due to the difference in diffusion constants.

A home-built electrospray ion source was installed on a VG-TRIO2 quadruple and the experimental conditions were optimized for good signals. The performance of this source, particularly with regard to protein spectra, was evaluated.

Electrospray mass spectrometry was used to probe conformational changes of proteins. The effects of acids and organic solvents in the electrospray solution and in the gas phase of the ion source as well as the effect of temperature on the protein mass spectra and conformations were investigated. Acids or methanol in the electrospray solution strongly promotes the unfolding of the native myoglobin, while the addition of acids or methanol to the gas phase can well retain the native conformation of myoglobin and greatly increase the native ion intensities.

Electrospray mass spectrometry was used as an off-line HPLC detector for tryptic digests of cytochrome c, unlabeled and labeled with a fluorescent Cascade Blue ligand. Almost all of the tryptic peptides were observed in the ESI mass spectra. The additional dimension provided by ESI mass spectrometry makes the combined HPLC/ESI/MS an extremely powerful analytical method, particularly for modified proteins.

INTRODUCTION

Electrospray Ionization

Electrospray is a new mass spectrometric technique that constitutes a major advance in the production of gas phase analyte ions from liquid solutions. This technique depends on dispersing analyte solution as a cloud or mist of small charged droplets, from which ions desorb into a bath gas at atmospheric pressure [1-4]. With electrospray, intact gas phase ions, with multiple charges, can be produced from remarkably large, complex, and fragile parent species. The pioneering efforts of Malcolm Dole [5-7] demonstrated the feasibility of electrospray ionization of non-volatile, liquid analytes. Later John B. Fenn [8-10] successfully interfaced an atmospheric pressure electrospray ion source to a quadrupole mass analyzer which revealed the remarkable ability of the technique.

Ionization methods for non-volatile species include laser desorption (LD), fast atom bombardment (FAB), plasma desorption (PD), and secondary ion mass spectrometry (SIMS). These are referred to as "desorption ionization" methods where sufficiently rapid heating vaporizes complex molecules before decomposition [11]. LD, FAB, PD, and SIMS are "soft" in the

sense that they can produce intact ions of species having molecular weights up to several tens of thousands [12-14]. These methods typically give only singly charged ions from parent species having molecular weights below ca 10,000 Da. In spite of this problem, these "energy-sudden" techniques have been very important in mass spectrometry for the analysis of large and complex molecules. However, electrospray ionization has become an effective complement to LD, FAB, PD, and SIMS because it overcomes some of the problems encountered in their use, such as limited mass range, large m/z values and extensive background noise.

The production of multiply charged ions by electrospray ionization (ESI) at atmospheric pressure presents an opportunity to study very large biomolecules [15-18]. Multiply charged molecular ions, which can be formed from proteins or oligonucleotides, can be efficiently mass analyzed and detected using magnetic and quadrupole MS due to the relatively low m/z values of these ions. With ESI, 100 or more charges can be placed on a large protein, bringing m/z down to below 2000 [20]. This is within the mass range of a quadrupole MS which are now extensively used for molecular weight measurements of large biomolecules [4,17,19]. Molecular weights of large biomolecules can be determined within 0.01%. There is, as yet, no evidence of an upper limit for the production of ions by ESI. However, the practical upper mass limit is ca. 100,000 Da due to increasing

congestion in the spectra coupled with the width of the peaks due to statistical variations in isotopic composition [10,17]. ESI is a near-ideal interface for liquid chromatography/MS because of its low m/z for large molecules [21]. The potential of this methods is further enhanced by tandem mass spectrometry (MS/MS), in which structural information is obtained by dissociating precursor molecular ion into product ions in a collision chamber [22].

Spray Ionization Process

Electrospray is one of several spray desorption techniques. The other two are aerospray (AS) and thermospray (TS). All three techniques are thought to share the same basic mechanism of ion production. Electrospray ion production requires two steps: (1) dispersal of highly charged droplets at near atmospheric pressure, and (2) subsequent droplet evaporation. An electrospray is produced by applying a high electric potential to a hypodermic needle through which 1-10 μL/min of liquid flows. A few kV potential difference between a spray needle and a counter electrode located 3 - 40 mm away is sufficient [23]. The electrical field at the needle tip results in charge accumulation on the surface of the liquid emerging from the needle terminus. The high electric field results in disruption of the liquid surface and formation of highly charged droplets. The liquid flow rate, resistivity, and surface tension are important parameters for droplet production. Positively and negatively charged

droplets are produced depending upon the needle voltage polarity. The negative ion mode requires the presence of SF_6 to inhibit electrical discharge [24,36]. Ions, charged clusters, and even charged droplets, depending on the extent of desolvation, are sampled by the mass spectrometer through either a small orifice or a narrow transport capillary.

The effects of experimental parameters on ESI voltage and current have been explored by several researchers. It is found that fluids with higher surface tension require a higher threshold voltage (onset voltage) for stable electrospray production. Thus about 8 kV is needed for water and 4 kV for methanol at a 10 mm spray needle to counter electrode distance [25]. The use of higher voltages does not substantially increase the electrospray ion current until the onset of corona discharge. High dielectric liquids produce higher currents [26]. ESI currents for a typical water/methanol/5% acetic acid solution are in the range of 0.1-0.5 μA. Conducting liquids can produce much higher ESI currents (up to 500 μA for liquid metals) [27]. The total electrospray ion current increases only slightly with increasing liquid flow rate. Increasing the flow rate results in the formation of large droplets and so decreases the evaporation of charged droplets [28].

The formation of molecular ions from charged droplets requires effective evaporation of the initial droplets. In some instruments, this is accomplished at atmospheric pressure

by forcing the ions to drift through dry nitrogen gas at a temperature of ca. 60 °C. The dry bath gas provides the enthalpy for vaporizing the solvent from the droplets. Both the internal and translational temperatures of the desorbed ions are maintained at the bath gas temperature. Alternatively, desolvation can be promoted by heating during ion transport through a interface capillary.

Spray Ionization Mechanisms

Two mechanisms are commonly cited: droplet fission at the Rayleigh limit [29] and direct field evaporation of ions [30]. The mechanism of ion formation from charged droplets is, however, still unclear and this is a very active area of research [31-33].

One electrospray ionization mechanism, described by Dole over 20 years ago, is known as the "charge residue" mechanism [5-7]. As the solvent evaporates from charged droplets, the surface charge density increases until the Rayleigh limit is reached. At this point the forces due to electrostatic repulsion are large enough to overcome the surface tension. The resulting instability, sometimes called "Coulomb explosion", tears the droplet apart and produces charged daughter droplets that evaporate further. Dole's idea was that the "Coulomb explosion" repeats until the ultimate droplets contain not more than one solute molecule each, provided that the original solution was sufficiently dilute. As the last solvent molecule evaporate from these ultimate

droplets, the charge would be retained by the solute molecule to produce a free ion.

Since the experimental data show that there are large number of multiple charged ions in electrospray ionization, Dole's mechanism to produce singly charged free ions seems to be a remote possibility.

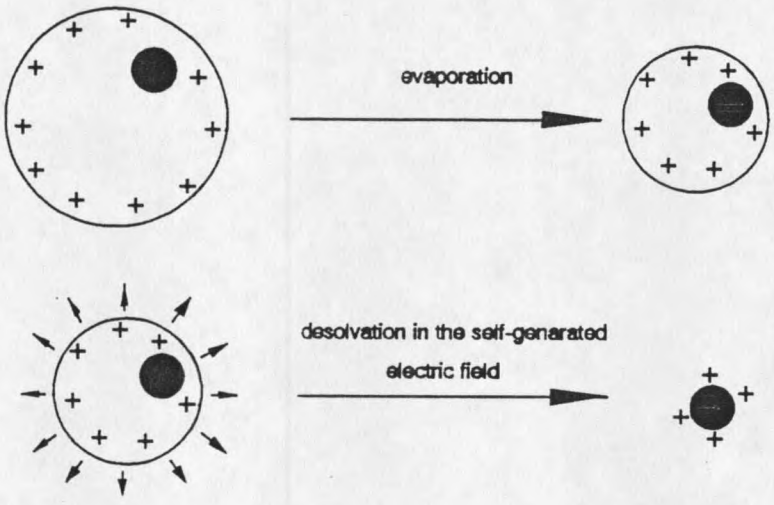

Figure 1. Sketch of the ion desolvation process [10].

An alternative to the "charge residue" mechanism was proposed in 1976 by Iribarne and Thomson, known as "field ion evaporation" [34,35]. According to this model, the Rayleigh equation (eq. 1) predicts that the electric field at the droplet surface increases as the droplet radius decreases during evaporation. Charged droplets are torn up by "Coulomb explosions" into smaller droplets. This sequence repeats

until the daughter droplets become so small that the electric field due to the surface charge density is strong enough to desorb ions directly from the droplet into the ambient gas. This process is often referred to as "ion evaporation" [1,34]. Figure 1 shows an artist's conception of the sequence of events.

When a droplet radius reaches the Rayleigh radius R_R as a result of evaporation, the droplet becomes disrupted (for a given charge) due to the Rayleigh instability [20]. The Rayleigh radius, R_R, for a charged droplet is given by

$$\frac{N^2 e^2}{R_R} = 16\pi\sigma R_R^2 \qquad (1)$$

where N is the number of elementary charges in the droplet and σ is surface tension of the droplet.

Iribarne and Thomson analyzed the energy relations and kinetic aspects controlling the possible separation of small ions from the bulk of an evaporating charged droplet. The droplet radius $R=R_E$ at which ion evaporation takes place can be related to charge number N and an energy barrier ΔG. The resulting formula is

$$R_E = A + \sqrt{A^2 + B} \qquad (2)$$

where A and B are functions of N and ΔG [34]. They wondered if the ions produced by vaporization of charged droplets were charged residues or small individual ions evaporated from the liquid. The ion mobility measurements with higher resolution persuaded them that desorption of small ions did occur. On the basis of a very simple model they estimated values for solvation energies of the ions and calculated the fields necessary for their desorption. They found that for droplets in the right size range, the required fields could be achieved without exceeding the Rayleigh stability limit [34,35].

The droplet radius $R=R_R$ from eq.(1) of Rayleigh instability and $R=R_E$ from eq.(2) of ion evaporation as a function of N have been plotted in Figure 2 [34].

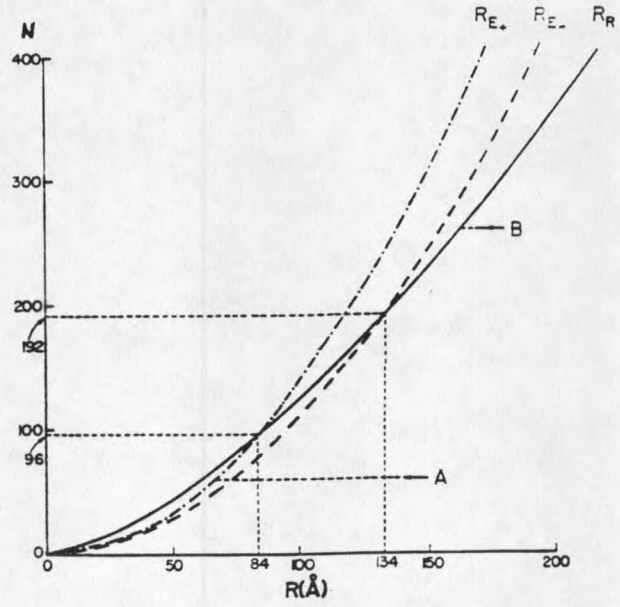

Figure 2. Critical radius for ion evaporation (R_{E+}, R_{E-}) and Rayleigh instability (R_R) [34].

As evaporation proceeds, N remains constant while R decreases until reaching either the curve R_R or curve R_E in Figure 2. The curve R_E will be reached first (path A in Figure 2) resulting in ion evaporation if N<192 for negative ions and if N<96 for positive ions (the critical radii are 134 and 84 Å, respectively). If instead N is larger than these critical values, the curve R_R will be reached first (path B in Figure 2), and at this point the droplet will lose a considerable fraction of its charge. After one or more steps, the charge on the droplet falls below the critical limit, and ion evaporation takes place.

Ion Transport Through Capillaries

In contrast to EI, CI, FAB, and other common MS ionization methods, the electrospray source operates at atmospheric pressure. This means that the ions must be transferred from the high pressure environment into the vacuum of the mass spectrometer, i.e. the ions must be separated from the neutrals. This is not a new problem in mass spectrometry. Atmospheric pressure ionization (API), usually using a corona discharge or a β-emitter such as ^{63}Ni, has a long history. There are two basic designs for the interfacing of an API source with a mass spectrometer. In one, the ions pass directly from atmospheric pressure into the vacuum chamber through a single, pin-hole orifice [81]. Here, the gas flow

through a ca. 100 μm diameter orifice is pumped by a very efficient cryopump on the vacuum side. DC or RF electrical fields are used to extract the ions from the gas jet. Extensive cooling in the super-sonic jet may result in unwanted cluster ions, particularly with water molecules. Therefore, a dry, nitrogen interface gas is covering the high pressure side of the orifice [81]. This API design is presently used in the Sciex electrospray sources [82].

In a second API design, the pump-down is achieved in two stages. The ions pass through a first orifice and enter a chamber with a pressure in the torr range. This chamber is usually pumped by a mechanical rough pump. The ions are then sampled into the mass spectrometer through a conical skimmer. By applying an electrical field in the intermediate pressure chamber, the ions can be declustering and even fragmented. This API design is very common for electrospray interfaces. Also in this design, it may be beneficial to force the ions to drift through a layer of dry gas on the atmospheric pressure side of the first orifice.

Capillary ESI/MS Interface

A remarkable new atmospheric pressure/MS interface was designed by Fenn and his co-workers [1,3,9]. In this interface the ions were sampled through a $\phi 0.2 \times 60$ mm glass capillary that connected the atmospheric ESI source with the intermediate pressure chamber. Ions are entrained in the flow of high pressure gas that enters the transport capillary. The

gas emerges at the exit as a supersonic free jet. The gas throughput was close to that of a 100 μm orifice and equally good mass spectra were obtained. It is particularly noteworthy that the capillary gas flow can drag positive ions against a potential difference between the inlet and the exit ends of the capillary. Thus, positive ions were transported 4.5 kV "uphill" in Fenn's experiment [3,9] and 15 kV "uphill" in another experiment reported in the literature [9].

Figure 3 shows a schematic drawing of Fenn's electrospray mass spectrometer [1,9,10]. Sample solution flows, typically at 5-20 μL/min, through a stainless steel hypodermic needle. Voltages were applied to each of the following components: needle (ground), cylindrical electrode (-3500 V), metalized inlet and exit ends of the glass transport capillary (-4500 V and +40 V, respectively), skimmer (-20 V).

In Fenn's early instrument, Figure 3, desolvation of the electrospray ions occurred in a drying gas in front of the capillary. However, in later designs by Chait et al., no curtain gas is required [38]. Instead ion desolvation is promoted by heating the ion transport capillary. Desolvation of the electrospray ions is carried out by heat transfer to the charged droplets during their transport through the capillary, and additional desolvation is induced by collisional activation in the region of reduced pressure between transport capillary and skimmer [37]. By controlling the temperature of the transport capillary and the potential

between capillary exit and skimmer, the degree of desolvation can be gradually increased to obtain either a desired solvated ion or a completely desolvated ion [15,22].

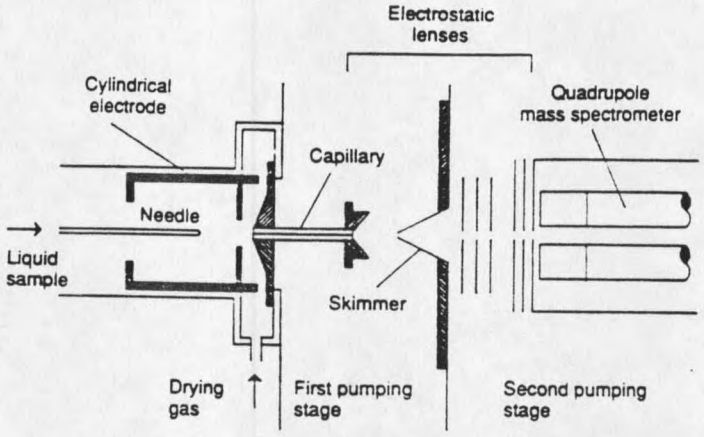

Figure 3. Schematic diagram of an ESI/MS apparatus [1].

For mass spectrometrists used to work at low pressures, ion transport through a narrow capillary seemed a surprising and strange arrangement. One might have guessed that only very few ions could have avoided collisions with the walls. Furthermore, the lore among ESI practitioners has been that ions would pass through very long capillaries. There has, therefore, been some doubts as to the mechanism of ion transport through the capillary tubes. There are several possibilities. For example, with electrospray, it is possible that it is mainly charged droplets and not gas-phase ions that

pass through the capillary. Further, with glass capillaries, the insulating walls must become charged as the first ions hit the wall. It could be argued that the repulsion between like charges must, at some point, prevent the further charging of the wall. Thus, ions that enter the capillary would have no choice but to pass through the full length of the capillary.

Ion Mobility in Gas Phase

If a weak and uniform electric field is applied to an ionized gas, a steady flow of ions develops along the field lines. The average velocity of the ions, or the "drift velocity", V_d, is directly proportional to the electric field strength E. Thus,

$$V_d = K * E \tag{3}$$

where the constant of proportionality K is called the mobility of the ions. K is a property of the ions and the bath gas.

McDaniel et al. have studied the ion mobilities extensively and they found that the drift velocity is a unique function of E/N for a given ion-gas combination at a given gas temperature [39], where E is the electrical field and N is the number density of neutrals. Therefore, the mobility of a given ionic species is inversely proportional to the number density of the neutrals and relatively insensitive to a small change of gas temperature (a few degree Kelvin) if the number density is held constant.

Ion Diffusion in Gas Phase

Inside the capillary, ions and charged droplets undergo axial as well as radial ion diffusion. Axial diffusion is small compared to the gas velocity through the capillary and will be ignored here. The radial ionic diffusion is discussed here.

According to Fick's law of diffusion,

$$J = -D\nabla n \tag{4}$$

where J is the ion flux, D is the ion diffusion coefficient, and ∇n is the ion density gradient. Therefore

$$\nabla \cdot J = -\nabla \cdot (D\nabla n) \tag{5}$$

and the equation of continuity gives

$$\frac{\partial n}{\partial t} = \nabla \cdot (D\nabla n) \; . \tag{6}$$

Consider a number of ions (S) located at the origin of a two-dimensional coordinate system. If the ions are released at time = 0 and allowed to diffuse through a field-free gas space at uniform pressure, the number density of the ions at a distance from the origin, r, and at a time t is,

$$n=\frac{S}{4\pi Dt}e^{-r^2/4Dt} \tag{7}$$

The root-mean-square displacement from the origin is,

$$\sqrt{\overline{r^2}}=\sqrt{4Dt} \tag{8}$$

In a conducting wall cylinder, eq. 7 and 8 have to be modified. Because the ions are discharged as they hit the wall, the number density N must be zero at the wall. The Gaussian error function in eq. 7 is replaced by a Bessell function [39]. For a infinitely long cylinder, the ion density is given by,

$$n(r,t)=\sum_{i=0}^{\infty}[G_i J_0(\alpha_i r)\cdot e^{-t/\tau_i}] \tag{9}$$

where G_i is a constant, J_0 is a Bessel function of order zero, $\alpha_i r_0$ is the ith root of J_0, and τ_i is a time decay constant. Thus, the ion density in the cylinder can be seen as a sum of diffusion modes each with a different decay time, τ_i. The average life time, τ, of ions against collision with the cylinder walls for a infinitely long tube of radius r_0 is

$$\tau=\frac{1}{D}\left(\frac{r_0}{2.405}\right)^2 \tag{10}$$

Types of Gas Flow Through Capillaries

Two types of gas flow inside tubes are commonly described, laminar flow and turbulent flow. At low flow velocities, fluids tend to flow without lateral mixing, and adjacent layers slide past one another like playing cards. There are neither cross currents nor eddies. This regime is called laminar flow. At higher velocities, turbulence appears and fluids move erratically in the form of cross currents and eddies. This type of motion is called turbulent flow.

Laminar and turbulent flow inside of tubes is distinguished by the Reynolds number (N_{Re}) [40]. Reynolds found that the critical velocity, at which laminar flow changes into turbulent flow, depends on four quantities,

$$N_{Re} = \frac{D\bar{v}\rho}{\mu} \qquad (11)$$

Where D = diameter of tube

ν = average velocity of fluid

μ = viscosity of fluid

ρ = density of fluid.

The type of flow in the tube depends on the Reynolds number and the roughness of tube inner surface. Laminar flow is always encountered at Reynolds number below 2100, but it can persist up to Reynolds numbers of several thousands if the tube entrance is well-rounded. Typically, the flow is turbulent at Reynolds numbers above 4000. Between 2100 and

4000 a transition region is found, where the type of flow may be either laminar or turbulent, depending upon the conditions at the entrance of the tube.

The velocity distribution of laminar flow in tubes can be derived using the definition of viscosity, μ,

$$\mu = -\frac{\tau \cdot g_c}{du/dr} \tag{12}$$

where τ is shear stress and g_c is Newton's-law constant. The negative sign in the equation accounts for the fact that u decreases as r increases in a pipe. After integration from tube center (r=0) to tube wall ($r=r_w$), the ratio of the velocity at radius r and the maximum velocity at $r=r_0$ is obtained as

$$\frac{U}{U_{max}} = 1 - \left(\frac{r}{r_w}\right)^2 \tag{13}$$

This equation shows that the velocity distribution in laminar flow with respect to radius is given by a parabola with maximum flow velocity at the centerline of the tube and with zero velocity at the wall, as shown in Figure 4. The average velocity is one-half of the maximum velocity.

In turbulent flow, the dependence of the average flow velocity on radius is more complicated. A typical velocity distribution for a Newtonian fluid moving with turbulent flow

through a smooth pipe at a Reynolds number of 10,000 is shown in Figure 4 [40]. The curve for turbulent flow is much flatter than that for laminar flow, and the difference between the average velocity and the maximum velocity is considerably less. At still higher Reynolds numbers the curve for turbulent flow would be even flatter than that in Figure 4.

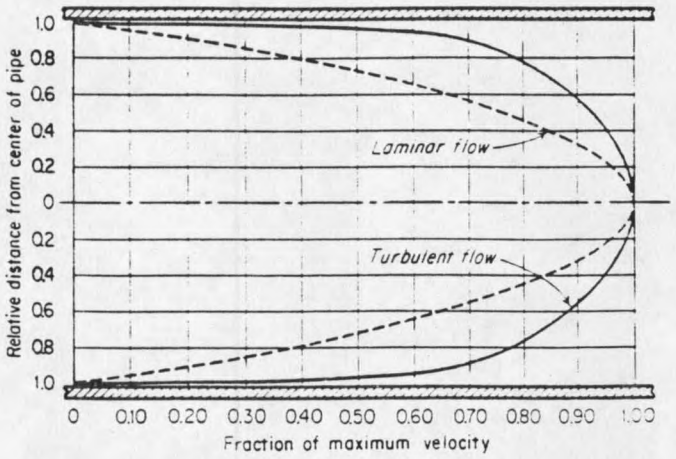

Figure 4. Velocity distribution in pipe for laminar low and for turbulent flow at N_{Re}=10,000 [40].

Protein Studies Utilizing ESI/Mass Spectrometry

ESI/MS for Protein and Peptide Analysis

Electrospray mass spectrometry (ESI/MS) has become an indispensable tool for peptide and protein structures analysis [1,112]. There are several unique capabilities that enable ESI/MS to be used to solve structural problems not easily handled by conventional techniques. First, ESI/MS is able to

provide accurate molecular weight information on low pico-mole amounts of peptides and proteins [41,42,100]. Second, molecular weight information is obtainable for peptides present in complex mixtures [43,44,48]. Third, the multiply charged ions can bring m/z down to the range accessible by conventional quadrupole mass spectrometers, even for large proteins (>150,000 Da)[1,23]. Fourth, by using tandem MS, partial to complete sequence information may be obtained for peptides containing up to 25 amino acid residues, even if the peptides are present in mixtures [45,46]. Fifth, adaption of ESI to on-line LC/MS is easily implemented and such an interface offers superior characterization of protein and peptide mixtures [47,49,50,63].

A key feature of the electrospray process is the formation of multiply charged molecular species. Such ions can be formed if the analyte contains more than one possible site of cation attachment. In the case of peptides, the maximum number of charges observed equals the number of basic amino groups (i.e., Arg, Lys, His, plus the free α-amino terminus). However, the maximum number of charges observed for proteins is often smaller than the number of basic side chains. This is presumably because the native folded state of the protein makes certain protonation sites inaccessible to the solvent [23]. Proteins usually exhibit a smooth progression of multiply charged molecular ions. Proteins with molecular masses up to 150,000 Da have been successfully analyzed by

ESI/quadrupole MS. A rough ratio of 0.5 - 1.0 charge/kDa is observed for most proteins, which means that an instrumental mass/charge range of < 2000 - 3000 is sufficient [51]. Electrospray has also been successfully interfaced to Fourier transform ion cyclotron resonance [52], magnetic sector [53], and ion trap mass spectrometers [54].

Desolvation of Electrospray Ions

Numerous investigations of the ionization mechanism of electrospray have been reported [1,34,35,56,57]. Considerable doubts remain concerning the detailed mechanism of ESI. Thus the nature of the charged species that are desorbed, evaporated, or "ejected" from the surface of highly charged and rapidly evaporating droplets is not known. Such questions are difficult to resolve using mass spectrometry because only the final ions are observed, and these have been transported through the ion source and the atmosphere-vacuum interface.

Droplet evaporation and desolvation are required to produce ions in electrospray. Two methods are used to assist droplet evaporation and ion desolvation, countercurrent gas flow and heated transport capillaries. An advantage of ESI interfaces using countercurrent gas flow is that the dry nitrogen environment minimizes the clustering of ions with water molecules that is caused by the cooling as gas expands into the vacuum. Condensation of nitrogen, on the other hand, is generally found to be negligible and is not observed for small molecules. Such condensation should be even less

important for large molecules that are less efficiently cooled in a supersonic expansion. In the absence of a countercurrent gas flow, desolvation of the ions can be carried out by heat transfer to the charged droplets during their transport through a heated ion transport metal capillary.

As the ions pass through the atmosphere-vacuum interface, they undergo collisional desolvation. The extent of such desolvation is determined by the nozzle-skimmer (or capillary-skimmer) potential bias (ΔV). At $\Delta V = 0$, the collisional desolvation can be minimized and adduct association is seen in the ESI mass spectra. As the potential difference is increased, such adducts disappear because of collisional excitation [108,112]. As the potential bias increases even further, the collisional excitation can be very extensive and analyte ions may even be fragmented. This is useful in order to obtain structural information.

ESI/MS Sensitivity

The ionization efficiency of ESI can be very high, providing the basis of sensitive measurements. Smith et al. measured a typical current (shown in table 1) for an electrospray mass spectrometer with a nozzle-skimmer interface [23]. A 10^{-4} M analyte solution at a flow rate of 1 μL/min has sufficient concentration of electrolyte ions to account for the total electrospray current, 1.6×10^{-7}A. A total of 10^{-12} - 10^{-11} A, or 10^{7} - 10^{8} counts/sec can be supplied to the detector for singly charged species. The ion transmission

efficiency is typically 10^{-5} [112]. On this basis, analyte concentrations as low as 10^{-10} M at a flow rate of 1 μL/min can give detectable ion currents (>10 counts/sec) [47].

Table 1: Typical electrospray ion source characteristics.

	frac. of total ionization	current A	total ions/s
total spray current[b]		1×10^{-7}	
through nozzle[a]	~ 10^{-2}	~2×10^{-9}	~10^{10}
focused into quadrupole	~ 10^{-4}	~2×10^{-11}	~10^{8}
detected	~ 10^{-5}	~2×10^{-12}	~10^{7}

[a] 1 mm diameter nozzle or a slightly large capillary bore giving an equivalent gas flow.
[b] Estimated at ca. 3 mm from spray needle using 10^{-4} N electrolyte solution of water/methanol (50:50) solution.

The ionization efficiency in the ESI can approach unity for large molecules. For example, with the flow rate of 2.7×10^{-16} moles/sec, cytochrome C molecular ions reach the detector at a rate of about 3000 counts/sec. The overall ion transmission efficiency is 2×10^{-5} [112].

The mass spectra of high molecular weight compounds depends on instrument sensitivity and other factors. When the molecular weight increases, the average number of charges also increases, so does the number of peaks with different charge state. In addition, an increased peak width is often observed due to the unresolved contributions from solvent attachment, electrolyte ion adduct [37,58]. In electrospray ionization, the concentration for proteins is 10 times lower than that of

singly charged species since large proteins have higher charge state. The detection of a protein molecular weight of 100,000 Da would require instrumental performance estimated to be 10^3 to 10^4 better than those necessary for singly charged species ionized with equal efficiency. However, higher molecular weight species may be ionized somewhat more efficiently than singly charged species.

Useful ESI/MS for very large proteins will require both more efficient mass spectrometers as well as a reduction in the "peak width" contributions. Studies with proteins of molecular weight > 200,000 Da have been reported with unresolved peaks [71]. The relative ion intensity is compared in Table 2 for different molecular weight [47]. Large proteins have much lower peak intensities. Spectra of oligonucleotides suggest that the maximum molecular weight may be somewhat lower (perhaps < 100,000 Da) due to the slightly lower ion currents in negative ion mode and the greater peak widths due to unresolved sodium attachment.

Table 2: Dependence of signal intensity upon MW.

MW (Da)	approx. # of charges[a]	peak width (amu)	maximum intensity (counts/s)
1,000	1	1	10^{12}
10,000	5	1	2×10^{10}
40,000	20	3	4×10^{8}
100,000	50	6	3×10^{7}
200,000	100	6	8×10^{6}

[a] Estimated form existing data and assuming all charges state are equally intense.

Molecular Weight Determination

The molecular mass of a protein can be easily determined from mass spectrum, assuming that adjacent peaks of a series differ by only one charge, and that charging is due to proton attachment (for positive electrospray ionization) [59,100]. This has been found to be good assumptions for proteins. In the case of subunit proteins, typically only the individual subunits are observed. The relationship between a peak position m/z of a protein with charge number i and molecular weight M_r is given as

$$K_i = \left(\frac{m}{z}\right)_i = \frac{M_r + m_a i}{i} = \frac{M_r + 1.0079\, i}{i} \qquad (14)$$

where K_i is the apparent $(m/z)_i$ for the peak and m_a is the mass of the adduct ions. With the proton attachment, m_a is 1.0079. The corresponding equation for a second multiply protonated ion at a peak position $(m/z)_{i+n}$ with charge number i+n is given by

$$K_{i+n} = \left(\frac{m}{z}\right)_{i+n} = \frac{M_r + 1.0079\,(i+n)}{i+n} \qquad (15)$$

Equation (14) and (15) can be solved for charge number i at $(m/z)_i$ while eliminating M_r,

$$i=\frac{n(K_{i+n}-1.0079)}{K_i-K_{i+n}} \qquad (16)$$

With the charge number i resolved and taking it as the nearest integer value, the ion mass M_r can be obtained from any one peak, or averaged from several peaks,

$$M_r=\frac{1}{n_0}\sum_i i(K_i-1.0079) \qquad (17)$$

where the adduct ion mass is 1.0079 and n_0 is the number of peaks used.

The quality of the spectrum with respect to mass determination can be measured by weighing factors from each peak. This method is most useful for noisy spectra with only few relatively large peaks [108]. The precision of mass measurement for proteins up to 100,000 Da has, in practice, been shown to be better than 0.02% [9,23,60,108].

Electrospray of Aqueous Solutions

Smith et al. [84] and Hayati et al. [61] investigated the effects of several experimental parameters on the onset and stability of electrospray. The parameters included solution properties such as surface tension, dielectric constant, viscosity, and conductivity, as well as applied voltage, flow rate, and spray capillary diameter. Smith found that stable electrospray in air could not be obtained if the surface

tension was above 0.05 N/m. The failure to spray liquid with higher surface tensions was explained as a result of the required field for electrospray exceeding that required for a corona discharge. The surface tension for distilled water is 0.073 N/m, well above the upper limit for the liquids that could generate a stable spray.

In electrospray ionization, peptides and proteins are usually dissolved in a acidic aqueous solution that contains a substantial proportion (typically 50%) of an organic solvent such as methanol. The presence of methanol lowers both the surface tension and the conductivity of the solution. Such solutions produce stable electrospray and generate reproducible ion signals in mass spectrometer. However, electrospray of purely aqueous solutions is indeed required because many proteins are not soluble in solutions containing large proportions of organic solvent. Furthermore, proteins can be denatured in solutions with a high percent of organic solvent [62,101]. The mass spectrometric sensitivity and the charge state distribution of protein ions in the spectra are also affected by the solvent composition.

Electrical discharges, such as corona, can be suppressed by a suitable choice of ambient gas. SF_6 is relatively non toxic and odorless and has found widespread use for the suppression of electrical discharges [64,65]. Many ESI investigators have used SF_6 to suppress corona and to successfully electrospray aqueous solutions [42-47,66,67,86].

The SF_6 flow rate is typically low, 50 to 300 ml/min. The higher ion signal stability and sensitivity are achieved by using SF_6 discharge suppression.

An alternative method of spraying aqueous solution was developed by Chait et al [68]. Instead of using SF_6, they use a different shape of spray needle. A flat tip syringe needle (710μm o.d. and 150μm i.d.) was sharpened by electropolishing in a mixture of water, glycerol, and phosphoric acid (1:1:1, v/v). As the tip of the syringe needle was made increasingly sharp, the water existing the needle tends to form finer droplets when a high voltage was applied. A stable electrospray from pure acidic water in ambient air was obtained.

STUDY OF PROTEIN CONFORMATIONS

Most proteins in their native state are tightly folded, compact structures. The conformation in solution can be altered by subjecting proteins to high temperatures, extremes of PH, detergents, or high concentrations of compounds such as urea and organic solvents [69]. A variety of physical techniques has been used to monitor these conformational changes, such as optical rotation, spectrophotometry, viscometry, fluorescence, circular dichroism, and nuclear magnetic resonance (NMR) [70].

More recently it has been shown that electrospray

ionization can also be used for such studies [62,72,73,104]. The reason is that proteins in different conformations have different numbers of basic sites exposed to the solvent. For this reason, the charge distribution in the ESI mass spectra are different.

Solvent Composition Effect

In general, a protein in a tightly folded conformation is expected to have fewer basic sites available for protonation compared to the same protein in an unfolded conformation. Chait [72] has reported a study of conformational changes in bovine ubiquitin induced by the addition of organic solvent, methanol, to aqueous acidic solutions of the protein. Bovine ubiquitin, in its native form, is a small, tightly folded protein (MW=8565 Da) that is very resistant to denaturation. When ubiquitin is dissolved in an aqueous solution with 1% acetic acid, the ESI/MS spectra show a distribution of low charge state (charge number < 8). Under these conditions, the protein is in the tightly folded native conformation. When ubiquitin is dissolved in a mixture of water and methanol, the ESI distribution is switched to higher charge states (6 to 13). Circular-dichroism measurements indicated that the protein underwent a large conformational change.

Loo et al [43] studied the effect of solvent composition to the denaturation of proteins. A bimodal charge state distribution was observed in the ESI mass spectrum of ubiquitin in solutions containing small amounts (< 20%) of

organic solvents. The distribution of peaks at high m/z (low charge state) was found to represent the native protein conformation. The distribution of high charge states is characteristic of the denatured protein conformation. Berman et al [106] reported the suitable results for the globular protein, cytochrome c. With addition of methanol to the cytochrome solution (<15%), the high charge state distribution totally disappeared [78].

Solution PH Value Effect

The denaturation of a protein at low or high pH is generally viewed as a global effect precipitated by the ionization and charging of residue side-chains. Columbic repulsion among the charged centers is the driving force that destabilizes the native protein structure. For some proteins, e.g., α-lactoglobulin, denaturation can be attributed to the ionization of a very limited number of residues buried in the native structure [74].

As a globular protein is under acidic conditions, the non-covalent bonds can be weakened due to the protonation to the available residues. This may result in the separation of a cofactor from the protein. For example, the oxygen-carrying protein myoglobin contains a non-covalently bound heme group in the hydrophobic pocket of the native globin chain. This chain can be induced to unfold under acidic conditions, thus weakening the heme-globin interactions. The acid denaturation of myoglobin has been studied extensively under a variety of

conditions [75,76]. In the case of horse myoglobin [77], the onset of denaturation occurs in the PH range 4.5-3.5 and depends strongly on the ionic strength of the solution.

Recent finding [104] demonstrates that electorspray ionization mass spectrometry can provide information on the conformation of myoglobin under different solution conditions and that the extent of heme-globin dissociation can be measured mass spectrometrically. At a pH value of 3.9, a bimodal charge state distribution showed that the two conformations of myoglobin were coexisting. The high charge state distribution corresponded to the apomyoglobin, the denatured protein conformation without heme; the low charge distribution corresponds to the native state of myoglobin with heme. Myoglobin and heme interaction is reversible under the solutions with low and high pH values [73].

Combined Separations ESI/MS of Polypeptides

Extensive structural characterization of proteins, particularly those converted to mixtures prior to analysis by chemical or enzymatic procedures (e.g., tryptic digestion), has become an important aspect of biochemical system. Since detailed knowledge of the primary structure is required as part of biochemical research, and sample size is generally limited, there are strong encourages to conduct biochemical

research on the combined separation/ESI/MS analysis. These combined analytical methods always give greater sensitivity in most cases. Reversed-phase high-performance liquid chromatography (RP-HPLC) has been shown to give high-resolution separation for mixtures of peptides and proteins [83,84,85].

The Separation Process of HPLC

Chromatography involves the separation of the components of a mixture by differences in the equilibrium distribution of the components between two phases: the mobile phase and the stationary phase. Migration of component molecules may be assumed to occur only when the molecules are in the mobile phase. The rate of migration of a component is inversely proportional to its distribution coefficient, so components with a high distribution in the stationary phase will move more slowly through the column and hence be separated from the components with a lower distribution in the stationary phase. Differential migration therefore depends upon the experimental variables that affect the distribution, i.e. the composition of the mobile phase, the stationary phase, and the temperature [86].

Component retention of HPLC The exact mechanism of component retention in PR-HPLC is not presently well understood. Component retention is believed to depend upon partition, adsorption, dispersive interaction, solubility in the mobile phase, and solvophobic effects. At present it

appears that solvophobicity is the primary mechanism for component retention.

The principle of solvophobicity as presented by Horvath et al. [87] is based upon the tendency of the mobile phase to minimize the site of the cavity occupied by the component molecules in the hydroorganic mobile phase. The magnitude of the solvophobic effect for a given solute molecule is largely due to the properties of the hydroorganic solvent system. The properties of dielectric constant and surface tension play important roles in governing solute retention [88].

UV-detectors Detectors used in HPLC must function with high precision, high sensitivity, and high stability, and must not significantly affect the separation achieved by the column. LC detector should be capable of detecting 1 part or less of solute in 10^6 parts of eluent. UV detectors were among the first detectors used in liquid chromatography and they are still the most popular today.

The solutes, which contain a UV chromaphore at the monitoring wavelength, absorb the incident light as they pass through the flow cell. Measurements of the amount of light absorbed produces a signal proportional to the concentration of the solute as described by beer's law. For highly absorbing species detection limits of 1 ng on column are feasible. The standard flow cell in most instruments has an optical path length of 10 mm and a volume of 7.5 - 10 µl. The design of the flow cell is important to prevent turbulence

which can cause refractive index changes in the eluent [89,90]. Figure 5 shows two cell designs which are commonly used in commercial instruments.

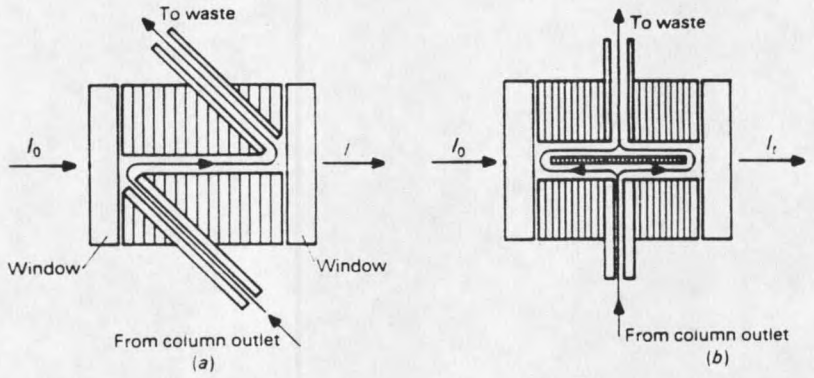

Figure 5. Common flow cell designs used in UV detectors for liquid chromatography [89]. (a) Z-pattern flow cell. (b) H-pattern flow cell.

Combined Separation Mass Spectrometry

The mapping for a tryptic digest protein conventionally utilizes RP-HPLC separation with UV-absorbance detection, typically operated at λ=214 nm. The combination of mass spectrometric detections have been provided a tremendous information (mass/charge) for the identification of the eluting components. The conventional combinations of liquid chromatography - mass spectrometry (LC-MS) are thermospray and continuous-flow fast atom bombardment (flow-FAB). In

thermospray ionization, peptides up to 2000 Da can be detected with an analyte qualities of 100 pmole. It has been reported that flow-FAB can detect as large as 5000 Da peptides and analyte quantities could be even less than that in thermospray. However, it was recently recognized that both techniques have their limitations in detecting glycopeptides. In the case of flow-FAB, the matrix interference decreases the detecting ability for small molecules (<500 Da). Also, the hydrophilic character of carbohydrates limits their concentration on the surface, thus the sensitivity drops off very rapidly for the peptides larger than 3000 Da.

Electrospray ionization has shown its ability to ionize peptides and proteins efficiently from analyte solutions. Because of multiple charge character, electrospray can be used for very large peptide and protein studies. The use of reverse phase HPLC combined with ESI for the analysis of peptide mixtures, particularly enzymatic digests of proteins, is rapidly growing. For example, Carr and co-workers [84] and Hancock and co-workers [83] have obtained information on the primary sequence. Carr and co-workers noted the speed and sensitivity of these methods, and reported a significant sensitivity advantage compared to flow-FAB methods. Hancock and co-workers have reported a detailed tryptic map for recombinant human tissue plasminogen activator, a 527 residue glycoprotein, and glycosylation sites for tryptic digests of recombinant proteins. The additional dimension provided by

mass spectrometry gives more details about the complex tryptic map and significantly enhances the high resolution chromatographic separation by distinguishing mass of any coeluting components.

OBJECTIVES

The purpose of this research is to obtain an understanding of the mechanism of ion transport by viscous gas flow through narrow capillaries, to model such ion transport, and to study applications of electrospray mass spectrometry to biochemistry using the narrow capillary interface. The objectives are:

Study the mechanism of ion transport through narrow capillaries by viscous gas flow and propose a suitable model to simulate ion transport and loss.

Install, put into operation, and optimize a home-built electrospray ion source as an interface to a mass spectrometer.

Investigate the characteristics of the electrospray ion source, particularly with regard to protein mass spectra.

Study protein conformational changes induced by acids, organic compounds, and high temperatures, and their effects on the electrospray mass spectra.

Develop an experimental protocol to study covalently modified proteins by tryptic digestion followed by HPLC separation and electrospray mass spectrometry.

EXPERIMENTAL

Effect of Experimental Parameters On Capillary Ion Transport

Instrumental Set Up

Figure 6 shows the flow chart and equipment components for investigation of electrospray ion transportation. The instruments included five basic parts, electrospray ionization source, ion transportation, ion current detection, vacuum system, and bath gas system.

The electrospray ionization source is composed by a syringe pump and an electrospray chamber. Details are given in Figure 7. Sample solutions, typically 10^{-4} M analyte in methanol entered electrospray chamber through a stainless steel capillary needle (1.0 mm O.D. and 0.5 mm I.D.) at a flow rate of 0-7 μL/min by means of a motor-drive syringe pump (SAGE Model 355).

A flow of air was maintained to keep the electrospray chamber at atmospheric conditions. A mist of positively charged droplets were produced at the tip of the spray needle under high electric field. About 4-6 kV (GLASSMAN high power supply, PS/EH 60R01.5) was applied to the spray needle and 0-50 V to the cylindrical electrode. Positively charged electrospray droplets drifted toward the ground plane electrode. A small fraction of those were "sucked into" the

transport capillary by viscous gas flow. A heating tape was coiled outside of the spray chamber to provide temperature control, typically from 25°C to 80°C. Higher temperatures would assist the electrospray and the charged droplet evaporation. The distance between spray needle tip to ground plane electrode is one of the most important parameters. This distance was adjusted by means of a screwed motion rod.

Ion transportation was accomplished by capillaries connecting the spray chamber at atmospheric pressure and an ion collector at vacuum condition. The capillaries used in this study were glass, teflon, and metal tubes with different bore sizes (0.97 to 3.8 mm) and lengths (25 cm to 15 m). Gas throughput of transport capillaries was varied by valve A, shown in Figure 6. This valve also controlled the vacuum of the ion collector.

Ions that successfully transferred through capillaries were received by an ion collector. The ion collector was designed as a Faraday cup. A shielding cell was built up outside of the ion collector to overcome the surrounding noise and to stabilize the ion current signals.

A counter current flow of nitrogen was introduced to the ion drifting region near the capillary entrance to assist the evaporation of charged droplets. Nitrogen gas flow rate was changed from 0-100 mL/min at room temperature. A gas purifier containing silica-gel was connected in line to obtain dry, clean nitrogen gas. This curtain gas chamber was different

from that of many other researchers (see Figure 7) and was expected to give more efficient counter-current flow.

The vacuum system was provided by a rough pump (30L/min). The vacuum inside the ion collector was varied from 0 to 200 torr. A mercury U tube pressure gauge was used to monitor the vacuum of ion collector. Two flowmeters (Rotameter), in different ranges, were connected after a filter to the pump exhausted and measured gas throughput of transport capillaries. The gas throughputs were changed from 0 to 15 L·atm/min.

Data Acquisition

In order to study the electrospray ionization and the ion transport efficiency through capillaries, the current signals at four different positions in the equipment were monitored and recorded. Details are shown in Figure 7. They are electrospray current from the spray needle, entrance current at the capillary entrance, wall current of the conducting capillaries, and transmitted current at the exit end of capillaries.

The electrospray current (I_{sp}) was monitored by Keithley 169 DVM which was connected to the current monitor of the high power supply. A washer shaped, "entrance" electrode was mounted at the front butt end of transport capillary and isolated from the capillary with a thin ceramic spacer. The inner diameter of the entrance electrode was the same as that of the transport capillary in order not to disturb the air

flow into the capillary. The "entrance" current, I_{en} , from that electrode was fed into a home built current amplifier that used two 071 OP-amps. In the case of conducting capillaries, the current due to the ions hitting the inner wall of the capillary, I_{wall}, was monitored by Keithley 485 pico-Ammeter. Keithley 485 pico-Ammeter also amplified the wall current signals and sent them to a computer interface for data recording.

The ion collection at the end of the transport capillary had to be highly efficient. This presented a problem because of high gas throughput and relatively high pressures. In the final design, the ion collector at the end of the transport capillary consisted of two concentric cylindrical electrodes. The inner cylinder consisted of a fine metal mesh and the outer of a perforated copper cylinder. This dual electrode was connected through a doubly shielded cable to a pico-ammeter (Keithley 617). Two 9 volt batteries were used in order to apply +18 volt to the vacuum housing relative to the dual collection electrode. This ion collector design proved to be highly efficient and to give a stable ion signal. The electrode assembly was housed in an aluminum vacuum jacket.

The four current signals from each position were sent to a computer interface in order to record them. The Montana Laboratory interface was used in these experiments. The computer spreadsheet was used for data storage of I_{sp}, I_{en}, I_{wall}, I_{trans}, and spray chamber temperature, T_{sp}.

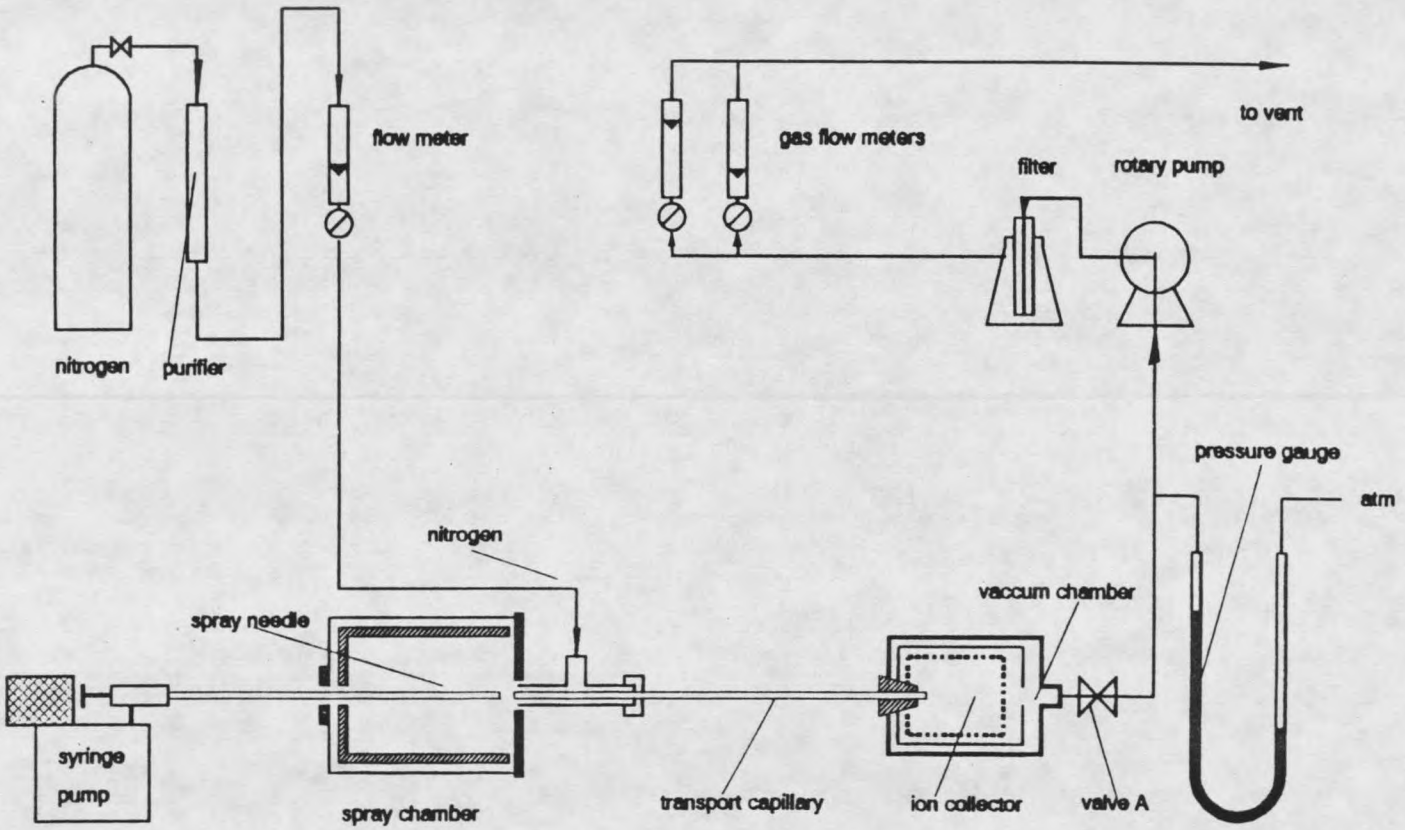

Figure 6. Equipment set up for ion transport through narrow capillaries.

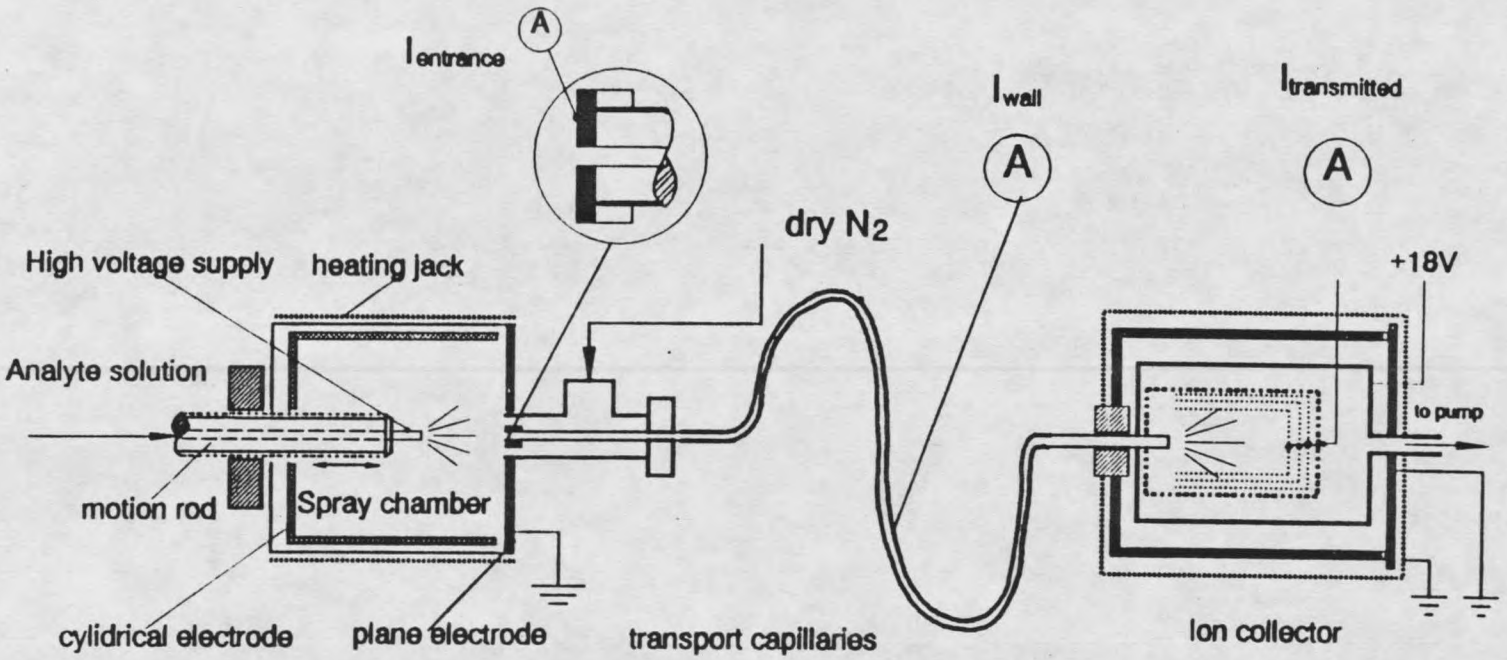

Figure 7. Detailed schematic drawing for electrospray chamber, ion collector, and current measurements.

Instrumentation of ESI/Quadruple MS

Figure 8 shows the instrumental set up for electrospray/quadruple mass spectrometer. This instrumentation mainly consists of electrospray chamber, narrow capillary interface, focusing lenses, and single quadruple mass analyzer. Each part in the instrumental set up has been improved since beginning of this work. The final construction of this instrument is presented here.

Narrow Capillary Interface

The most important part in our instrumental set up is the narrow capillary interface. Whitehouse et. al. [8] first introduced a capillary interface and obtained mass spectra of proteins by this interface (see Figure 3). The mass spectrometry facility at Chemistry Department of Montana State University designed a narrow capillary interface which has the required dimensions to mount on the ion source of VG-TRIO2 quadruple mass spectrometer. The interface was made by the mechanical facilities of Montana State University.

Figure 9 illustrates the basic structures and principles of this narrow capillary interface. A stainless steel transport capillary, $\phi 0.5 \times 200$ mm, connects the electrospray at 1 atmosphere and mass spectrometer under vacuum system. The transport capillary, after improvements, was surrounded by a heating jack (nichrome heating wire was wrapped between two

ceramic tubes) so that a controlled temperature was supplied to it. Details of the heating jack are also shown in Figure 9. The optimum temperature of transport capillary is maintained between 75 °C and 85 °C for most experiments. Voltage was also supplied to the transport capillary to obtain the potential bias between the transport capillary and the skimmer.

The distance between transport capillary and skimmer (d_{cs}) is very critical for ion signal intensity of mass spectrometry. In order to obtain a required vacuum in analyzer of mass spectrometer (< 2×10^{-5} mbar) and an optimized ion transport efficiency at the same time, the distance (d_{cs}) was adjusted as 3 - 4 mm for the best operation condition, shown in Figure 10. At the best operation condition (shadowed area in Figure 10), pressure was maintained lower than 2×10^{-5} mbar in the mass analyzer, meanwhile the ion signal intensity gained highest level. In fact, vacuum can be increased to 7×10^{-6} mbar when transport capillary is heated. The distance was set at 3.5 mm for most experiments.

Electrospray Chamber

Electrospray analyte sample was injected into a syringe loading injector (Rheodyne Model 7125, Supelco), 10 µL at a time. The sample was then pumped to the spray needle tip at solution flow rates from 1 to 1.5 µL/min through a motor-drive syringe pump (SAGE Model 355). Details of sample injection and sample loop connection are shown in Figure 11.

The stainless steel capillary with 0.7 mm i.d. and 1.5 mm o.d. was first used as a spray needle. The mixture of 50% methanol in water can be sprayed by using this needle, but it was not successful for spraying analysts in a 100% distilled water since water has higher surface tension, and under a higher on set voltage, corona discharge occurred. In order to spray protein sample dissolved in pure water, a much thinner stainless steel capillary with 150 μm i.d. was then used. Additionally, a fused silica capillary, 50 μm i.d. and 130 μm o.d., went through the stainless steel capillary in order to obtain an even sharper spray needle tip. Gold was coated on the tip of silica capillary (by gold sputtering) for a best electrical conducting. Details are described in Figure 11. The introduction of SF_6 gas to the spray needle tip was also made to suppress corona discharge. When SF_6 flow was on, the spray voltage can be turned up to a very high level without corona discharge. In practice, the flow of SF_6, when using gold platting silica capillary as a spray needle, is not necessary to suppress corona because the sharp needle supplied more stabilized spray. In electrospray of water solution, the on set voltage was greatly decreased with the use of sharp needle. The supplied voltage was from 2.3 to 3.8 kV with a 5 mm distance between spray needle and capillary entrance.

Vacuum System

Figure 12 shows the pumping system for the ESI/quadruple mass spectrometer. The interface pump needs a high capacity

to obtain a few torr in the capillary interface. The other pump are fixed to VG-TRIO2 instrument. The gas throughput of transport capillary and skimmer were also measured as described in Figure 12. The pump capacities and pressure distribution in each part are show in Table 3.

Table 3: Pump capacity and pressure distribution.

section	type	model	capacity	pressure
spray chamber	---	---	---	640 torr
interface	rotary pump		700 L/min	1 - 5 torr
ion source	rotary backing pump diffusion pump	E2M8 100/300P	137 L/min 280 L/s	$< 3\times10^{-4}$ mbar
mass analyzer	rotary backing pump diffusion pump	E2M2 63/150P	40 L/min 135 L/s	$< 1\times10^{-5}$ mbar

Ion Signal Optimization

Structure of Lenses

Lots of effort had been made to optimize the electrospray ion intensity. Except the improvements of spray needle and transport capillary, focusing lens structure is a very important system to be optimized. Two lenses have been added to the instrument after the original design. One is a screen

right after the skimmer for ion extraction and another is between the skimmer and the lens #2. Figure 13 shows a lens structure and approximate dimension of lenses. The potentials of lenses were controlled by a home made multi-channel potentiometer (DC volt, battery power supply). The potential of transport capillary was controlled by a high voltage supply (Glassman PS/EH 60R01.5).

The potential distribution for transport capillary and each lens are listed in Table 4.

Table 4: Potential distribution of lenses.

lenses	potential (DC volt)
transport capillary	20 - 180 V
skimmer	+ 11 V
screen	- 14 V
lens # 1	+ 9 V
lens # 2	+ 11 V
focus # 1	- 80 V
focus # 2	- 16 V

SIMION program [99] had been used to simulate ion trajectory under a given lens dimensions and potential distribution. Figure 14 plots the electrical fields and ion trajectories by using SIMION program. In this simulation, ions were started at the center hole of skimmer. Initial kinetic energy of ions was 10 eV. It could be seen that almost all ions are focused into mass analyzer (quadruple)

under the same lens structure and potential distribution listed in Table 4.

Signal Amplification

In the study of very large protein using electrospray ionization, the sensitivity of the instrument is required to be 10^4 better than those for the singly charged species. A pre-amplifier (VG F16, FA3) was adopted to the VG TRIO2 signal amplification system. Figure 15 shows the diagrams of current amplification before and after the addition of a pre-amplifier. Ion signal intensity of electrospray has been increased more than 5 times when the pre-amplifier was used.

Protein and Peptide Studies

Sample preparation

All samples, except the modified cytochrome C that was provided by the Department of Microbiology at MSU [98], were obtained from commercial sources and used without further purification. Table 5 listed the sources and catalog numbers of proteins and peptides that were used for this project.

HPLC grade methanol and Glacial acidic acid were used. High purity water (17.8 MΩ/cm) was obtained from deionization of water by Barnstead NANOpure II system.

Two analyte solutions were prepared for different studies. In one, proteins were dissolved in a mixture of 50/50 (v/v)

water and methanol. Acetic acid (HOAc) was added to the mixture to obtain a required pH. In another, proteins were dissolved in 100% pure water and no acid addition to the solution. Concentration of proteins were ranged from 10 to 40 μM. Solutions with different methanol concentrations and pH values were used for protein conformation studies. More details of each analyte solution will be shown in the Results and Discussions sections.

Table 5: Summary of samples.

Sample	Catalog number	Source
Myoglobin (from horse heart)	M1882	Sigma Chemical Co., St.louis, MO
Cytochrome C (from horse heart)	C2506	Sigma Chemical Co., St.louis, MO
Avidin (from egg white)	A9275	Sigma Chemical Co., St.louis, MO
Trypsin (from bovine)	T8253	Sigma Chemical Co., St.louis, MO
α-chymotrypsin (from bovine)	C7762	Sigma Chemical Co., St.louis, MO
α-chymotrypsin (from bovine)	1430	Worthington Biochemical Co. Freehold, NJ
Chymotrypsinogen (from bovine)	5630	Worthington Biochemical Co. Freehold, NJ
Carbonic anhydrase(II) (from Bovine)	C2522	Sigma Chemical Co., St.louis, MO
Alcohol dehydrogenase (from yeast)	A7011	Sigma Chemical Co., St.louis, MO
Angiotensin II	A9525	Sigma Chemical Co., St.louis, MO
Lys-Bradykinin	B4889	Sigma Chemical Co., St.louis, MO

Gas Phase Conditions At The Spray Region

In the study of gas phase acidity effect and gas phase temperature effect on the protein conformation, different conditions in gas phase of the spray region have been used. Figure 16 illustrates such arrangement for gas phase conditions. Acid addition into the gas phase at spray region was accomplished by loop A where N_2 bubbled through the solutions of acetic acid (0.23 M), hydrochloric acid (0.08 M), p-tolunesulfonic acid, and methanol, respectively. Flow rate of N_2 through each solution ranged from 0 to 6 ml/sec under room temperature.

The spray region temperature was accomplished by the preheated N_2. Shown in loop B in Figure 16, N_2 was first heated in a thermostat and then flowed to the exit of tube B. Tube B is also a glass with 2 mm i.d. and is thermally protected. The resulted temperature at spray region was measured by a thermocouple.

Separation of Tryptic Cytochrome C by HPLC

Materials

Horse heart cytochrome c (catalog number C2506) was obtained from Sigma Chemical Co. The modified horse heart cytochrome c was provided by A. Jesaitis and M. Quinn from Department of Microbiology at MSU [98]. TPCK-trypsin was

obtained from Sigma Chemical Co. HPLC grade acetonitrile was from Fisher Scientific. Distilled water (17.8 MΩ/cm) was obtained from NANopure II (Barnstead) system. Ammonium bicarbonate was from Matheson Coleman & Bell Manufacturing Chemists.

Tryptic Digesting of Cytochrome c

The tryptic digestion conditions and procedures were referred to personal communication [129] and Caprioli [130]. Cytochrome c was dissolved in pure water (750 μM) and 6 μl ammonium bicarbonate (1 M) was added to adjust the sample solution pH between 7.5 and 8. To this cytochrome c solution, TPCK-trypsin was added to give a final enzyme-to-substrate ratio of 1:50 (w/w). The digestion proceeded at 37 °C for 16 hours. The tryptic solution pH was checked again at the end of digestion and to make sure it was maintained at 7.5 - 8. The digestion was stopped by refrigeration of the sample immediately after 16 hours.

The tryptic digestion of modified cytochrome c followed the same procedures and conditions as for cytochrome c except that the concentration of original modified sample was only 50 μM, so that less TPCK-trypsin was used to keep enzyme-to-substrate ratio of 1:50.

HPLC Chromatography

The HPLC system used consisted of a Gilson Model 811B Mixer gradient liquid chromatograph and a UV-detector (Spectra-Physics). A injection of 20 μL of the tryptic

mixture from cytochrome c (750 μM) was made onto the C18 reversed-phase column. About 15 nmol sample was consumed to collect the spectrum. Elution was accomplished using a linear gradient of solvent A and B at a total flow rate of 1 mL/min. Solvent A was 1% HCl in distilled water; solvent B was 1% HCl in acetonitrile. Separation of the tryptic peptides was effected with a gradient of 6 - 60% solvent B over 30 minutes. A UV detector was used to monitor the effluent absorbance at λ=214 nm and 230 nm. Effluents with different absorbance and retention time were manually separated and collected into test tubes. Same HPLC equipments and procedures were used for the separation of tryptic mixture of modified cytochrome c. However, only 1 nmol of the peptide mixtures was injected on to the same column.

The fractions obtained form HPLC separation process were then kept at 0 °C for the storage and were ready for the mass spectrometry analysis. Since the effluent concentrations were too low to obtain ion signals from ESI mass spectrometer (about 3×10^{-8} M), they were evaporated under a vacuum system to increase the concentration. The total volume of effluents were decreased from 30 mL to 5 mL so that the concentration of fractions were increased 6 times higher.

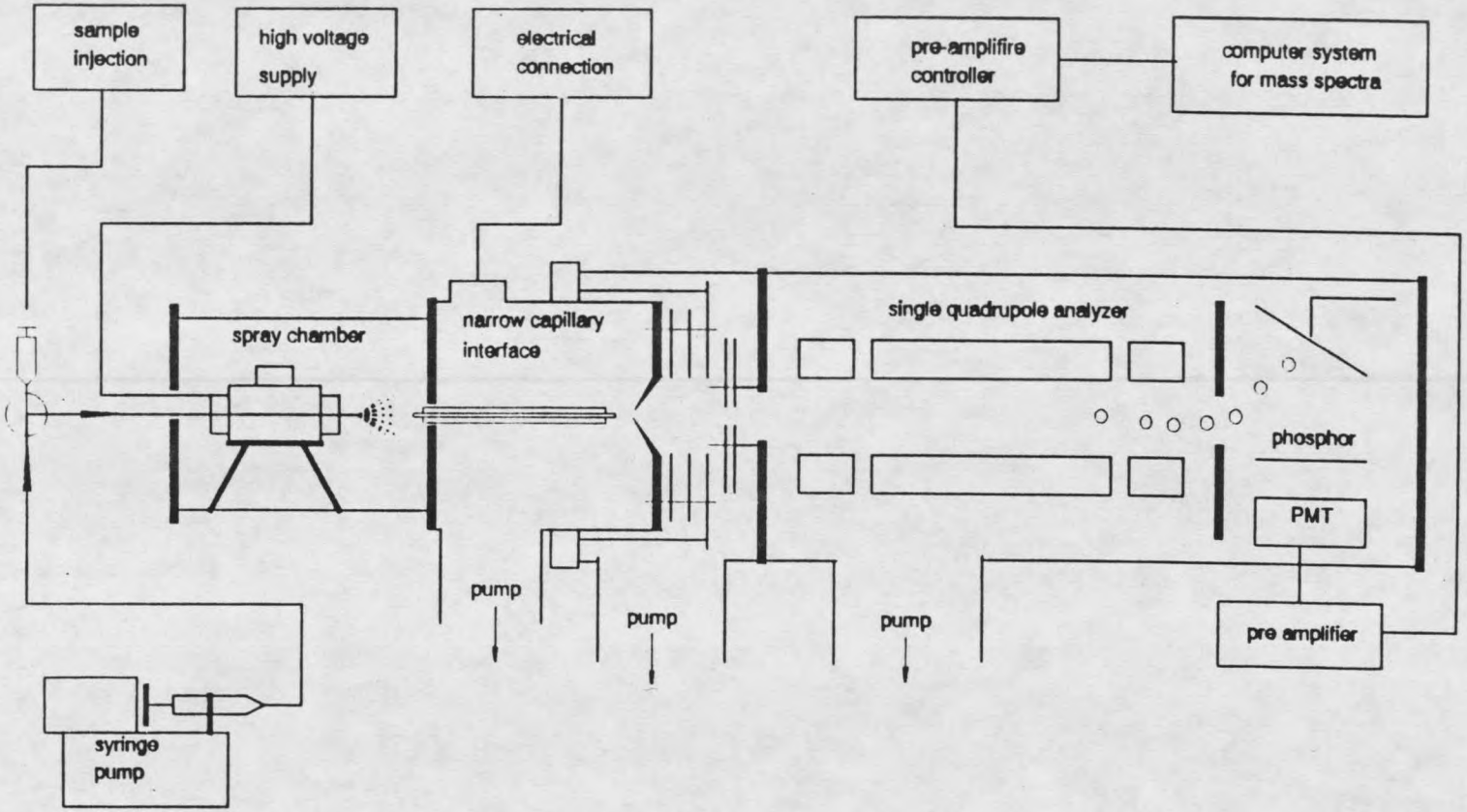

Figure 8. Schematic drawing for electrospray interfaced quadruple mass spectrometer.

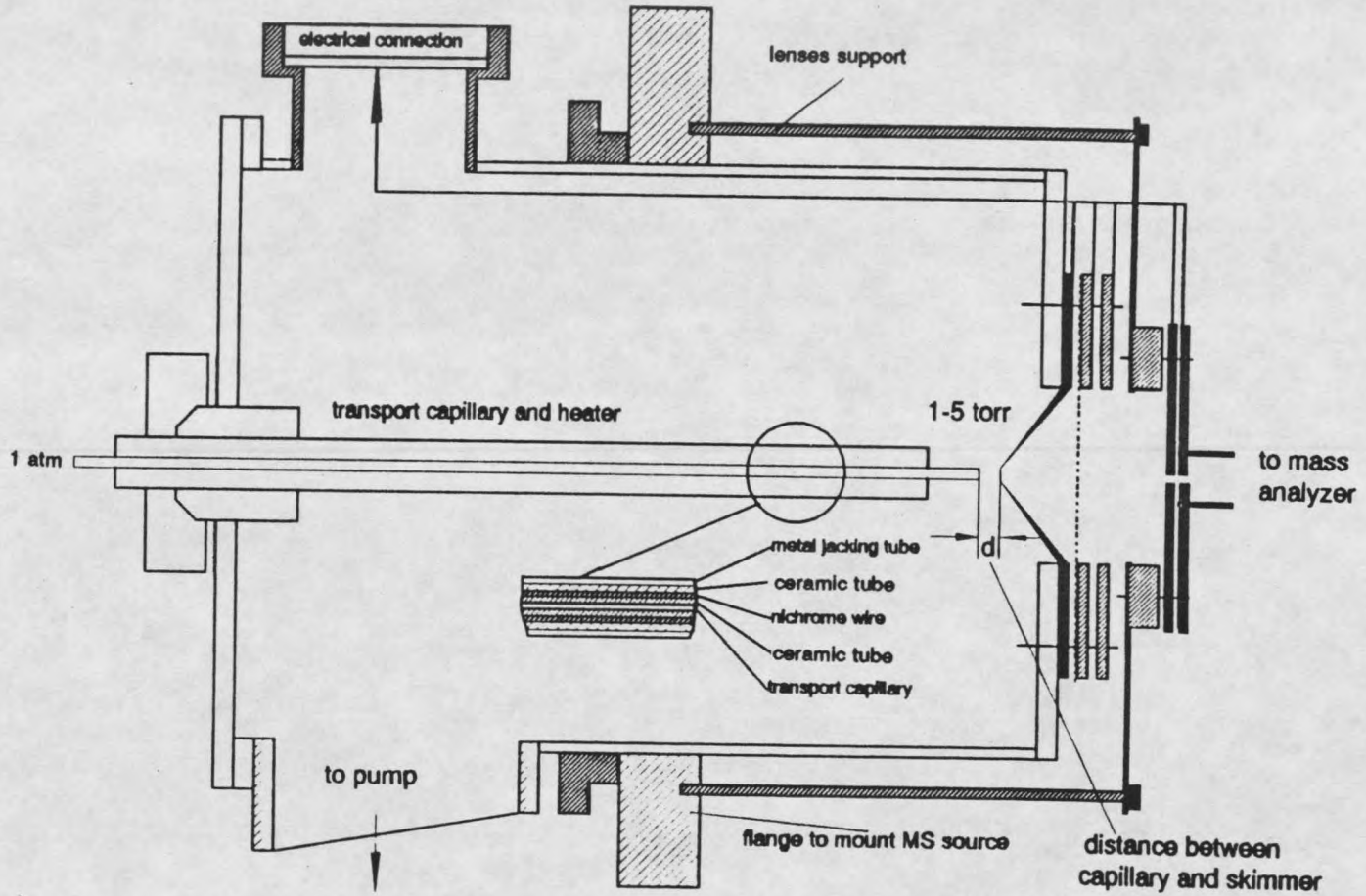

Figure 9. Narrow capillary interface designed for electrospray/mass spectrometer.

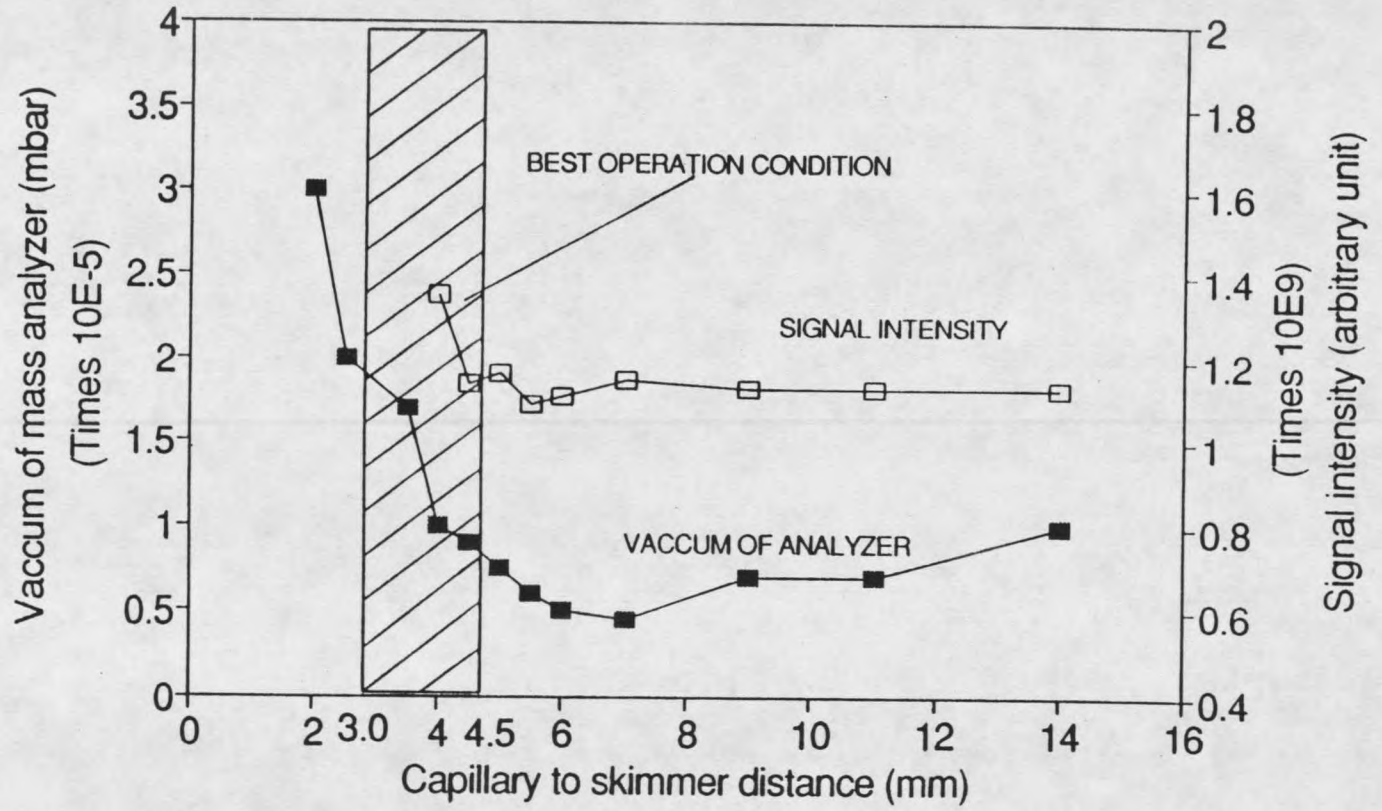

Figure 10. Optimization of the distance between a transport capillary and a skimmer.

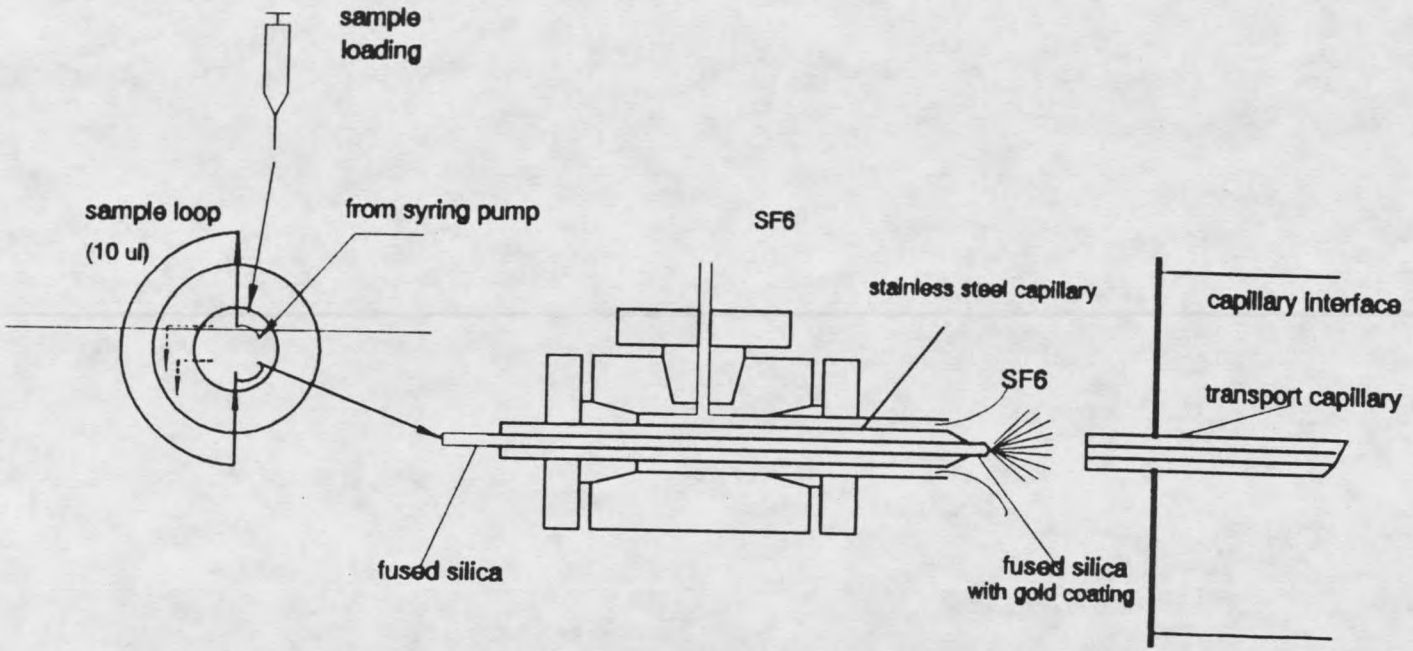

Figure 11. Construction of electrospray needle and sample injection.

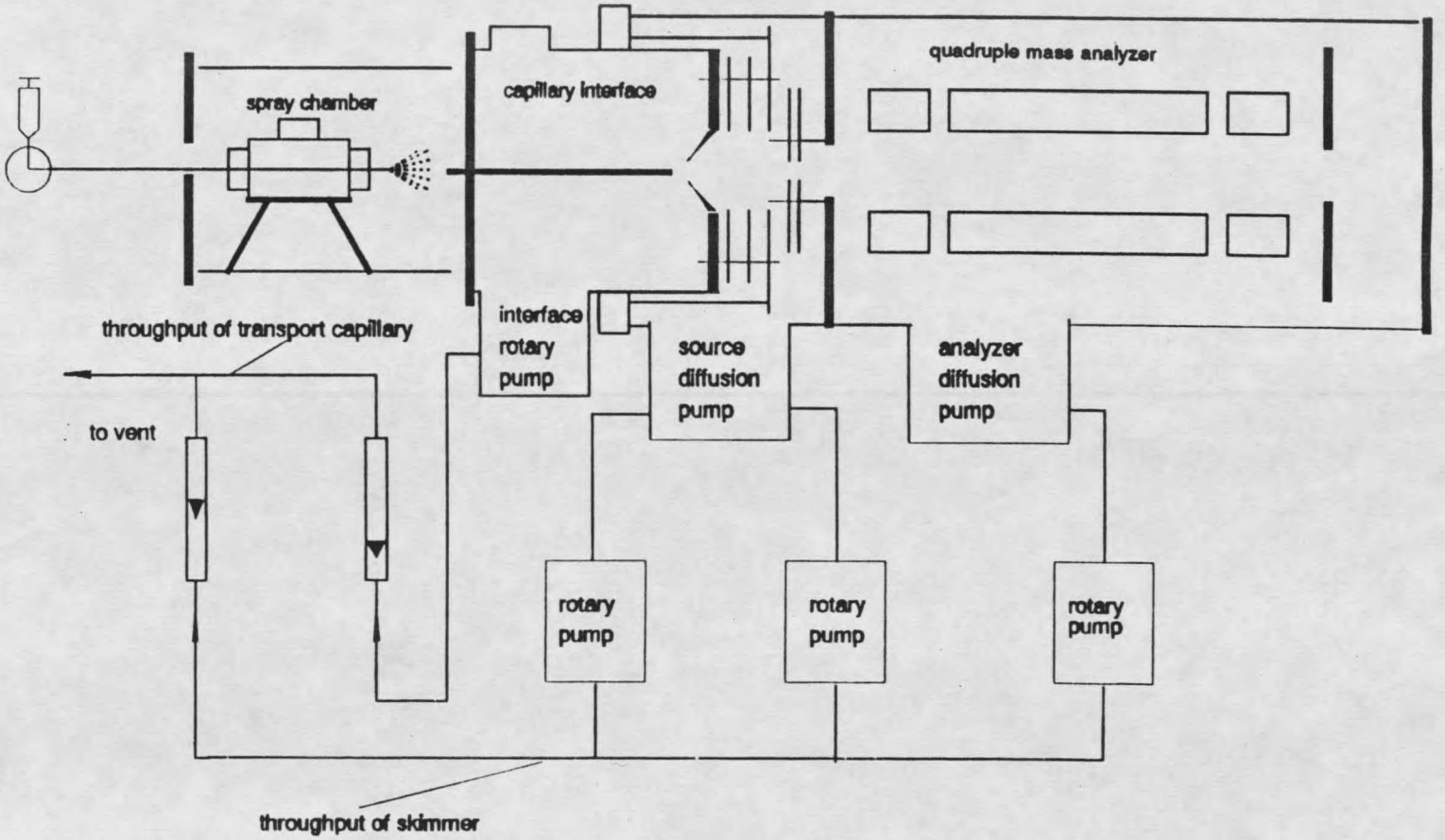

Figure 12. Pumping system in electrospray/quadruple mass spectrometer.

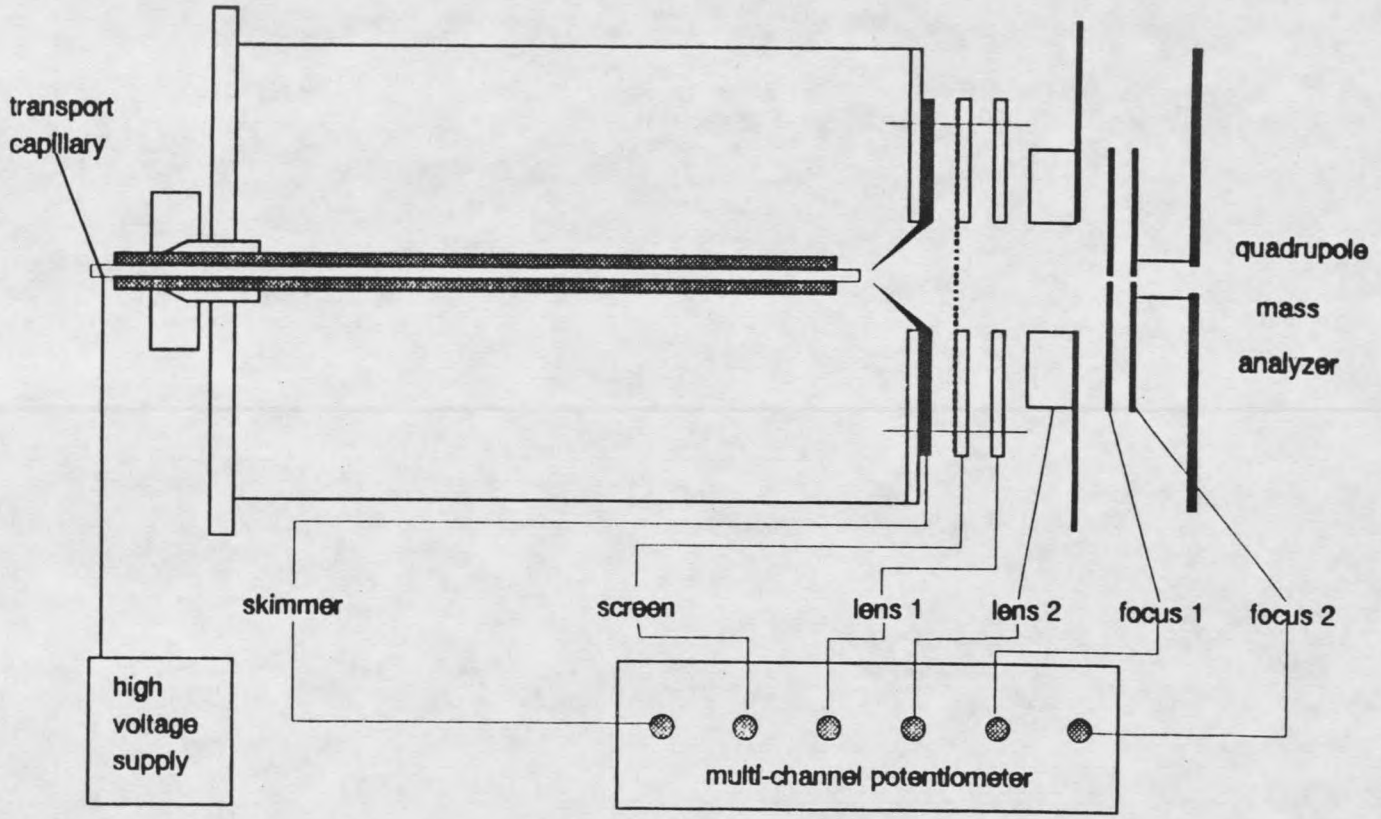

Figure 13. Structure of ion focusing lenses and voltage distribution.

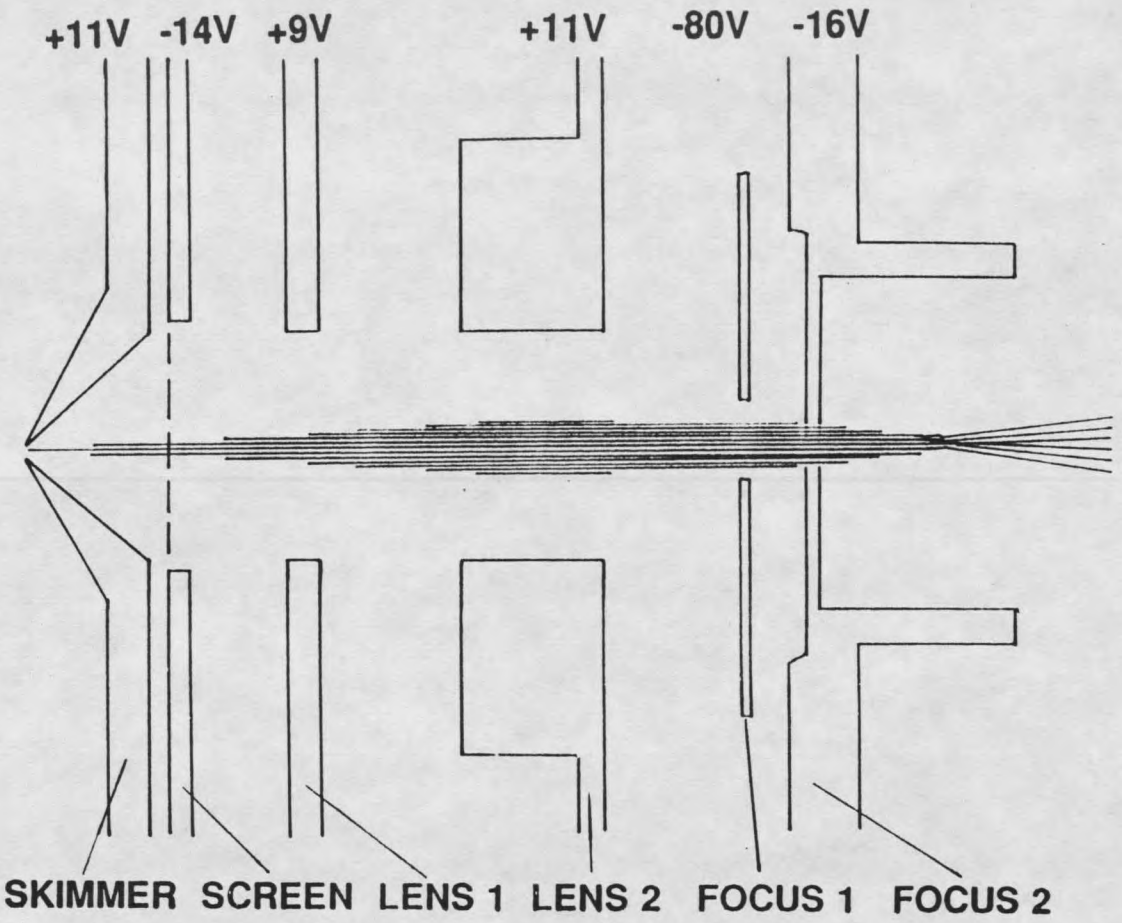

Figure 14. Ion trajectories simulated by SIMION program. Voltage distribution is shown in Table 2 and the initial ion energy is 10 eV.

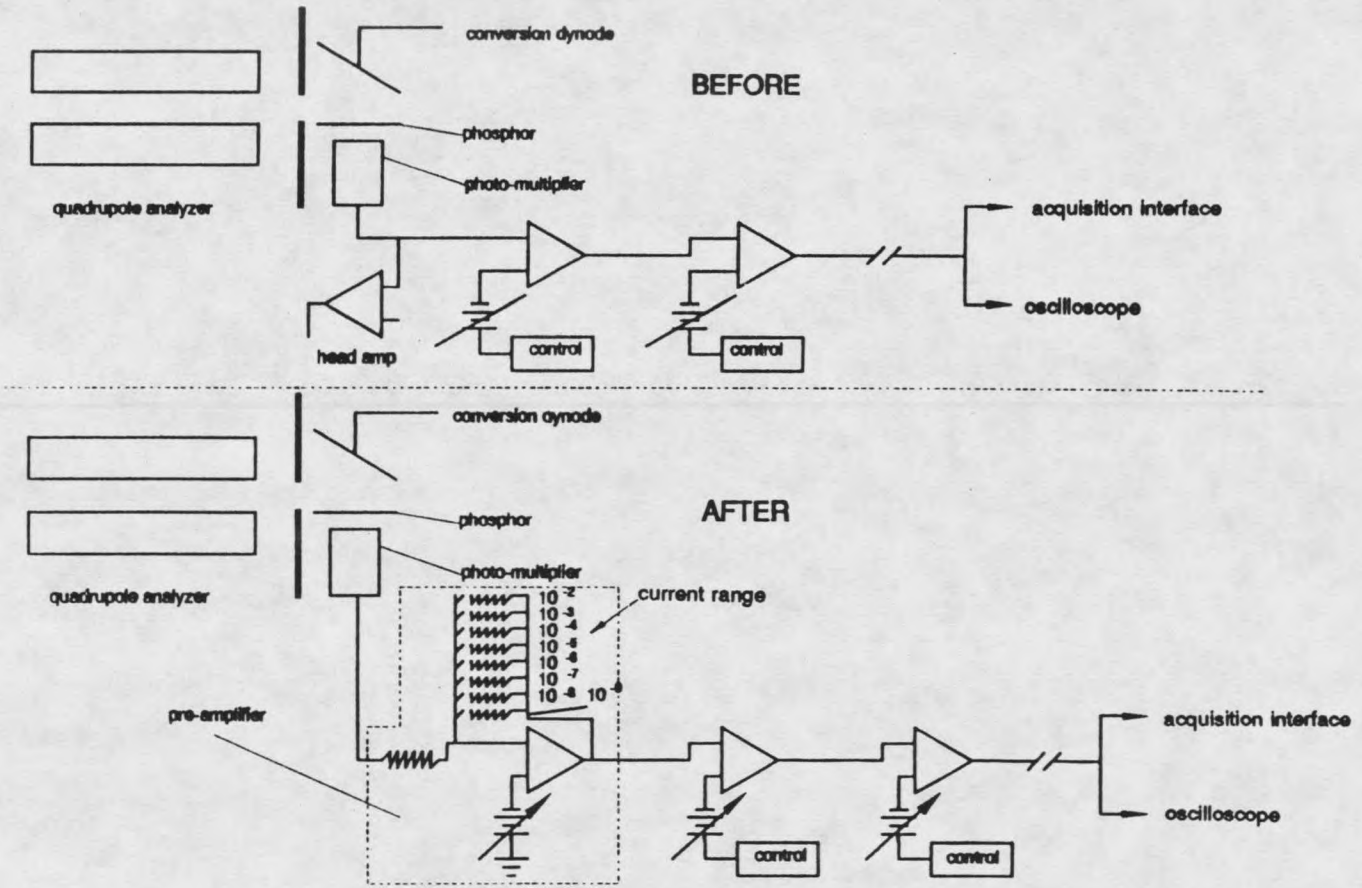

Figure 15. Methods of ion signal amplification before and after the applying of pre-amplifier.

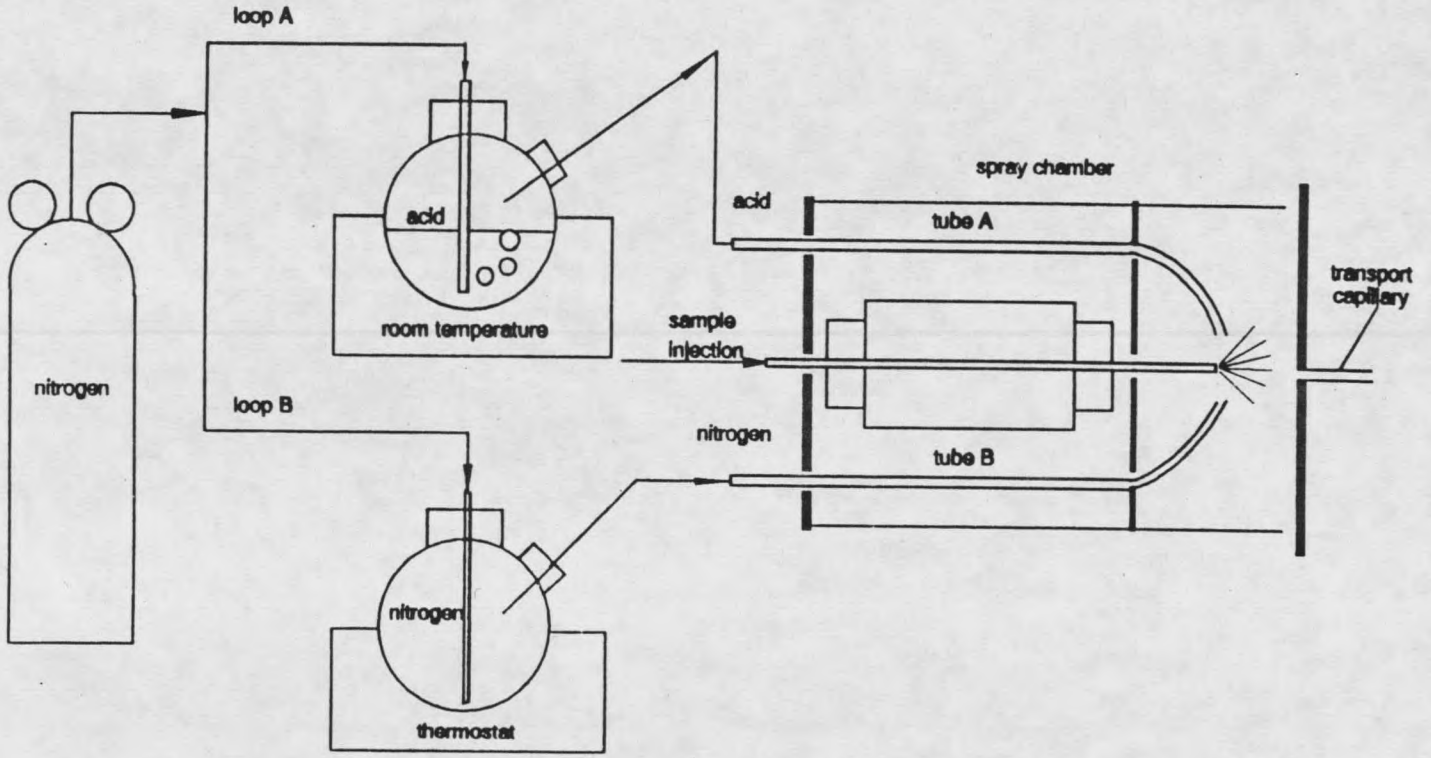

Figure 16. Equipment set up for acid and hot nitrogen additions to electrospray region.

RESULTS AND DISCUSSIONS

Ion Transport by Viscous Gas Flow Through Capillaries

Effect of Experimental Parameters

The entrance and transmitted currents were measured as described in Figures 6 and 7 (Experimental) and the effects of experimental conditions are presented here. Electrospray was produced using methanol solutions containing 10^{-4} M NaOAc and a flow rate of 4-6 μL/min. Ions were transferred through a ϕ1.47×250 mm glass capillary in these experiments.

(a) Electric field effect Electrospray ion currents were first measured as a function of the voltage applied to the spray needle (V_c) and the distance between the spray needle tip and the plane electrode (d_{ES}). Figure 17 (a) shows the entrance and transmitted currents as a function of spray voltage. Both I_{en} and I_{trans} gradually increase with increasing spray voltage V_c. The onset voltage for electrospray was 3700 V as shown in the figure. This is in good agreement with the calculated onset voltage for methanol, V_{on} = 3900V. When the spray voltage was above 7 kV, a corona discharge occurred and this caused the spray current to be unstable. Figure 17 (b) shows the entrance and transmitted currents as a function of spray needle tip to plane electrode distance. This distance was increased from 5 to 40 mm. It is

seen that the entrance current, I_{en}, decreased by a factor of ca. 50, where the transmitted current, I_{trans}, only decreased by a factor of 5.

In order to see the effect of the electric field, the transmitted ion current is plotted as a function of the electric field in Figure 18 using the same data as in Figure 17 (a) and (b). The electrical field, E_c, is affected by the voltage applied to the spray needle, V_c, and the distance between the spray needle tip and plane electrode, d_{ES}, and can be calculated from the equation

$$E_c = \frac{2V_c}{r_c \ln(\frac{4d}{r_c})} \qquad (18)$$

where r_c is the outer radius of the spray needle [91-93,97].

In Figure 18 (a), it is seen that I_{trans}, as a function of the electric field, follows the same trend whether the electrospray voltage or the spray needle tip to plane electrode distance is varied. However, at a constant and high electric field, the transmitted current was more unstable at a shorter needle to electrode distance. Figure 18 (b) shows the ion transmission efficiency (I_{trans}/I_{en}) as a function of the electric field using the same data as in Figure 18 (a). This efficiency is seen to reach a constant level for electric fields larger than 3500 kV/m. The transmitted efficiency is lower at a shorter needle to electrode distance.

It is possible that a corona discharge occurred when the needle to electrode distance (d_{ES}) was short and the electric field thus very high. Since droplets have slow diffusion, the ion transport efficiency for droplets is expected to be higher than for the "small" ions. Thus the charged species produced with a shorter needle to electrode distance may have been mainly the corona discharge ions which would explain the lower transmitted efficiency.

(b) Ion source temperature The temperature of the electrospray chamber (T_{sp}) is another parameter which affects the electrospray ionization and capillary ion transport. Literature results indicate that a slight heating allows aqueous solutions to be more readily electrosprayed, possibly due to the decrease of viscosity and surface tension of the solution. Figure 19 shows the entrance and transmitted ion currents as a function of spray chamber temperature from 25 °C to 75 °C. The spray needle tip to electrode distance was 20 mm and the spray voltage was 4.5 kV. Figure 19 shows that I_{trans} increased by more than three times from 25 °C to 75 °C and I_{en} increased by 1.4 times. It is possible that I_{en} increased only because the electrospray current increased.

(c) Solution flow rate Figure 20 (a) shows the entrance and transmitted currents as a function of solution flow rate from 0-7 μL/min. It is seen in the figure that I_{en} increased with increasing flow rate. This is in agreement with the dependence of electrospray current on solution flow rate (Q_l)

[87], according to following equation,

$$I_{sp}=KQ_l^{4/7}(\sigma E_c)^{3/7} \qquad (19)$$

where K is a constant, Q_l is the solution flow rate, σ is the threshold conductivity, and E_c is electric field at the needle tip. Assuming that the entrance current is proportional to the electrospray current, I_{en} can be estimated from eq. (19) as

$$I_{en}=K'Q_l^{4/7} \qquad (20)$$

where K′ is a constant that depends on σ and E_c.

Figure 20 (b) shows I_{en} calculated from eq. (20) and fitted to the experimental data. The agreement is seen to be very good.

Gas Throughput

Both glass and metal capillaries with different dimensions were used to study the effect of gas throughput on the ion currents. A series of ϕ2.1 mm metal capillaries with lengths of 2, 5, 7, 10, 15, 25, 35, and 50 ft were used to study the effect of capillary length on ion transport efficiency. A series of 250 mm long glass capillaries with ϕ0.97, ϕ1.47, ϕ1.84, and ϕ3.81 mm were used to study the effect of bore size on transport efficiency. Methanol solutions containing 10^{-4}

M NaOAc was electrosprayed at a flow rate of 4.44 μL/min at room temperature in these experiments. The spray voltage was 4.5 kV and the spray needle tip to plane electrode distance was 20 mm.

Metal Capillaries Figure 21 (a) shows the entrance, wall, and transmitted currents as a function of the gas throughput, from 0 to 11 L•atm/min, for a 2 foot long capillary. The entrance current at about 10 nA constitutes about 5% of the total electrospray current. It is seen that the entrance current shows a moderate increase from 9 to 16.5 nA. This is probably due to the ions being "sucked" into the region around the capillary entrance by the gas flow. The wall current at zero gas flow is seen to be not zero, but 0.2 pA. The reason is that some ions diffuse past the entrance electrode into the capillary through the stationary gas. However, as the gas flow increases, the wall current also increases to a maximum of 6 nA. The transmitted current, on the other hand, increases from 0 to 2.5 nA. The ion transmission efficiency increases from 0 to 29% with increasing throughput in Figure 21 (a).

Figure 21 (b) presents the same type of result as Figure 21 (a) but for a 50 foot capillary. The graphs look qualitatively very similar. (I_{en} is smaller because the electrospray discharge current was smaller.) As in Figure 21 (a), the wall current, I_{wall}, increases moderately and the transmitted current, I_{trans}, rapidly with increasing gas

throughput. A tendency towards saturation of I_{trans} is seen at the highest throughput. This was observed for all the longer capillaries and contrasts with the behavior for the shorter capillaries. The maximum transmission efficiency for the 50 ft capillary is only 0.5% compared to 21% for the 2 foot capillary at the same throughput.

Electrospray versus corona. With the electrospray ion source, it is always possible that charged droplets are responsible for much of the transmitted current. Therefore, a corona discharge ion source was used for comparison. The ion population in such a source consists of a distribution of hydrates of either a hydronium or possibly a protonated impurity ion. Figure 22 (a) shows the result for the ϕ2.1 mm, 2 foot metal capillary. Comparing with the electrospray experiment in Figure 21 (a), it is seen that the result is very similar except that the transmitted corona current is considerably smaller. Thus, the transmission efficiency through the 2 ft capillary at maximum throughput is about 7% for the corona versus 29% for the electrospray.

The results from different length capillaries were plotted in different ways. For example, Figure 23 (a) shows the transmitted current for several I.D. 2.1 mm metal capillaries with lengths between 2 and 50 feet and for gas throughput between 1 and 5 L$\cdot$atm/min. In this graph, the current is plotted versus the "1 atm" residence time defined through,

$$t^{o}_{res} = \frac{V_{capi}}{Q_{gas}} \qquad (21)$$

where V_{capi} is the capillary volume and Q_{gas} the gas flow rate. This would be the actual residence time for the ions in the capillary if there was no pressure drop through the capillary. It is noteworthy that in Figure 23 (a), all the ES data nearly fall on the same line even though a wide range of gas flow rates, and thus exit pressures, was used. Though, not obvious from the picture, there is a tendency for the transmission efficiency to decrease with increasing throughput at a constant, "1 atm" ion residence time.

Figure 23 (b) shows the same result as Figure 23 (a) except that a corona discharge was used instead of electrospray. A comparison between the figures shows that the transmitted current decreases much faster with residence time for the corona than for the electrospray.

Glass Capillaries. It was more difficult to obtain reproducible results with glass than with metal capillaries and teflon capillaries gave very unstable signals. Presumably this was due to charging of the insulating surfaces. With glass capillaries there is no wall current. Thus, only the entrance and the transmitted currents were recorded. Figure 24 (a) shows the transmitted current as a function of gas throughput for three glass capillaries with the same length, 250 mm, but with different diameters, 0.97, 1.47, and 1.84 mm.

The transmitted current is strongly depending on the gas throughput, similar to what was observed for metal capillaries, see Figure 21. It is remarkable, however, that all the data points fall nearly on the same line even though they were obtained with different I.D. capillaries. This result will be explained below. Figure 24 (b) shows I_{trans} from the same experiment as in Figure 24 (a) but plotted as a function of the "1 atm" ion residence time, eq. (21). Clearly, fewer ions survive in the narrower capillaries at the same t^0_{res}. There is an initial sharp decrease in I_{trans}. This may be due to ion losses at the capillary entrance. At longer times, however, the transmitted current is seen to decay exponentially with increasing ion residence time. Further, the decay is slower for the larger diameter capillaries.

The ion transmission efficiency of glass and metal capillaries were compared under identical conditions. For example, in one series of experiments, capillaries from 0.3 m to 3.0 m were used. With ion residence times from 10 to 140 ms, it was found that the transmitted current with glass consistently was about a factor of two lower than that for the metal capillary. In no case did we observe a higher transmitted current for a glass than for an equivalent metal capillary.

Mechanism of Ion Loss In Ion Transport Capillaries

The main objective of this work was to obtain an understanding of the nature of ion transport by viscous flow

through narrow capillaries. It was described in the Introduction that the mechanism was uncertain and much discussed among researchers. The first consideration must be that ions are lost through diffusion to the wall. However, as we will see shortly, simple diffusion calculations tend to show that significant ion transport through very long and narrow capillaries (for example, ϕ2.1mm×50ft) should not be possible. However, the experimental data described above shows that the transmitted current decreased exponentially with capillary length, which indicates that radial diffusion of ions in the capillary wall is occurring. Thus, ion loss by radial diffusion will be discussed first. The mathematical treatment of diffusion in cylindrical tubes was outlined in the Introduction.

For the fundamental diffusion mode in a infinitely long cylindrical tube, the ion density, as a function of position and time is given by eq. (9),

$$n(r,t) = \sum_{i=0}^{\infty} [G_i J_0(\alpha_i r) \cdot e^{-t/\tau_i}] \qquad (9)$$

The symbols G_i, J_0, and $\alpha_i r_0$ were explained in the Introduction. For an infinitely long cylindrical tube, the time decay constant, τ_1, is given by eq. (10),

$$\tau_1 = \frac{1}{D}\left(\frac{r_o}{2.405}\right)^2 \qquad (10)$$

The higher diffusion modes decay faster. For example, the lifetime of the second diffusion mode is 5.3 times shorter than that of the first.

Equations 9 and 10 are applicable to the diffusion of ions in a stationary gas in an infinitely long cylinder. The equations would still be valid if the gas was flowing through the tube and if the flow had a constant velocity throughout the tube cross section ("plug flow"). Now consider real gas flow through the transport capillary. The mean free path in the pressure range encountered in this study is much shorter than the radius of the capillaries. Therefore, the flow is viscous. As discussed in the Introduction, it is the Reynolds number, N_{Re}, that determines the type of flow inside the tube (eq. (11)). Under most conditions, the flow is laminar if the Reynolds number is below 2100 and is turbulent if the Reynolds number is above 4000. In the transition region, N_{Re} = 2100 and 4000, the flow may be either laminar or turbulent, depending upon the conditions at the entrance of the tube. For air flowing through the ϕ2.1 mm capillary, eq (11) predicts that the flow should be laminar for flow rates below 3 L/min and should be turbulent above 6 L/min. The treatment of ion diffusion loss is developed here only for laminar flow in order to simplify the analysis.

One of the problems with the application of equations 9 and 10 to capillary ion transport is that the pressure decreases significantly along the capillary under our experimental conditions. The diffusion constant, D, is known to be inversely proportional to pressure [39]. However, the gas velocity is also inversely proportional to the pressure. Therefore, the ion residence time in a segment of the capillary is proportional to the local pressure. Thus, according to equations 9 and 10, the increase in the diffusion constant will be exactly canceled by a decrease in the ion residence time. For this reason, the pressure drop in the capillary can be ignored when applying the diffusion equations, and the "1 atm" ion residence time, eq. (21), can be used.

In order to use eq. (9) to predict the extent of ion loss by diffusion in transport capillaries, the diffusion constant must be estimated. The mobilities of typical ions at 0 °C and 1 atm range from 0.5 $cm^2/V \cdot s$ and 3 $cm^2/V \cdot s$ [39]. By using Einstein's relation,

$$K = \frac{eD}{kT} \qquad (22)$$

where e is the charge of the ion, k is Boltzmann's constant and T is the absolute temperature, and adjusting to 30 °C and 660 torr, it is found that the diffusion constants range from 0.013 to 0.078 cm^2/s. The corresponding time constants, $\tau_{1/2}$,

for the 2.1 mm capillary are calculated from equation 10 and range from 146 to 24 ms. If we take a capillary length of 50 foot and a gas flow of 2 L/min, the "1 atm" ion residence time is 1.6 s. The expected transmission efficiency is given by,

$$T_{eff}=2^{-\frac{t_{res}}{\tau_{1/2}}} \tag{23}$$

and ranges from 5×10^{-4} to 8.5×10^{-21}. However, the observed transmission efficiency is higher, $T_{eff} = 3\times10^{-3}$. This could be explained by a rather moderate decrease of D to 0.010 cm^2/sec. This would result in a half-life of $\tau_{1/2}$ = 191 ms and in the observed $T_{eff} = 3\times10^{-3}$ for the 50 foot capillary.

In this calculation the effect of the parabolic flow profile on ion loss by diffusion was not considered. The velocity profile of laminar flow is known to be parabolic due to viscous drag. The local velocity is related to the average velocity by eq. (13), see Introduction,

$$U(r)=2\cdot U_{avg}[1-(\frac{r}{r_w})^2] \tag{24}$$

Because of the relatively high pressure, the velocity slip at the walls can be neglected [39]. The fact that the flow profile is parabolic means that equations 9 and 10 will not be correct. An improved treatment of diffusion in parabolic flow will now be presented.

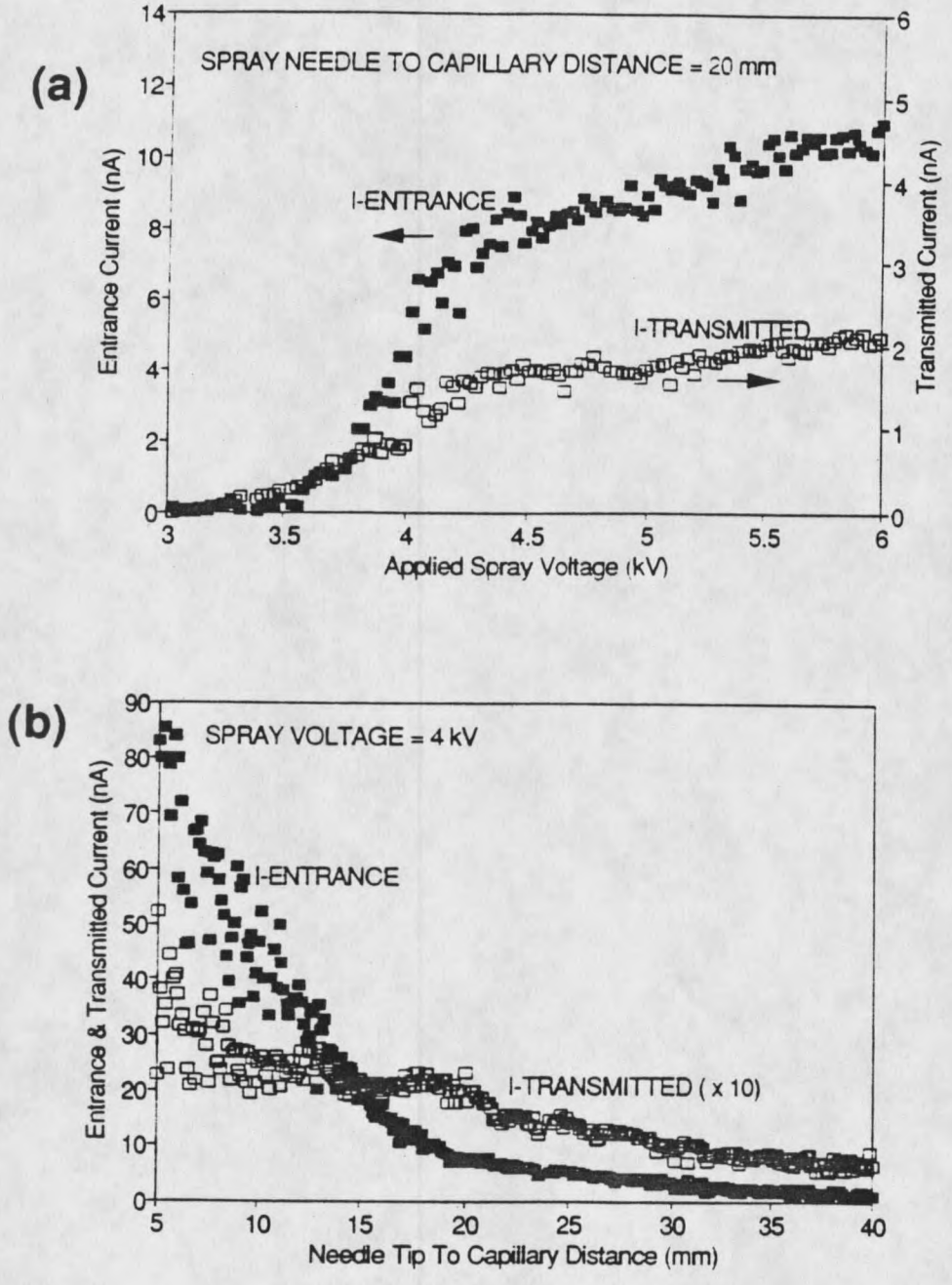

Figure 17. The entrance and transmitted ion currents affected by: (a) applied electrospray voltage and (b) distance between spray needle tip and transport capillary.

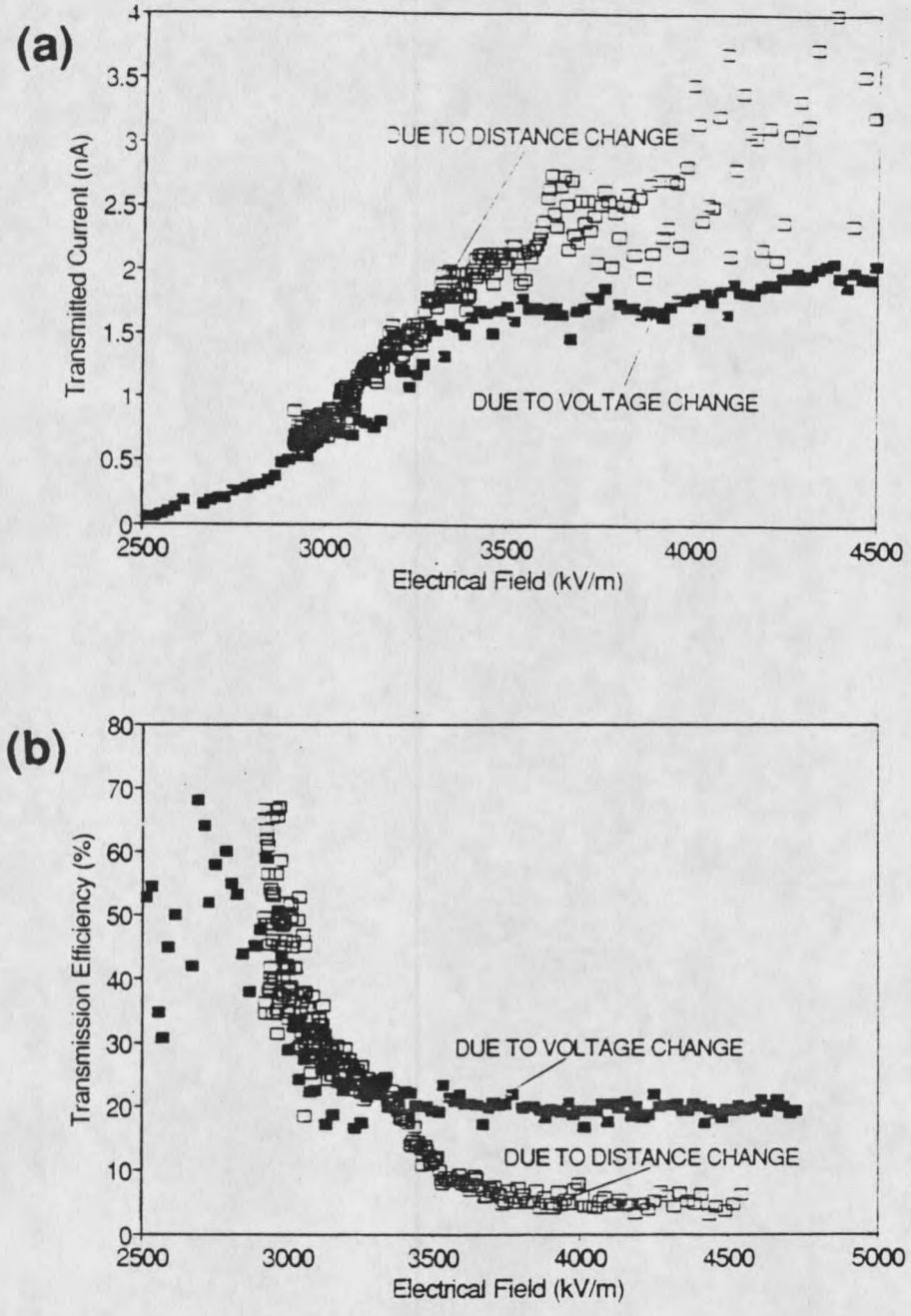

Figure 18. Ion currents affected by electrical field. (a) Transmitted current as a function of electrical field. (b) Transmitted efficiency (I-trans/I-entran) as a function of electrical field.

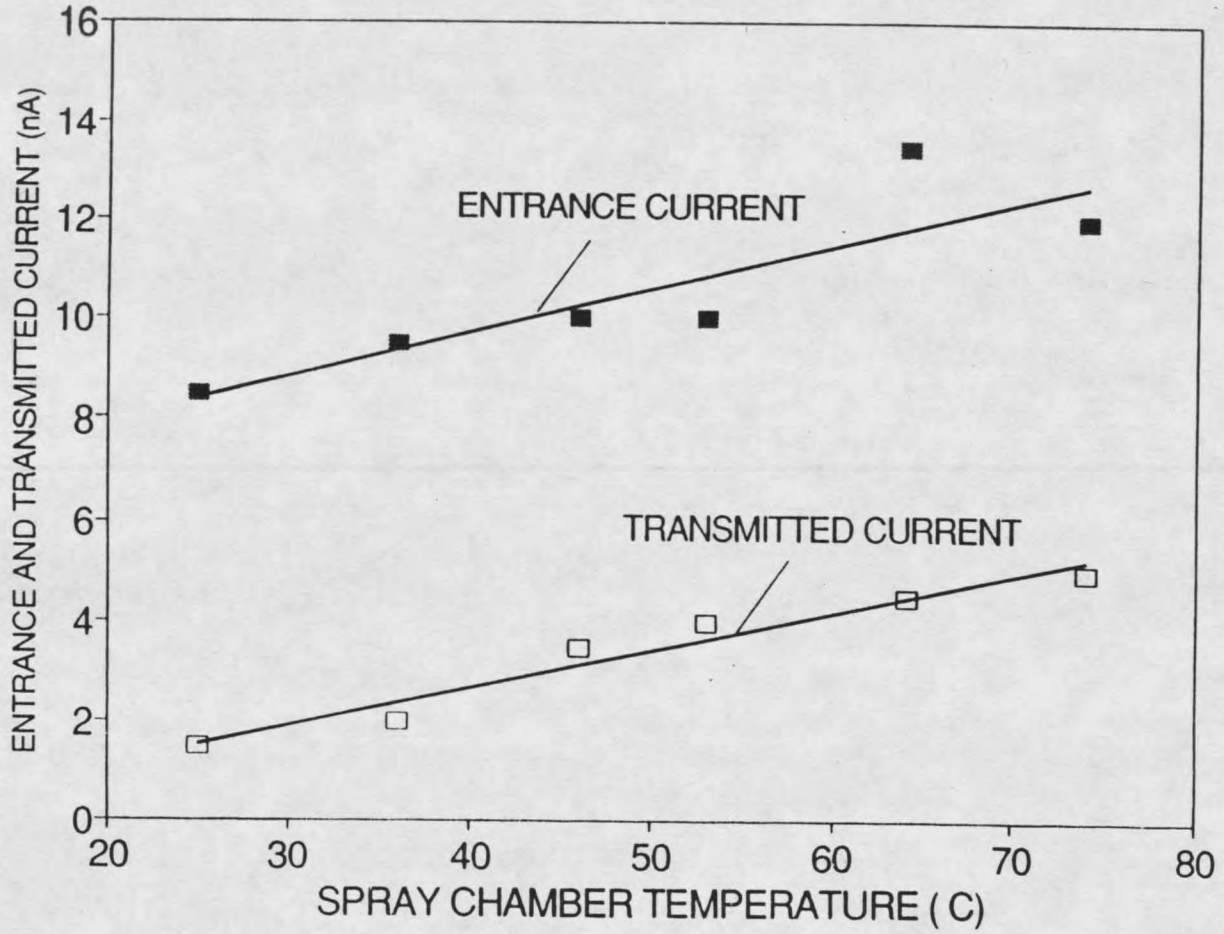

Figure 19. Entrance and transmitted currents affected by the spray chamber temperatures.

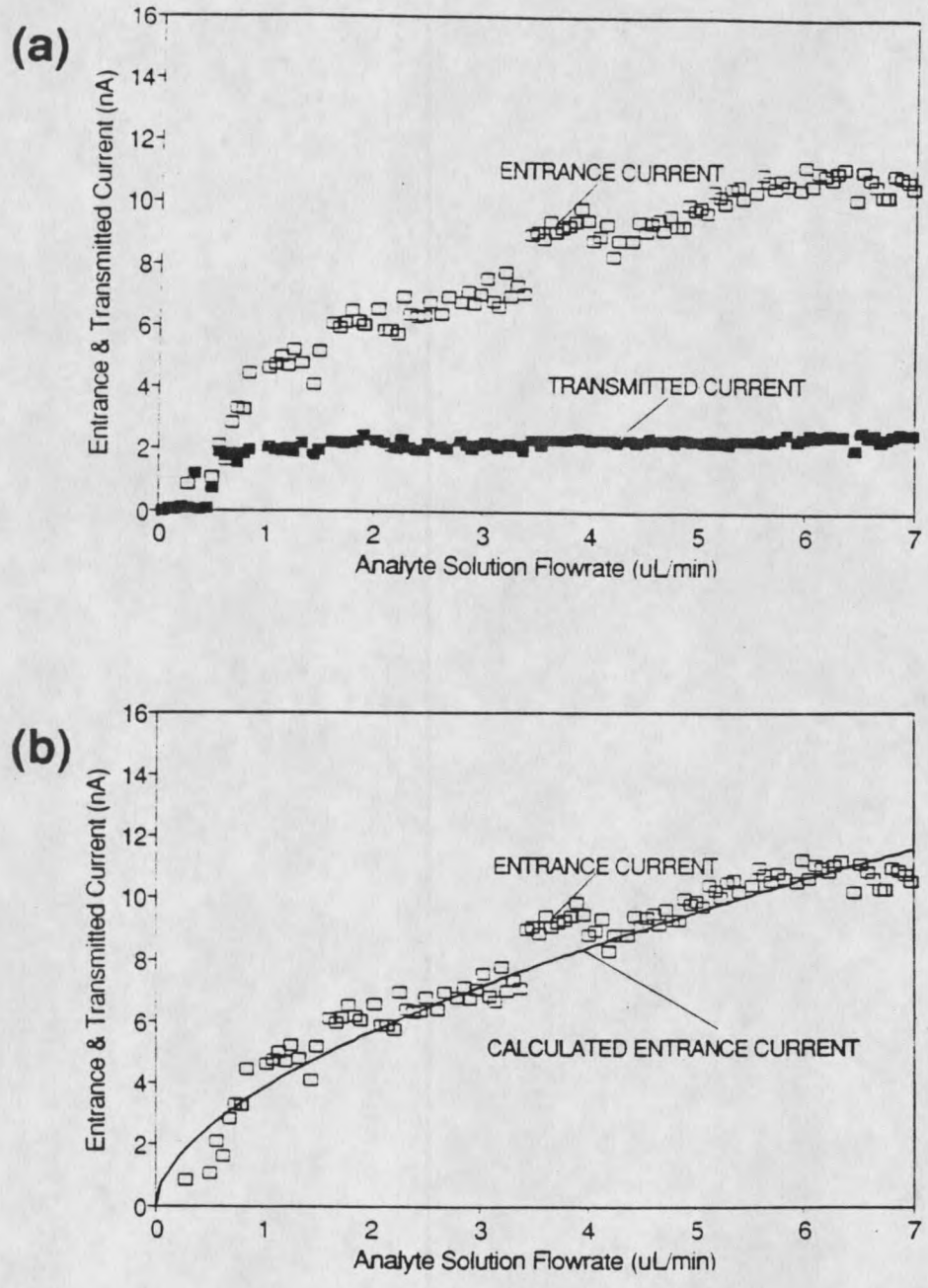

Figure 20. (a) Entrance and transmitted currents affected by the flow rate of analyte solution (µl/min). (b) Comparison of calculated entrance current and observed entrance current as a function of solution flow rate.

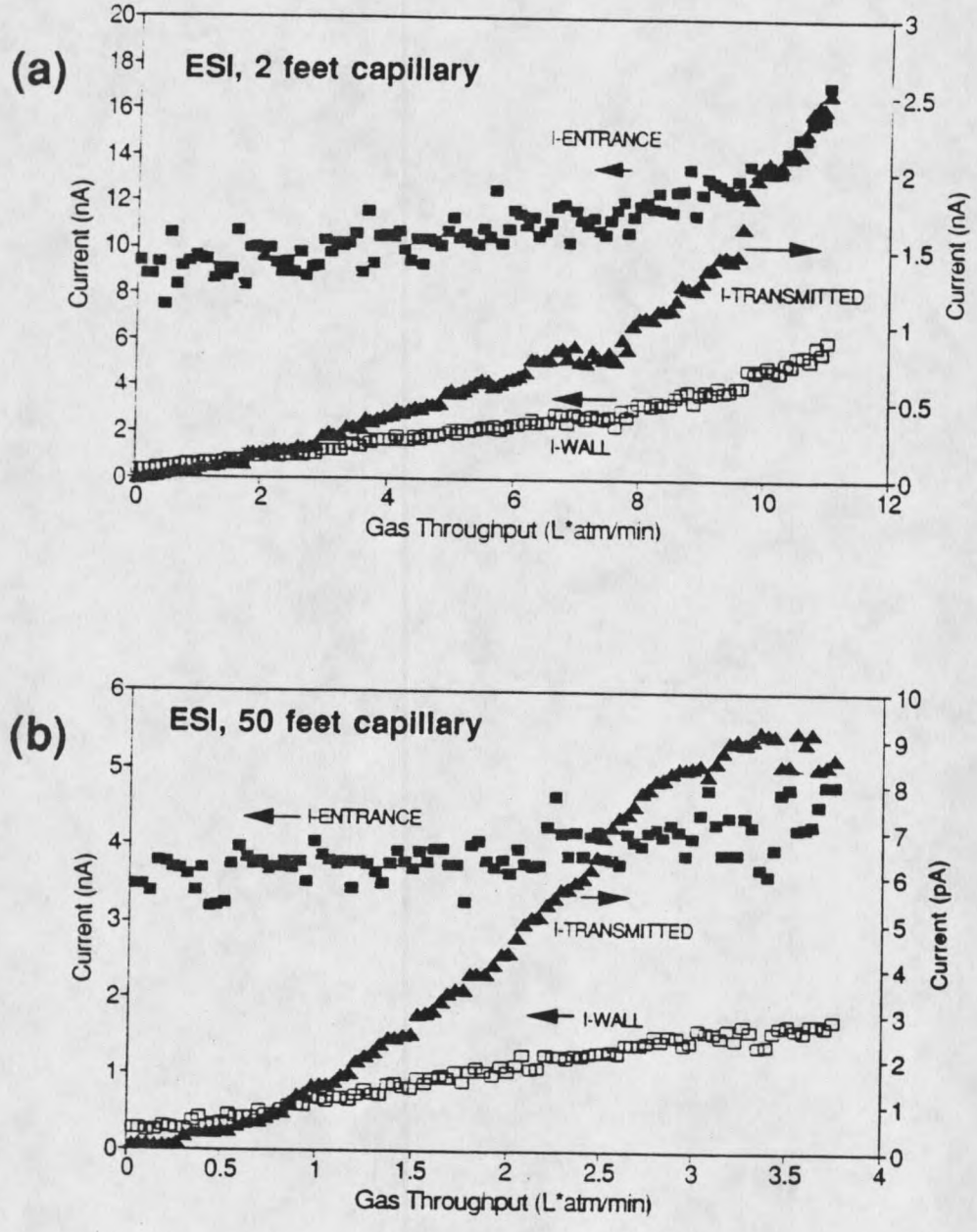

Figure 21. Entrance, wall, and transmitted currents as a function of gas throughput of metal capillaries. (a) For a metal capillary of 2 feet long. (b) For a metal capillary of 50 feet long.

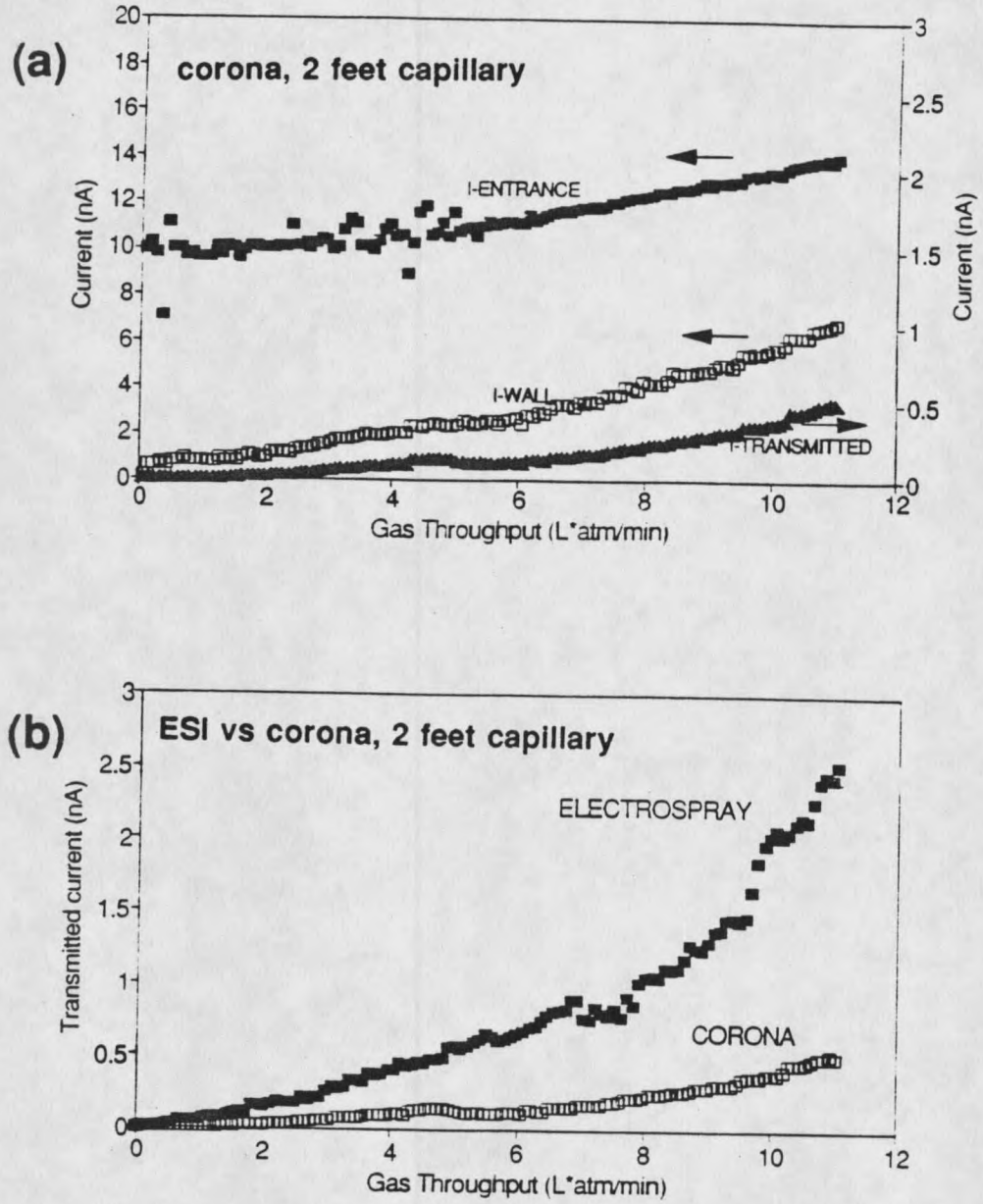

Figure 22. (a) Current measurements in corona discharge for a 2 feet metal capillary. (b) Transmitted current from electrospray versus corona for a 2 feet metal capillary.

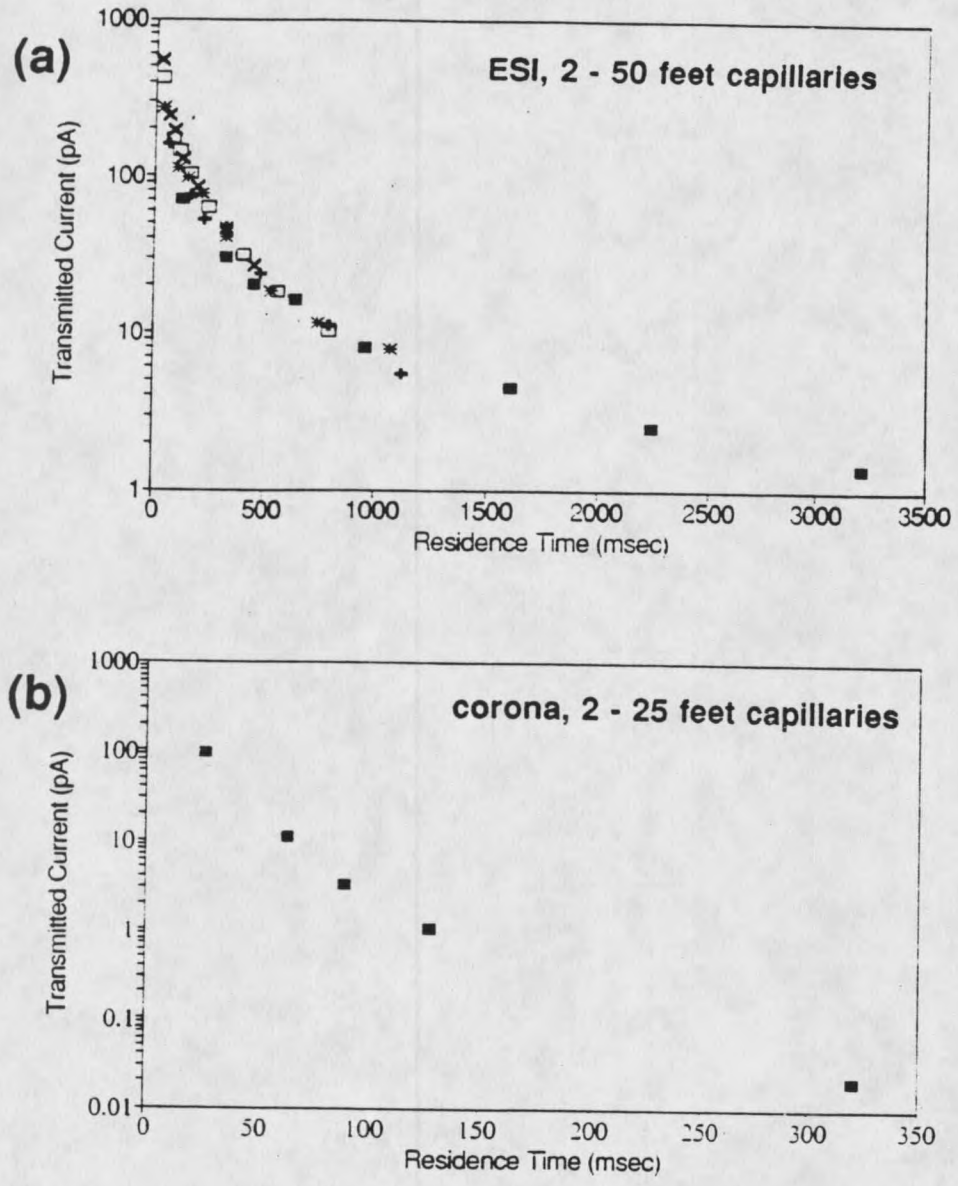

Figure 23. Transmitted current as a function of ion residence time through capillaries. (a) Transmitted current obtained from electrospray. Capillary length varied from 2 to 50 feet. (b) Transmitted current obtained from corona. Capillary length varied from 2 to 25 feet.

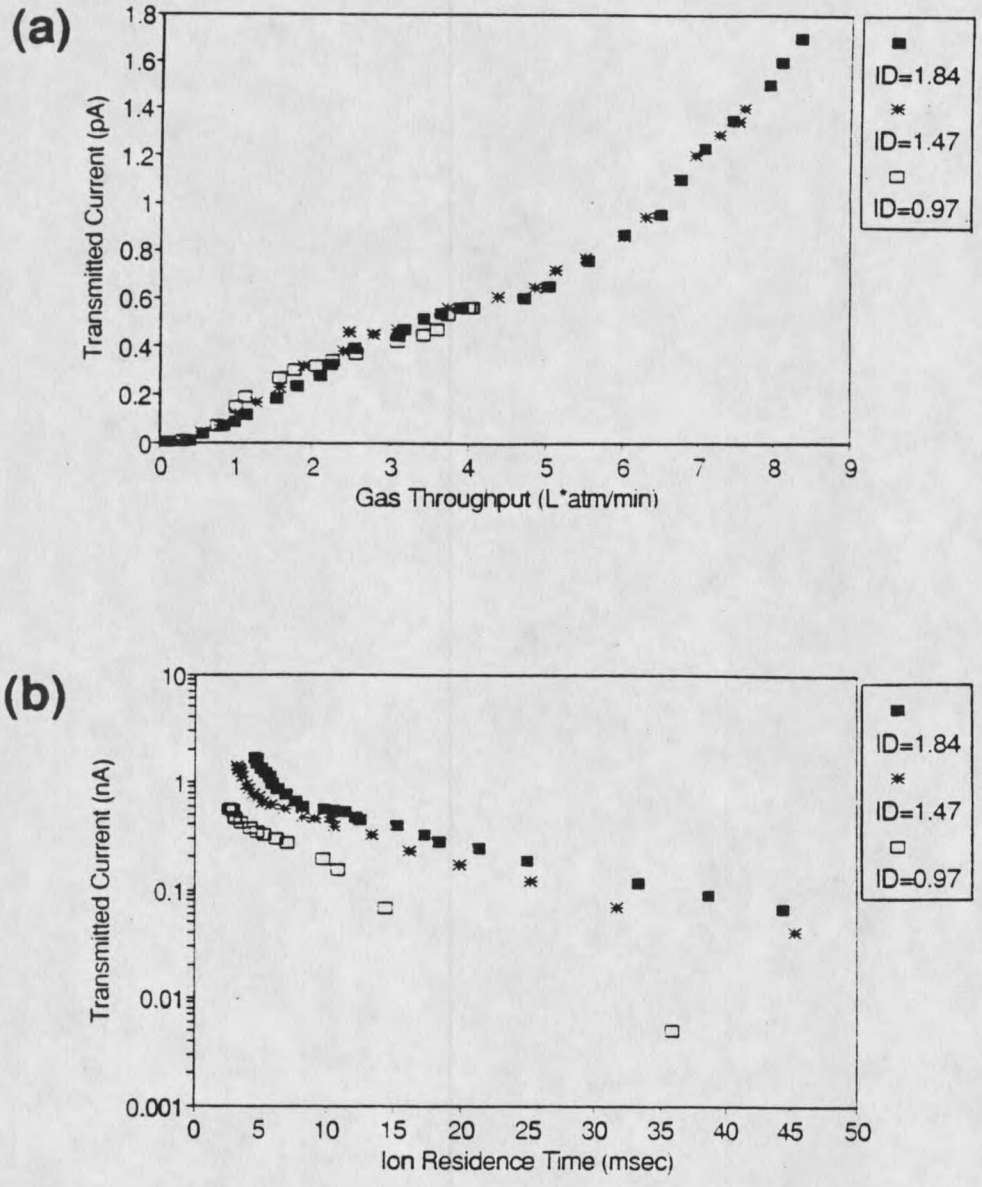

Figure 24. (a) Transmitted current through three glass capillaries with length of 250 mm and different I.D. as a function of gas through put of transport capillary. (b) Same data as in (a) but plotted versus the ion residence time.

Monte Carlo Simulations of Ion Diffusion in Transport Capillary

The parabolic velocity profile of the gas flow through a capillary complicates the solution to the diffusion problems. Indeed, there are no analytical solutions. Here, ion diffusion has been simulated using a Monte-Carlo method ("drunken sailor" method). In these simulations, one ion was followed at a time. First, the ion is injected into the entrance of the transport tube. The radial distance from the center was determined by a random number in such a way that a constant ion density in the gas was simulated. After injection, the ion is made to take a step, of length Δl, in a plane perpendicular to the direction of the gas flow, at fixed time intervals, Δt. The direction of the step in the plane was determined by a random number. At every step, the gas flow velocity was calculated such that the motion of the ion down the tube could be followed. As the ion either exited out of the tube or hit the wall, its position was recorded.

The diffusion constant, D, in the Monte Carlo simulation is obtained from [132],

$$D=\frac{\Delta l^2}{4\cdot\Delta t} \tag{25}$$

The accuracy of the simulation was tested by injecting the ions in the center of a wide tube and by using a gas flow velocity that was constant over the cross section of the tube

("plug" flow). Under such conditions, the ion number density is given by eq. (7),

$$n = \frac{S}{(4\pi Dt)^{(3/2)}} e^{-\frac{r^2}{4Dt}} \qquad (7)$$

where S is a constant [39]. The description of this equation was given in Introduction. Figure 25 shows a comparison between the radial number density calculated from equation 7 and the density obtained in a Monte Carlo simulation with 30,000 ions. The agreement is seen to be excellent.

The Monte Carlo program was next used to study the effect of parabolic flow on the diffusional loss of ions. Figure 26 shows a comparison between the transmitted current for parabolic flow (a), and for "plug" flow (d) for an ϕ2.1 mm capillary as a function of the "1 atm" residence time. The diffusion constant was 0.01 cm^2/s in both cases. The initial fast decrease in the ion signal is due to the rapid decay of the higher diffusion modes. However, after a (parabolic flow-modified) fundamental diffusion mode has been established, the transmitted current decreases exponentially with time (or capillary length). The decay time for the "plug" flow simulation was 0.198 s which is in excellent agreement with the 0.191 s calculated from equation 10. In contrast, the decay time for the parabolic flow profile simulation is 0.33 s. Thus, the effect of the parabolic flow is to nearly double the half-life of the ions in the capillary. For a long

capillary with many half-lives, the effect on the transmitted current is dramatic.

For the long, 50 feet capillary, we saw that 0.3% of the ions that entered the tube was transmitted at a gas flow rate of 2 L/min, Figure 21 (b). After correcting for the effect of parabolic flow, it is now seen that this is the transmission efficiency expected for ions with a diffusion constant of $D=0.02\ cm^2/s$. This is certainly within the range of typical diffusion constants for gas-phase ions [39].

It is clear from the discussion above that all our results can be explained by assuming that ions are lost primarily by diffusion to the walls as they pass through the capillary. For example, it was observed that the transmitted current was independent of capillary radius (at the same throughput and capillary length), see Figure 24 (a). Now, the transmitted current is proportional to $\exp(-t/\tau_i)$, see eq. (9). In turn, the decay time, τ_i, is proportional to the square of the capillary radius, eq. (10). Also, the residence time, t, is proportional to the square of the radius. These two effects cancel, which explains the result in Figure 24 (a) and 24 (b). It is interesting that this holds for glass capillaries, where (presumably) the wall current is zero.

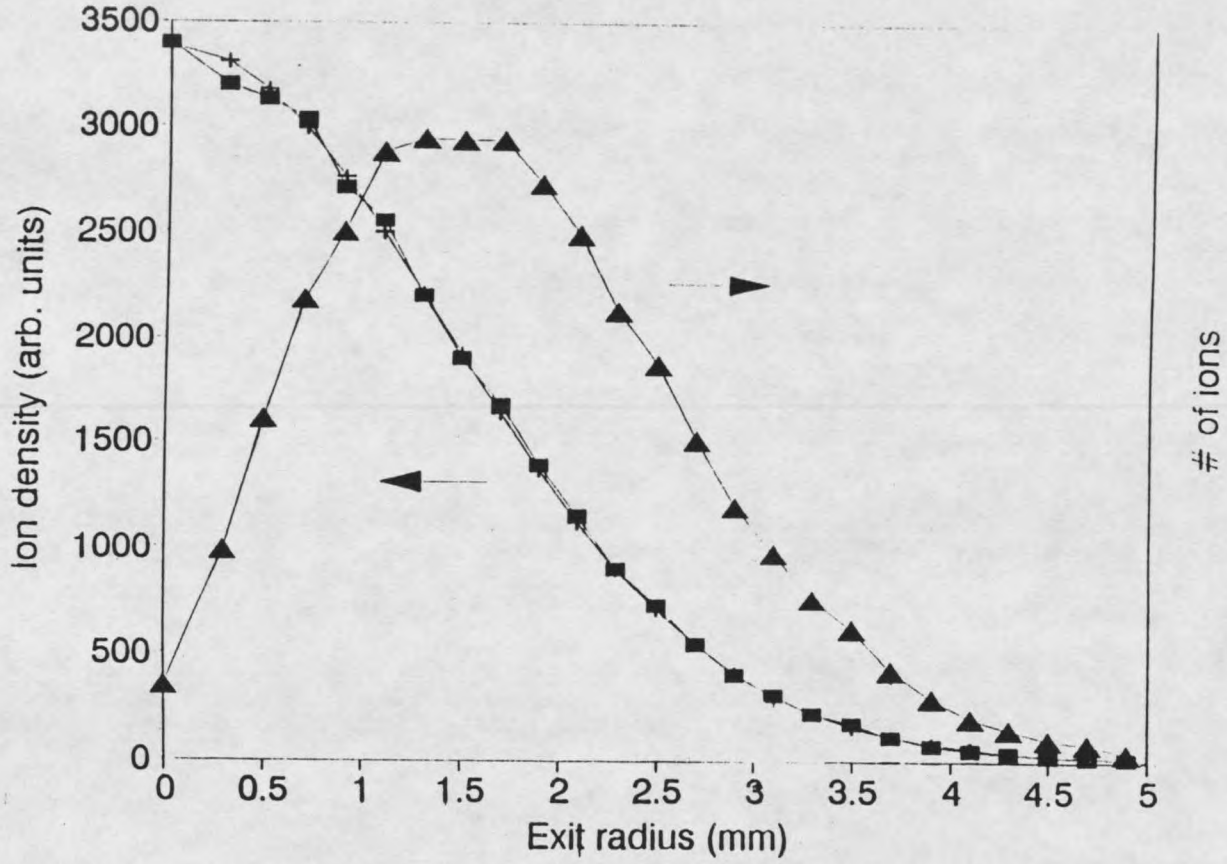

Figure 25. Calculated radial ion density distributions: (+) Monte Carlo simulation; (■) analytical solution, eq. ; (▲) # of ions. The following parameters were used: Δl=0.1 mm; Δt=0.0005 sec; and D=0.05 cm2/s. Number of simulated ions was 30,000.

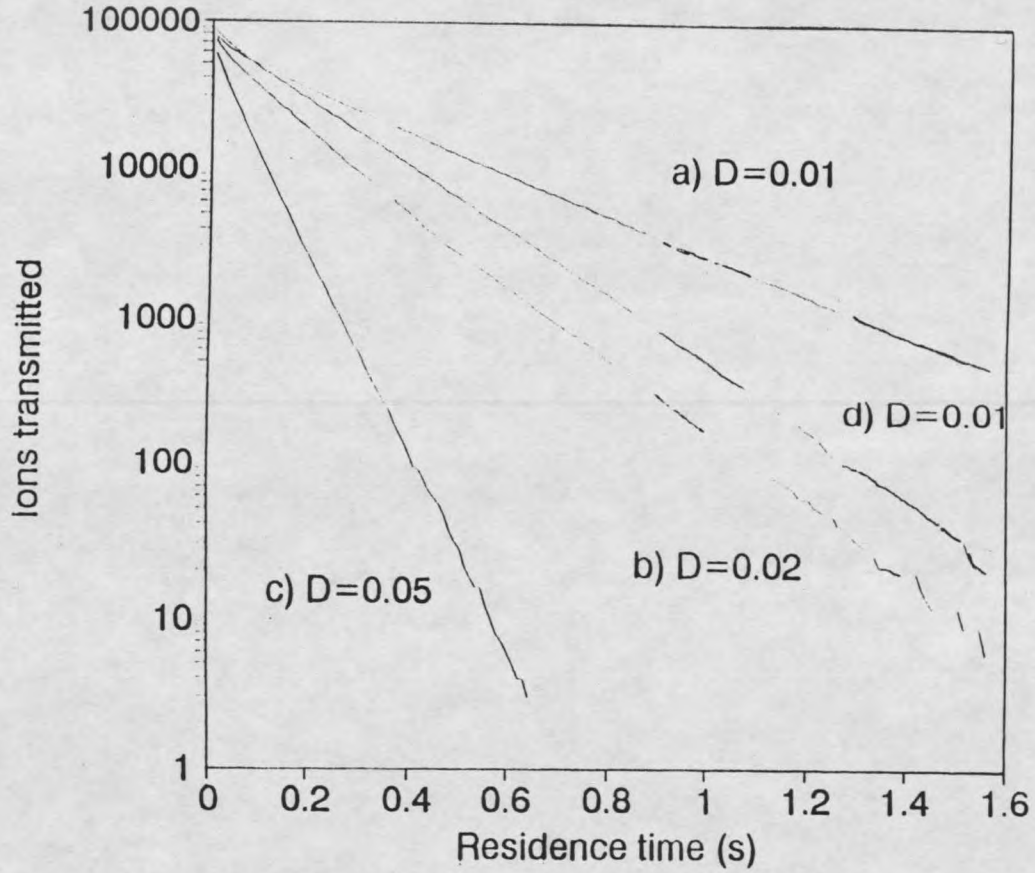

Figure 26. Monte Carlo result for transmitted current as a function of the normalized ion residence time (eq.) in the transport capillary. a-c) parabolic flow profile; d) plug flow profile.

Characterization of Proteins by ESI/MS

Electrospray ionization mass spectrometry has been found to be very useful for the analysis of large proteins. A very important factor is that the multiple charging of large proteins brings the m/z ratio down to values that can be measured on conventional mass spectrometer. Also, electrospray ionization is a soft ionization method that provides intact protein ions. In this project, proteins with molecular weight up to 40,000 Da have been electrosprayed.

Table 6: Protein solution conditions in ESI/MS.

protein	solvent	pH	concentration	flowrate μL/min	moles used[a] $\times 10^{-12}$
Myoglobin	H_2O/MeOH/HOAc	3	10 μM	1	5
Cytochrome c	H_2O/MeOH	5.5	40 μM	1.5	30
Avidin	H_2O/MeOH/HOAc	3.5	20 μM	1.5	30
Trypsin	H_2O/MeOH/HOAc	2.5	20 μM	1.5	30
α-Chymotrypsin	H_2O	4.0	40 μM	1.0	20
Carbonic Anhydrase	H_2O/MeOH/HOAc	4.0	20 μM	1.5	15
Alcohol Dehydrogenase	H_2O/MeOH/HOAc	3.5	12 μM	1.5	10

[a] Moles of a protein consumed to collect an ESI mass spectrum.

In the initial experiments with the electorspray mass spectrometer (ESI/MS), which was described in the Experimental section, mass spectra were obtained from 9 different proteins with molecular weights from 12,300 Da to almost 40,000 Da.

Table 6 contains a summary of the experimental conditions used. The protein samples were dissolved in mixtures of water and methanol, or in some cases, pure water. In order to achieve sufficient protonation in electrospray, it was often necessary to lower the solution pH by addition of small quantities of acetic acid (HOAc). Solutions with protein concentrations ranging from 10 to 40 μM were injected at flow rates from 0.5 to 1.5 μL/min.

Analysis of Mass Spectra

The electrospray mass spectra of proteins are characterized by a series of multiply protonated ions $(M+nH)^{n+}$. Assuming that the mass of the electrically neutral protein is M_r, the mass to charge ratio of these ions is $(M_r+m_a i)/i$, where i (i=1,2,3,...., etc.) is the charge of the ion, and m_a is the mass of the cations (protons) that impart the total charge i to the ion via cation addition [101,108]. The mass to charge ratio separation between successive peaks is not constant, and the mass spectrum has an appearance of peaks being more closely spaced at lower m/z ratios. The number of charges per ion has been indicated on each spectrum. The need for low pH in the sample solution, along with the results obtained from peptides, strongly support the assumption that protons are the most likely charge carrier in these experiments. The molecular weight of each protein was determined by the averaging algorithm method [100] that was

discussed in the Introduction section.

Horse Myoglobin. Myoglobin is an oxygen-carrying protein found in muscle, where it serves as an oxygen reserve and facilitates oxygen diffusion through the cell. Myoglobin has two molecular components, a single polypeptide chain containing 153 amino acid residues and a heme group, an iron-containing biomolecule [101,102]. Myoglobin from equine skeletal muscle has 23 acidic amino acids including the carboxyl terminus and 33 basic amino acids including the amino terminus (Lys, Arg, His, and N-terminus). Myoglobin can be denatured and caused to unfold by subjecting it to low pH. Columbic repulsions among the protonated centers lead to the destabilization and unfolding of the compact native conformation. Buried amino acids then become available for protonation. When pH is low enough, myoglobin is believed to be totally protonated, as a result of protein unfolding.

Figure 27 shows the electrospray mass spectrum of myoglobin. The protein was dissolved in a 50:50 water/methanol solvent and the pH was adjusted to 3 by addition of acetic acid. Under these conditions the protein is denatured. The number of charges on each peak ranges from 10^+ to 22^+, with the most abundant ions having charge 16^+. Excellent signal-to-noise is observed as 5 pmol of the protein was consumed. The observed average molecular weight was 16,954, which is 0.02% higher than the molecular weight calculated from the myoglobin sequence.

Cytochrome c. Horse heart cytochrome c has 24 basic amino acids (lysine, arginine, histidine, and α- amino terminus) and 15 acidic amino acids [115]. It is believed that the iron in the heme group is coordinated to a histidine and methionine residue [101]. Since the heme group is covalently linked to the protein through cysteine residues, the heme remains bonded to cytochrome c even at low pH and in the presence of methanol.

Figure 28 shows the electrospray mass spectrum of horse heart cytochrome c. The protein was dissolved in a 50:50 water/methanol solvent and pH was about 5 without any acid addition. The charge distribution appears to be a bimodal. The first charge distribution ranges form 7^+ to 9^+. These rather low charges is attributed to cytochrome c being in the native conformation in which the protein is tightly folded and fewer amino acids are available for protonation. The second distribution has charge numbers from 9^+ to 16^+, with 12^+ being the most abundant. This charge distribution is probably due to the denatured conformation, where additional basic amino acids are available for protonation. The cytochrome c spectrum has an excellent signal-to-noise ratio. The observed average molecular weight is 12,365, which is 0.01% higher than the molecular weight calculated from the amino acid sequence.

Avidin. Raw egg white contains a glycoprotein, avidin, that combines with biotin ($K_{assoc.} = 10^{15}$) and prevents biotin absorption from intestine. Avidin has a molecular weight of

about 70,000 and consists of four identical subunits. Each subunit has 128 amino acid residues with known sequence and can bind one molecule of biotin [117]. The specific binding is abolished by heat and other denaturing influences. The avidin subunit has 18 basic amino acids: 1 histidine, 9 lysines, and 8 arginines.

Figure 29 shows the electrospray mass spectrum of avidin from egg white. The protein was dissolved in a 50/50 water/methanol solvent and the pH was adjusted to 3.5 with the addition of HOAc. Avidin assumably denatured under these conditions. The charge state of the ions ranges from 9^+ to 15^+, with 13^+ being the most abundant. The observed molecular weight determined from the spectrum is 14,571.3, which is in agreement with the weight of avidin (14,332) plus biotin (244.3). This constitutes our first example of a non-covalent complex that survived in the electrospray process. The sensitivity, however, was low and more than 30 pmol was needed to collect this spectrum.

Trypsin. Trypsin, one of the digestive enzymes, is a serine protease. Bovine trypsin consists of 223 residues and catalyzes the hydrolysis of peptide bonds after the basic amino acids of lysine and arginine. Trypsin is formed in the small intestine by the activation of trypsinogen, which cleaves an amino-terminal hexapeptide from the surface of trypsinogen. Trypsin consists of 19 basic amino acids [116].

Figure 30 shows the electrospray mass spectra of trypsin

from bovine pancreas. For Figure 30 (a), the protein was dissolved in a 50/50 water/methanol mixture and pH was adjusted to 2.5 by adding acetic acid. The charge distribution ranges from 13^+ to 19^+, with 17^+ being the most abundant. The high charge states suggest that the protein was in a denatured conformation. This seems very likely because of the methanol content and the low pH. In contrast, Figure 30 (b) shows the trypsin spectrum with pure water and no added acid. The lower charge states can be explained if the trypsin remained in the native conformation. The intensity of bovine trypsin was relatively low and 30 pmol was needed to record the spectrum in Figure 30 (a). The observed average molecular weight is 23,292, which is 0.004% lower than the molecular weight calculated from the amino acid sequence.

Chymotrypsin. Like trypsin, chymotrypsin is a serine protease. The active enzyme, α-chymotrypsin, is formed from chymotrypsinogen A. It has a molecular weight of 25,234 Da and consists of three polypeptide chains that are covalently linked by five disulfide bridges. The native molecule is roughly ellipsoidal [102]. Bovine α-chymotrypsin has 19 basic amino acids including 3 arginines, 14 lysines, 2 histidines, as well as 3 N-termini.

Figure 31 shows the electrospray mass spectrum of bovine α-chymotrypsin. The protein was dissolved in pure water and the pH was about 4.0 without any acid addition. The charge states range from below 14^+ to 22^+, with the most abundant ion

being 18^+. The high charge state may indicate that the protein was not in its native conformation. The explanation could be that the original chymotrypsin sample was subjected to a low pH, since 0.01 N HCl is used in the pretreatment of the protein to eliminate autolysis products and low molecular weight contaminants. Twenty pmol of protein was needed to collect the ESI spectrum and the resulting peak intensity was very good. The observed average molecular weight was 25,230, an error of 0.01% relative to the molecular weight calculated from the amino acid sequence.

Carbonic anhydrase. Carbonic anhydrase is a zinc-containing enzyme which catalyzes the reversible reaction between carbon dioxide and water to form carbonic acid (in blood). Chemical and crystallographic studies show that the zinc atom, which is essential to the reaction, is located in a hydrophobic cavity, which is probably also the site of substrate binding. The protein has 264 residues of known sequence and a molecular weight of 29,025 Da. Bovine carbonic anhydrase has 37 basic amino acids: 11 histidines, 19 lysins, and 7 arginines [116], as well as N-terminus.

Figure 32 shows the electrospray mass spectrum of bovine carbonic anhydrase. The protein was dissolved in 50:50 water/methanol mixture and pH was adjusted to 4 with the addition of HOAc. The charge states of the protein range from 18^+ to 40^+, with 29^+ being the most abundant. Only 15 pmol of protein was used for this spectrum and the signal-to-noise

ratio is seen to be very good. The observed average molecular weight is 29,022, which is 0.01% lower than the molecular weight calculated from the protein sequence. The high charge state distribution indicates that the protein is denatured under the conditions used.

Alcohol dehydrogenase. Alcohol dehydrogenase occurs in a wide variety of organisms including plants, animals, and yeasts. It is a cytoplasmic, zinc-containing enzyme. Together with the coenzyme nicotinamide adenine dinucleotide (NAD), the protein reversibly catalyzes the conversion of organic alcohols to ketones or aldehydes [119]. The active enzyme molecule from horse liver is a dimmer with two chains and with four zinc atoms which are involved in the catalytic activity. The enzyme from yeast has four subunits with an approximate total molecular weight 141,000. Yeast alcohol dehydrogenase can be deaggregated into subunits that are enzymically inert [120]. Each subunit in yeast alcohol dehydrogenase has 347 residues and contains 42 basic amino acids: 10 histidines, 24 lysins, and 8 arginines.

The electrospray mass spectrum of yeast alcohol dehydrogenase is shown in Figure 33. The protein was dissolved in 50:50 water/methanol and pH was adjusted to 3.5 with the addition of HOAc. The protein is assumably denatured under these condition and deaggregated into subunits. The charge distribution of the protein range from 21^+ to 43^+, with 34^+ being the most abundant. The observed molecular weight is

36,733, which is 0.04% lower than the subunit molecular weight calculated from the protein sequence. The signal-to-noise ratio was excellent considering that only 10 pmol of protein were used to record the spectrum.

Mass Measurement Accuracy and Sensitivity

Table 7 contains a summary of the calculated and measured molecular weights for the proteins discussed above. No special effort was made to increase the accuracy of the ESI molecular weight measurement. The errors range from 0.01% to 0.04%. Presumably, the accuracy could be improved by using mass calibration. The mass accuracy for proteins with ESI/MS is at least 5 times higher than that with PD/MS [121]. The accuracy obtained by ESI/quadruple mass spectrometer is comparable to what has been reported [23,100,121].

Approximately 5 - 30 pmol of protein was consumed to obtain the ESI mass spectra of the proteins studied here. No attempt was made to determine the detection limits. In general, ESI sensitivity depends on the availability of basic sites of the protein, the solution pH, the presence of impurities, and on the composition of solvents.

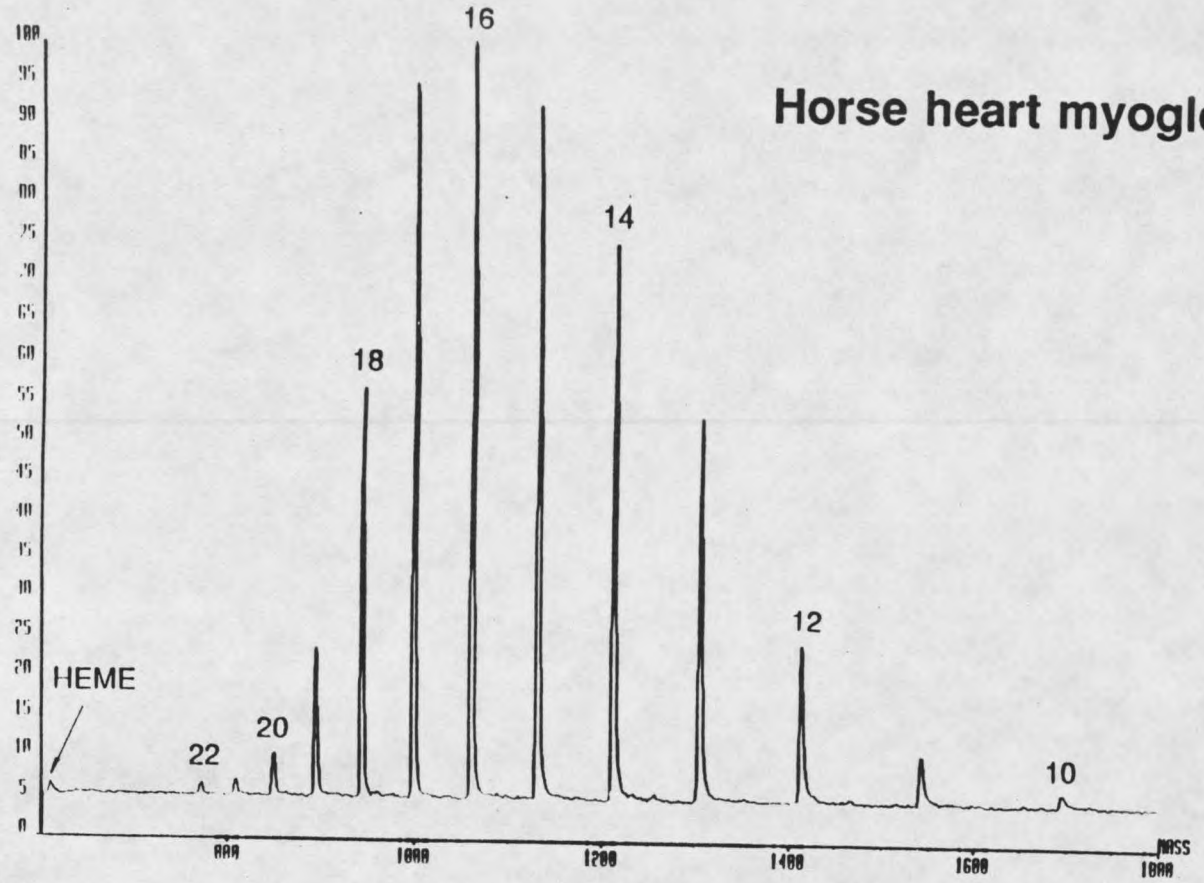

Figure 27. Electrospray mass spectrum of horse myoglobin in 50/50 water/methanol mixture. MW is 16,951 Da.

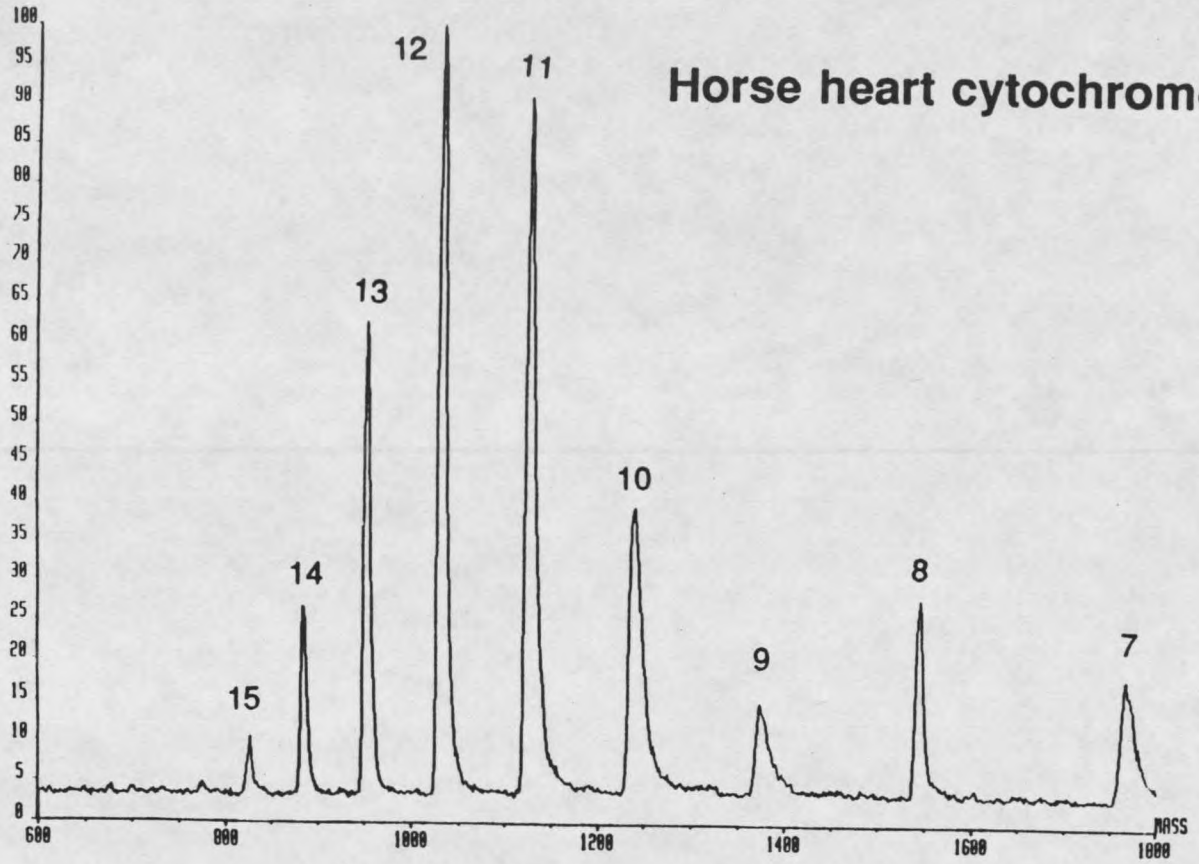

Figure 28. Electrospray mass spectrum of horse heart cytochrome c in 50/50 water/methanol mixture. MW is 12,360 Da.

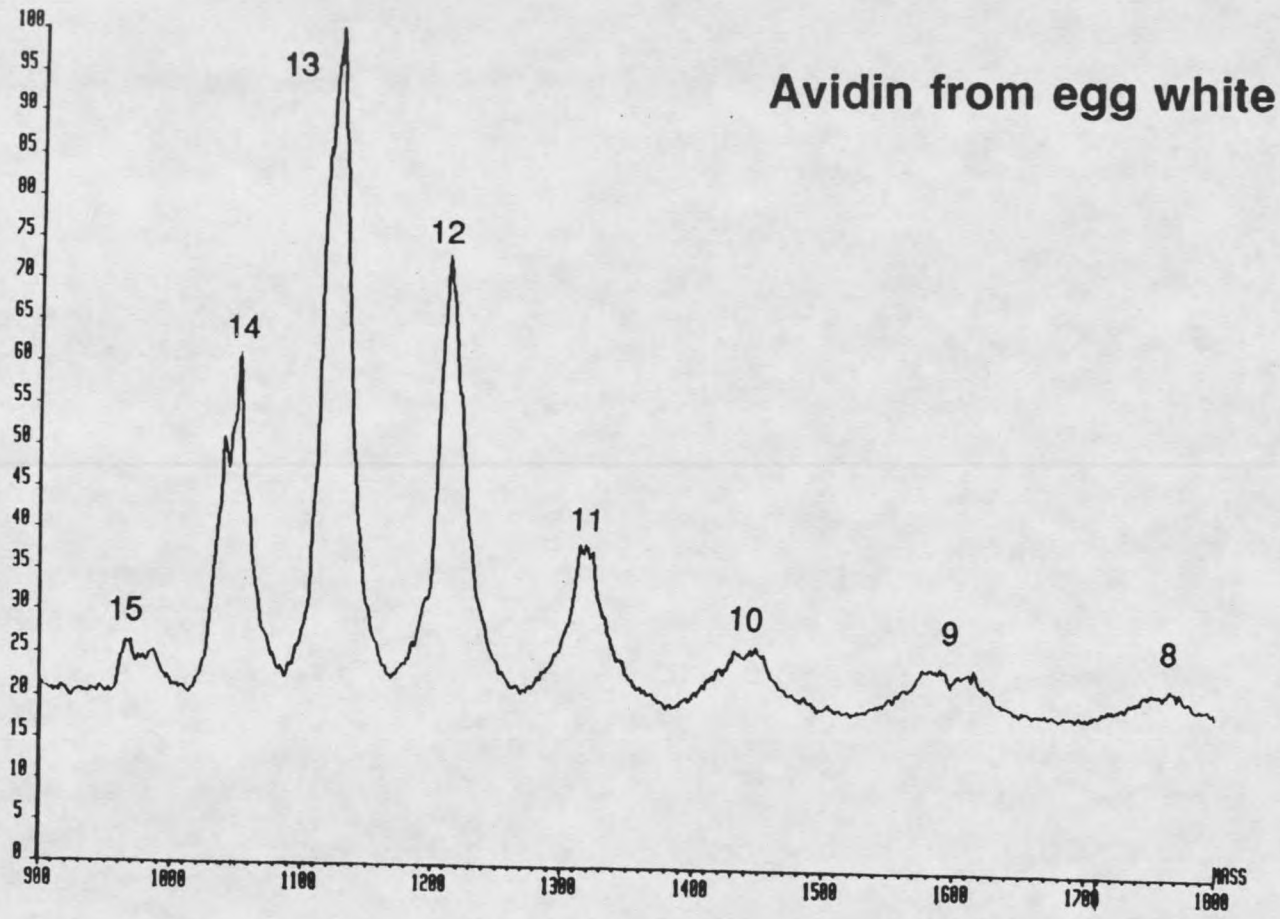

Figure 29. Electrospray mass spectrum of avidin from egg white in 50/50 water/methanol mixture. MW is 14,332 Da.

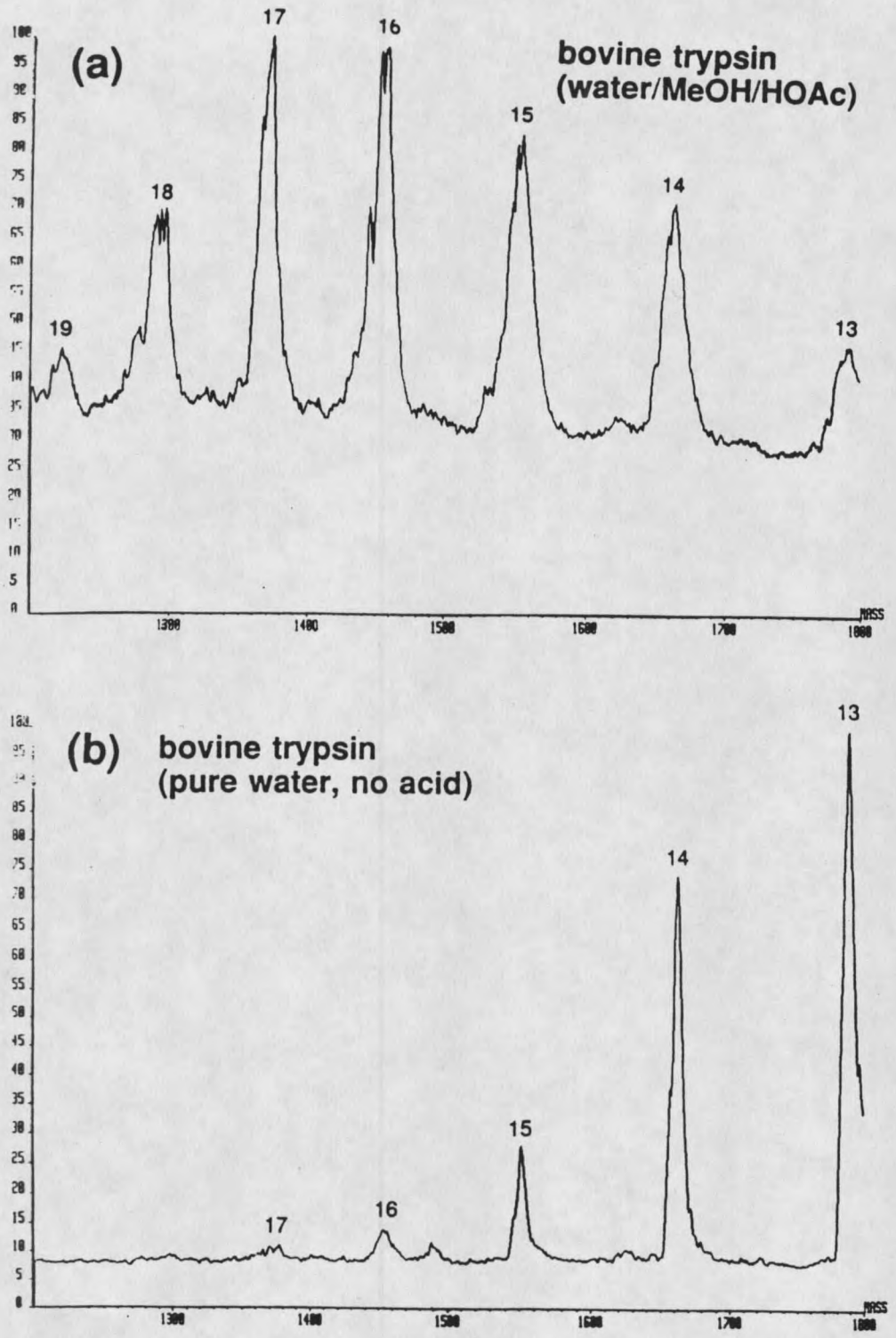

Figure 30. Electrospray mass spectrum of bovine trypsin. MW is 23,293 Da. (a) Trypsin was dissolved in 50/50 water/methanol mixture. (b) Trypsin was dissolved in pure water.

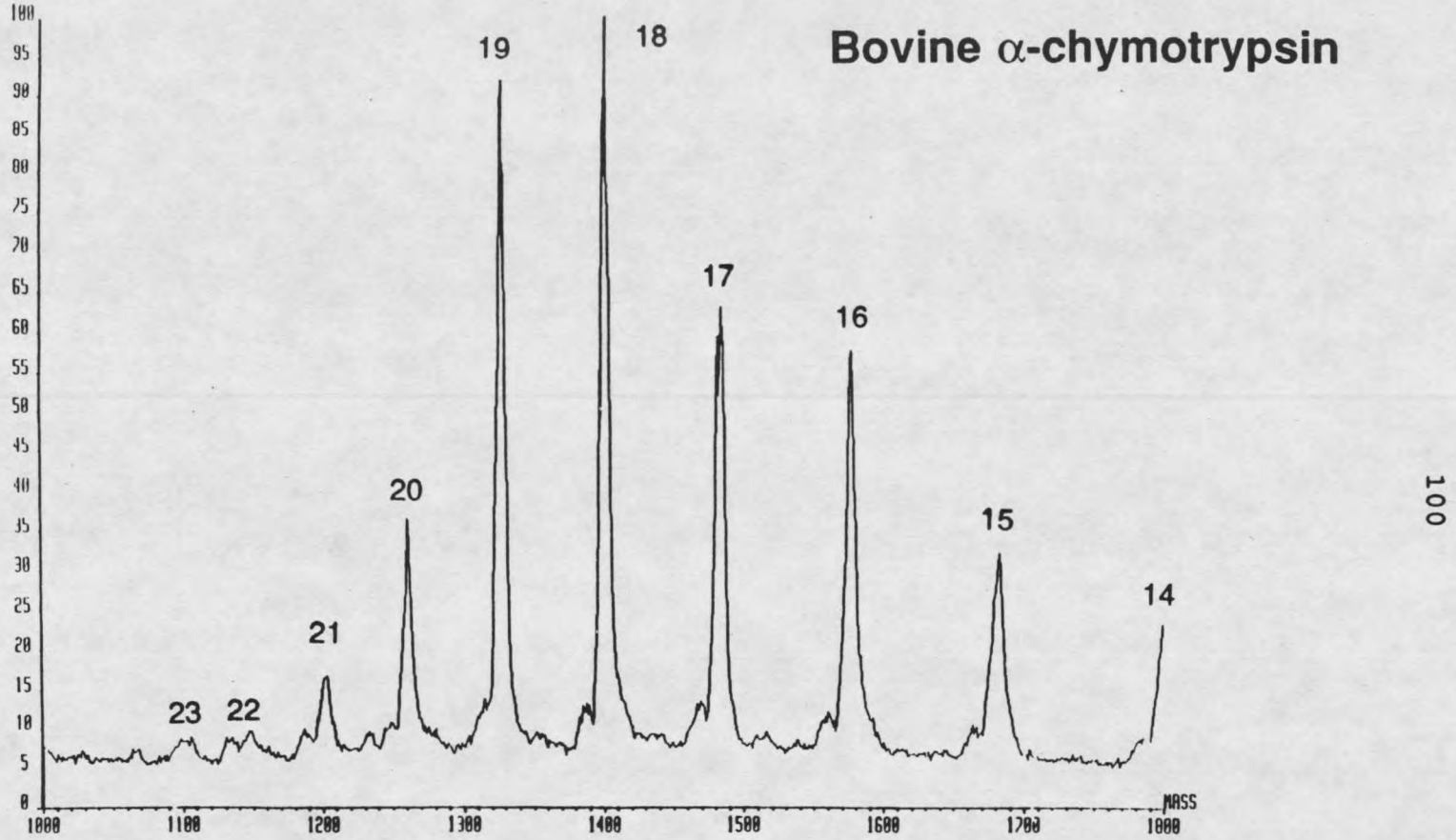

Figure 31. Electrospray mass spectrum of bovine α-chymotrypsin in pure water mixture. MW is 25,234 Da.

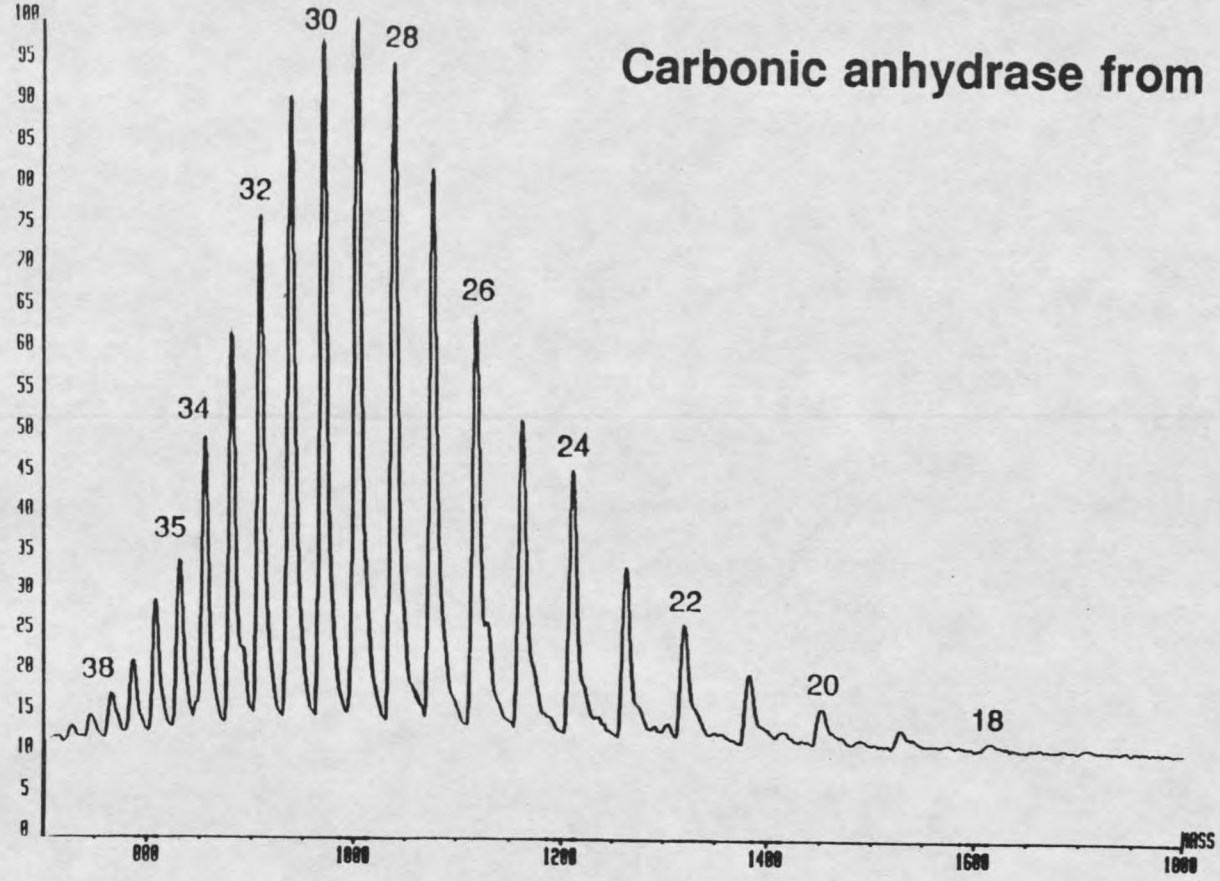

Figure 32. Electrospray mass spectrum of carbonic anhydrase from bovine in 50/50 water/methanol mixture. MW is 29,025 Da.

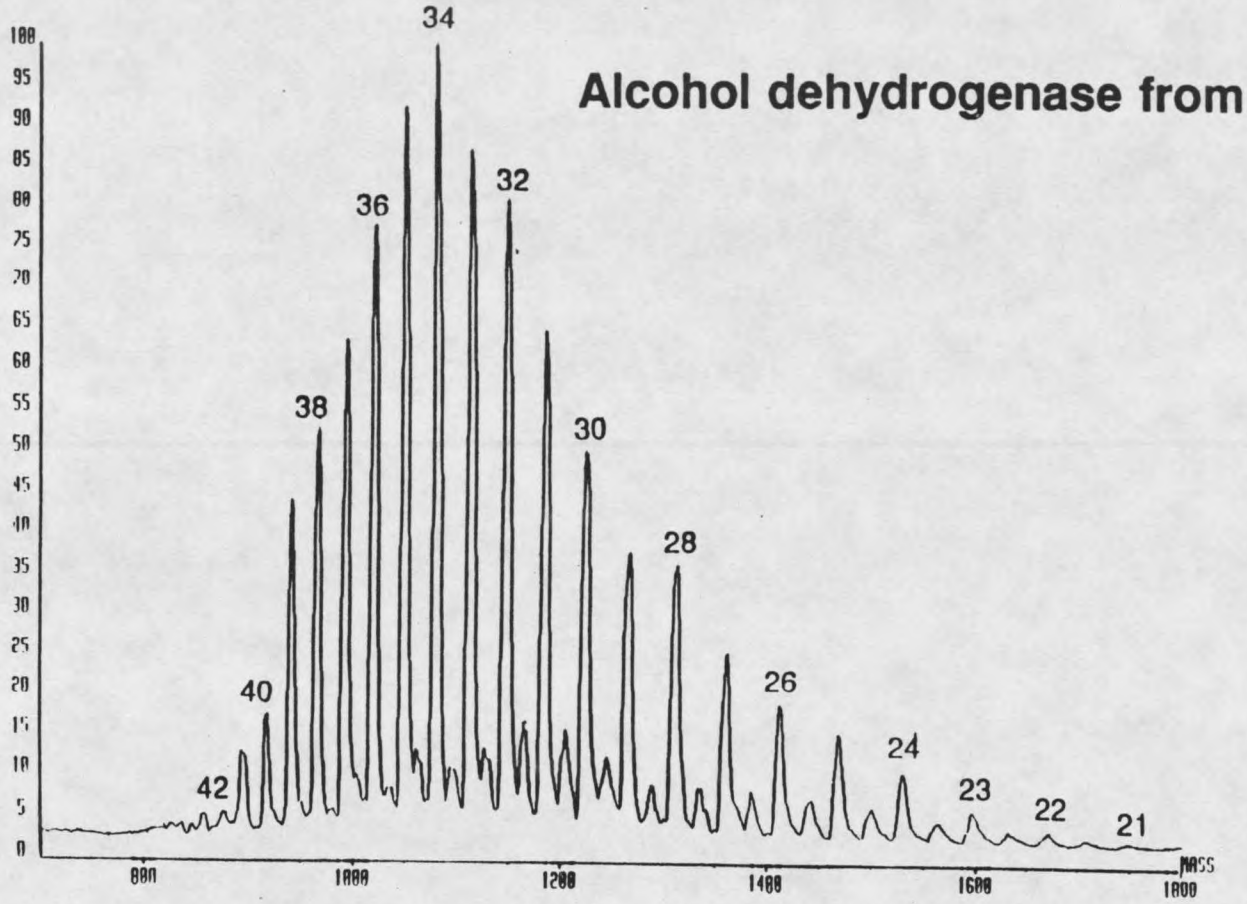

Figure 33. Electrospray mass spectrum of alcohol dehydrogenase from yeast in 50/50 water/methanol mixture. MW is 36,748 Da.

Table 7: Accuracy of mass measurement of proteins by ESI/MS.

protein	MW calculated from sequence	MW observed from ESI/MS	error%
Myoglobin (Horse)	16,951	16,954.4	+0.02
Cytochrome c (Horse)	12,360	12,361.0	+0.01
Avidin (Egg whites)	14,332	14,327.0	-0.03
Trypsin (Bovine)	β 23,293 ψ 23,329	23,292.4 23,339.4	-0.004 +0.04
α-Chymotrypsin (Bovine)	25,234	25,230.3	-0.01
Neo-Chymotrypsinogen (Bovine)	25,459	25,443.8	-0.05
Chymotrypsinogen A (Bovine)	25,656	25,663.5	+0.03
Carbonic anhydrase (Bovine)	29,025	29,021.8	-0.01
Alcohol dehydrogenase (Yeast)	36,748	36,732.9	-0.04

Heme Dissociation in Myoglobin

Conformations of Myoglobin

Horse myoglobin was used in this study because the protein undergo heme dissociation upon denaturation. The extent of denaturation of myoglobin is thus easily obtained from ESI mass spectra. The native myoglobin, with molecular dimensions of 45×35×25 Å, is a very compact macromolecule with little empty space in its interior [102]. A heme group containing protoporphyrin IX and iron resides inside the protein and is

non-covalently bonded to two histidine residues, as shown in Figure 34 (a). These specific interactions with iron are required for biological activity [102]. Since the native myoglobin holds the heme group very tightly, the total molecular weight should be that of myoglobin + heme group, MW=17,566 Da. Figure 34 (b) shows the electrospray mass spectrum of native myoglobin. The charges of the ions are low, 10^+ to 12^+. This is explained by the tightly folding conformation of the native protein.

Myoglobin can be denatured and induced to unfold by subjecting it to low pH. As a result of denaturation, the labile heme separates from the protein. Buried amino acids then become available for protonation. At a sufficiently low pH, the unfolding of the protein results in protonation of the histidine residues, which are the binding sites to the heme group. When the last histidine is protonated, the heme-myoglobin interaction is disrupted and the heme group separates from the globin. Myoglobin is believed to be totally protonated. Thus the denatured state can be characterized by the absence of the heme-myoglobin complex and a relatively higher charge state distribution. When myoglobin is in a denatured conformation, its molecular weight is that of the polypeptide chain, with a total of 153 residues, MW=16,951 Da. Figure 34 (c) shows the electrospray mass spectrum of denatured myoglobin. The charge state distribution is much higher than that for the native protein

because more available amino acids are protonated.

In this section, the conditions in the protein bulk solution and in the gas phase of the spray region, that are required to maintain the native conformation of myoglobin, will be discussed. Also, the effect of the protein conformation on the ESI mass spectra has been investigated.

Effect of Bulk Solution pH

The denaturation of proteins can be induced by high temperature, low pH, impurities, or high concentrations of organic solvent. In order to retain native myoglobin, such conditions must be avoided. When the protein is dissolved in pure distilled water with no salts and acid added, pH was 5.5, it is assumed that the protein is in the native conformation. As the pH is decreased, the extent of protein denaturation will increase. Figure 35 shows the effect of solution pH on the degree of myoglobin denaturation.

For the spectrum in Figure 35 (a), myoglobin was dissolved in distilled water with no added acid. Only the heme complex, and by deduction, the native conformation was observed in the ESI/MS spectrum. The low charges, 10^+ and 11^+, indicates that the protein was tightly folded. It is impossible to obtain a full charge distribution because of the 1800 m/z limitation of this instrument. Figure 35 (b) shows the myoglobin spectrum when a small amount of HOAc has been added to the protein solution to adjust the pH to 5. Two distinct charge state distributions are now seen: the native conformation ranges

from 10^+ to 16^+, with 10^+ being the most abundant; and the denatured conformation ranges from 10^+ to 20^+, with 15^+ being the most abundant. At this pH, the intensity for the native protein remained high, but the denatured protein were equally intense. When the pH was decreased to 4.5, the amount of native protein dropped to very low levels and the "denatured" peaks came to dominate the spectrum, Figure 35 (c). At an even lower pH, pH=3, the native form disappeared altogether, Figure 35 (d).

Effect of Methanol Solvent

Changes in the environment of a protein, such as addition of organic solvents to the protein solution may cause denaturation of the protein. Common organic solvents used in electrospray are methanol, acetonitrile, isopropanol, and acetone. For example, increasing the alcohol concentration in a protein solution results in a lowering of dielectric constant of the solution. Denaturation may result from alcohol binding to hydrophobic sites.

Figure 36 shows the effect of methanol concentration on the degree of myoglobin denaturation. Figure 36 (a) shows a spectrum of myoglobin sprayed in pure distilled water (methanol%=0). The native conformation was observed, with charge states of 10^+ and 11^+. In Figure 36 (b), (c), and (d) the methanol concentration was increased to 10%, 20%, and 50% by volume, respectively. With 10% methanol, the charge state distribution for the native form shifted to higher charges, up

to 15^+. At the same time, denatured peaks have appeared. With 20% methanol, these trends continued, Figure 36 (c). Thus, native peaks with charge states up to 17^+ are observed and the charge 11^+ ion is the most abundant. The intensities of denatured peaks are now similar to those of the native form. With 50% methanol, Figure 36 (d), the native conformation has disappeared and only the denatured form is observed.

There are two charge distributions for the denatured myoglobin conformation in Figure 36 (d). The first one consists of 10^+ to 11^+, and the second one ranges from 12^+ to 17^+. This result is very reproducible. It possibly means that two conformations of denatured myoglobin are coexisting. One conformation, with a lower charge state, could be relatively compact and only exterior side chains are protonated. Another, with a higher charge state, could be relatively loose and additional side chains are available for protonation. The details of these conformation have not been studied.

It is noteworthy that methanol up to ca 10% to 20% will increase the intensities of both the native and the denatured conformations.

Addition of Acids Into The Gas Phase of The ESI Source

It was seen above that the pH and the composition of the organic solvent have a great influence on the denaturation of myoglobin. However, it is not at all clear that all the

denaturation occurs in the solution before the electrospray. It is possible that some denaturation also occurs during the electrospray process itself. Therefore, the effect of the gas phase conditions in the electrospray region on the denaturation of myoglobin was studied. In a first series of experiments, three different acids, hydrochloric acid (HCl), acetic acid (HOAc), and p-tolunesulfonic acid (PTSA) were introduced into the gas phase of the electrospray source. These experiments were carried out at room temperature. Myoglobin was dissolved in pure distilled water with no acid added and the pH was 5.5. The set up in Figure 16 was used.

Figure 37 shows the effect of gas phase acid addition on the myoglobin conformation. Figure 37 (a) is a spectrum of myoglobin sprayed in pure water with no acid added into the gas phase. Only the native heme-complexed myoglobin with charge 10^+ was detected. The conditions for Figure 37 (b) were identical except that HOAc vapor was continuously released into the electrospray source. The concentration of the HOAc solution was 0.23 M. The appearance of HOAc in gas phase significantly increased the charges on the native myoglobin, up to 12^+. It is noteworthy that no denatured myoglobin was detected. However, the increase in the charge state may be interpreted to mean that the conformation of myoglobin somewhat loosened with the presence of HOAc in gas phase. However, the time during which the proteins were subjected to the acidic conditions was obviously too short for

unfolding to progress to the point at which the heme can dissociate. The consequences of the very first stages of unfolding may then be seen. An alternative interpretation is that the gaseous HOAc results in somewhat higher charges of the decomposing droplets. Addition of another acid, p-tolunesufonic acid (PTSA), showed very similar results to those of HOAc in Figure 37 (b).

Addition of HCl gave a very different result as shown in Figure 37 (c). The experimental conditions were the same as for Figure 37 (a) and the HCl vapor was introduced using the same set-up. However, it was difficult to obtain good myoglobin spectra even with a low HCl flow rate. At higher HCl flow rate no spectra at all could be obtained. Figure 37 (c) shows both native and denatured conformations with HCl added into the gas phase. The signal-to-noise level is seen to be low. Addition of HCl into the gas phase seems to suppress native myoglobin ions. It probably destabilizes the spray by increasing the electrolyte concentration beyond what is optimal in ESI. However, other differences in the effects between HCl and HOAc are not understood.

Figure 38 shows the myoglobin spectra obtained at different flow rate of HOAc in gas phase. Nitrogen gas was bubbling through a 0.23 M HOAc solution as shown in Figure 16. Figure 38 (a), (b), (c), and (d) show spectra of myoglobin with HOAc flow rates of 0, 1.7, 6, and 20 μmol/sec, respectively. The ion intensity and the charge state of

native myoglobin were seen to increase along with the increasing HOAc flow rate. The charge states increase gradually from 10^+ to 11^+ and to 12^+. The HOAc addition also greatly increased the intensities of native myoglobin peaks.

It is of interest to compare the effects of adding HOAc to the gas phase and to the bulk solution prior to electrospray. The myoglobin spectrum with no acid addition in Figure 39 (a) should be compared with that obtained with gas-phase HOAc addition, Figure 39 (b), and with HOAc addition to the bulk solution, Figure 39 (c). It is noteworthy that the flow rate of HOAc in the bulk solution was very small, 0.7 μmol/min, compared to the gas phase flow rate, 360 μmon/min, which was thus more than 500 times higher. Despite this, myoglobin is completely denatured with the much smaller HOAc addition to the liquid phase, whereas the native conformation was maintained under HOAc addition to the gas phase. It seems reasonable that HOAc in the gas phase absorbs into the liquid surface of the Taylor cone and the charged droplets and subsequently interacts with myoglobin inside the droplets. This interaction can last only 10^{-3} seconds before the ions or charged droplets arrive at the mass analyzer. In contrast, bulk solution HOAc has a much longer time to interact with myoglobin, complete the denaturation process and accomplish heme group dissociation.

In a different series of experiments, the effect of methanol vapor introduced into the gas phase in the spray

region was investigated. It was found that at room temperature, the mass spectra showed the presence of both native and denatured myoglobin conformations. Charge distributions were very similar to the results from 10% methanol in the bulk solution, shown in Figure 36 (b). The effects of methanol in gas phase and in bulk solution on the denaturation of myoglobin are apparently similar. It is possible, though, that the gas-phase methanol concentration was much higher.

The Effect of Ion Source Temperature

The conformation of proteins in solution can be altered by subjecting them to high temperatures. High solution temperature strongly denatures protein and finally breaks polypeptide chains of proteins. However the temperature at spray region has quite different effects to the conformational change of myoglobin.

Figure 40 shows spectra of myoglobin sprayed from a pure water solution at four different gas-phase temperatures. The temperatures in Figure 42 (a), (b), (c), and (d) were 23, 30, 38, and 50 °C, respectively. The temperature was determined by a N_2 gas stream that passed through a thermostated coil and entered the ion source. The temperature was measured at the spray region by a thermocouple, see set up in Figure 16. At temperatures below 25 °C, it was found necessary to add gas phase HOAc in order to obtain myoglobin spectra. Above 25 °C, no gas phase HOAc was added. At low temperatures, the

intensities of the native myoglobin ions were weak and only 10^+ and 11^+ charge ions were observed (Figure 40 (a)). Because of the addition of HOAc to the gas phase, the most intense charge state switched to 11^+. At higher temperatures, the intensity of the native myoglobin ions was greatly increased; at 30 °C, the intensity was 10 times higher than at room temperature and at 38 °C, more than 30 times higher. The charge state distribution also shifts toward higher charges. At 38 °C, weak denatured myoglobin peaks are seen. At a temperature of > 50 °C, Figure 40 (d), the heme group is totally dissociated from the myoglobin.

The increased gas-phase temperature in the ESI source causes the surface tension of the myoglobin solution to decrease. Lower surface tension decreases the electrospray on-set voltage and facilitates the breakup of the liquid into small charged droplets. Second, energy transfer from the hot gas assists the desolvation of the droplets. Also, at higher temperatures, the native conformation of myoglobin is destabilized. This increases the chance for protonation of protein side chains which would tend to increase the charge state.

Gas Phase Deprotonation

Dimethyldodecylamine (DMDA) vapor was introduced into the spray region by the same method as described above for gas-phase acid addition. The proton transfer reactions were carried out at room temperature.

The spectrum shown in Figure 41(a) was obtained by electrospraying a solution of 9 μM myoglobin in a water/methanol (50:50, v/v) mixture. The pH of the solution was adjusted to 4 with the addition of acetic acid. The protein is denatured under these conditions. A charge distribution from 12^+ to 19^+, with the maximum intensity at 16^+ was observed in this spectrum. No heme-complex was observed. The same myoglobin sample was again sprayed, under the same conditions as above, except that DMDA was introduced into the spray region. The result is shown in Figure 41 (b). A very different charge distribution was observed with only 10^+ and 11^+ ions, with charge state 10^+ being the most intense. The dramatic decrease of the charge states in the presence of a strong base indicates that proton transfer reactions have taken place,

$$(myog \cdot H_n)^{+n} + DMDA \rightarrow (myog \cdot H_{n-1})^{+(n-1)} + (DMDA \cdot H)^+ \qquad (26)$$

The occurrence of reaction 26 is further supported by the observation that the intensity of $(DMDA \cdot H)^+$ at m/z 214 increased (not shown in Figure 41). This gas phase reaction is very fast since DMDA has a higher proton affinity than the amino acid residues in the protein. Similar deprotonation has been reported for cytochrome c [114,131] and for myoglobin [73]. A second sequence of peaks is seen in Figure 41 (b). These peaks are likely due to an adduct between myoglobin and

DMDA.

The deprotonation of peptides by DMDA can be a useful technique. Figure 42(a) shows a ESI mass spectrum of 50 μM angiotensin II (MW=1046 Da) in a water/methanol (50:50, v/v) solvent. The pH was adjusted to 3.5 by adding acetic acid. The spectrum displays a singly charged ion peak (MH^+ at m/z=1047) and a doubly charged ion peak (MH_2^{2+} at m/z=524). The intensity of MH_2^{2+} ions is 4 times higher than that for MH^+ ions. The spectrum in Figure 42(b) was obtained after introducing DMDA for 20 seconds. The intensity of MH_2^{2+} has now decreased whereas the MH^+ peak is much more intense. The high intensity of $(DMDA \circ H)^+$ at 214 confirms that the gas phase deprotonation has taken place.

Analysis of Closely Related Forms of Chymotrypsin

Activation of Chymotrypsinogen

Chymotrypsin is one of several proteolytic digestive enzymes that are synthesized in the pancreas as zymogens, i.e. inactive precursors of the enzymes. Chymotrypsinogen, the inactive precursor of chymotrypsin, is stored in lipid-protein membranes in the mammalian pancreas and, when needed for digestive purposes, are secreted into a duct that leads into the duodenum, where they are activated.

Chymotrypsinogen A is composed of a single polypeptide chain with 245 amino acid residues and five disulfide bridges.

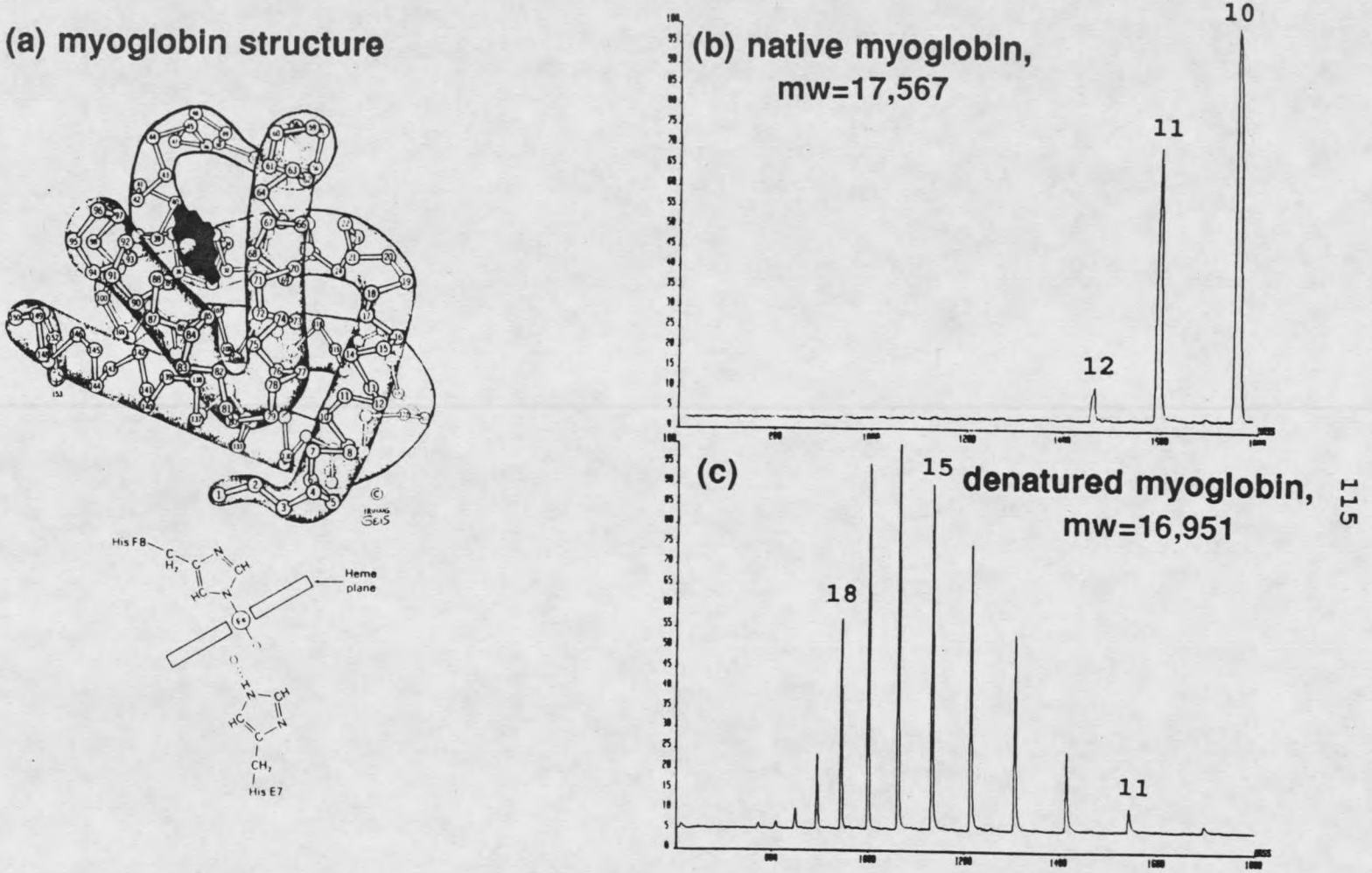

Figure 34. Conformations of myoglobin. (a) Three-dimensional structure of myoglobin. (b) Native myoglobin (heme is attached). (c) Denatured myoglobin (heme is dissociated).

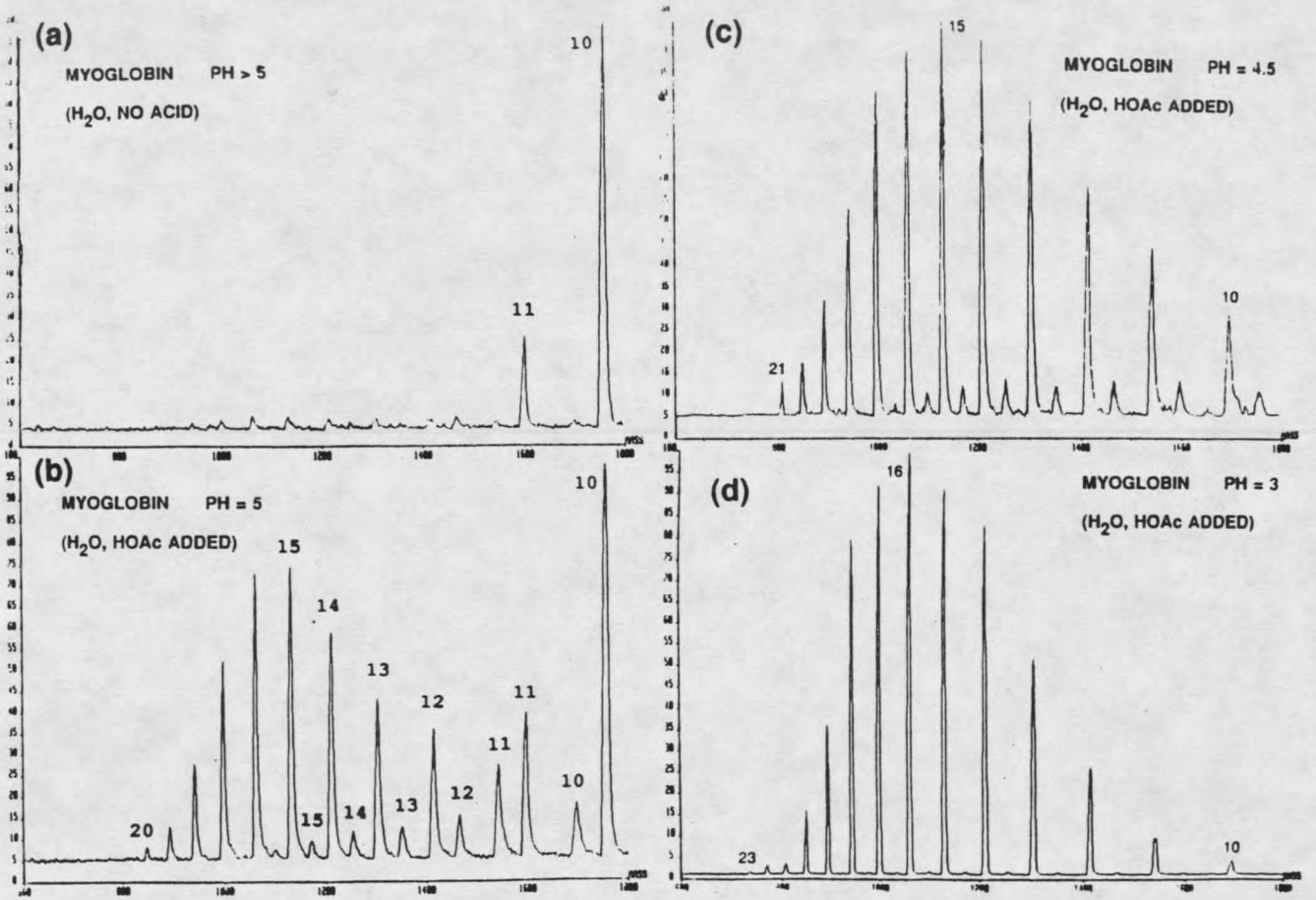

Figure 35. ESI mass spectra of myoglobin and its conformations effected by bulk solution pH. Myoglobin was diaaolved in pure water. (a) Solution pH was > 5. (b) Solution pH was 5. (c) Solution pH was 4.5. (d) Solution pH was 3.

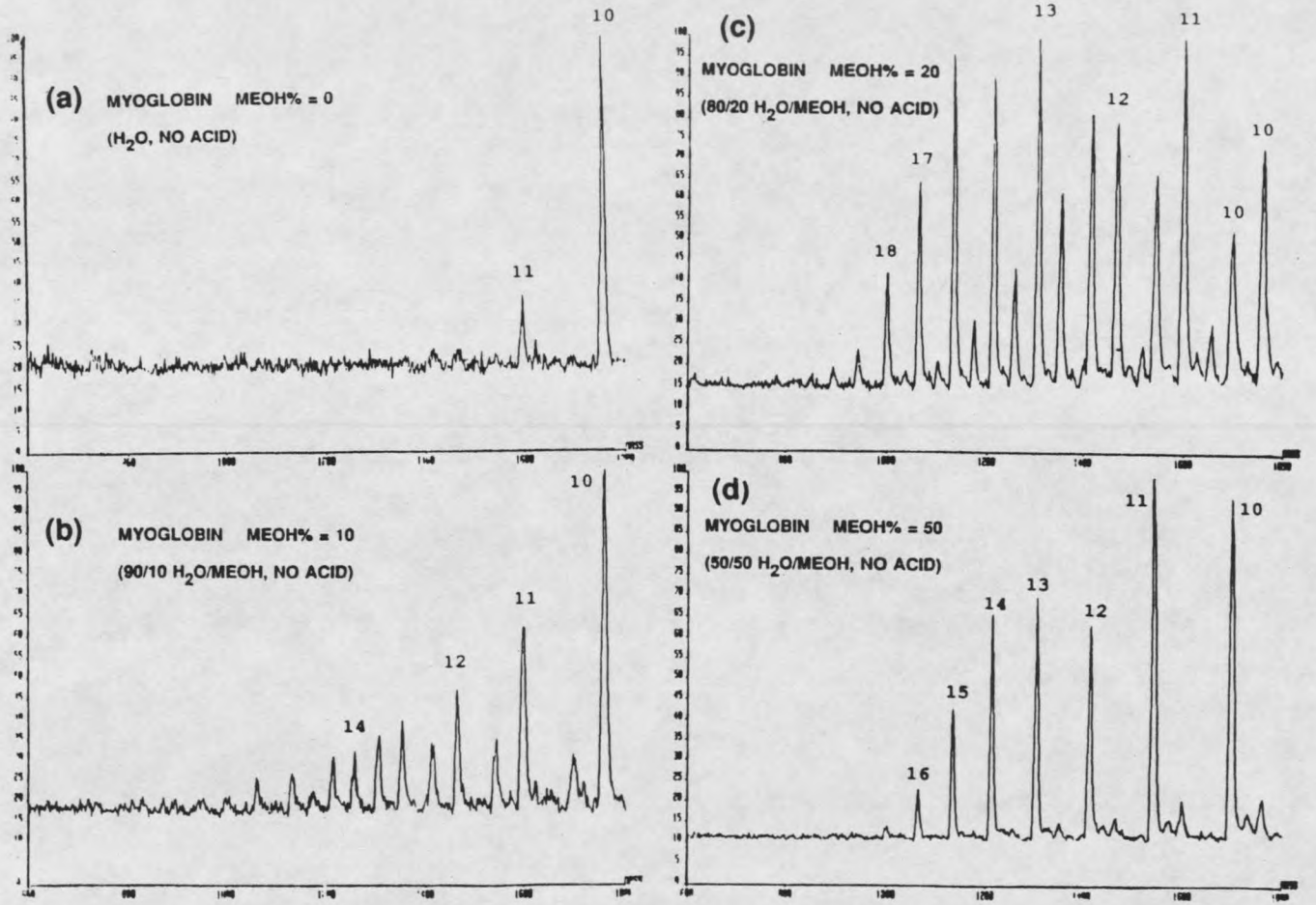

Figure 36. ESI mass spectra of myoglobin and its conformations effected by methanol compositions in bulk solution. (a) 0% methanol. (b) 10% methanol. (c) 20% methanol. (d) 50% methanol.

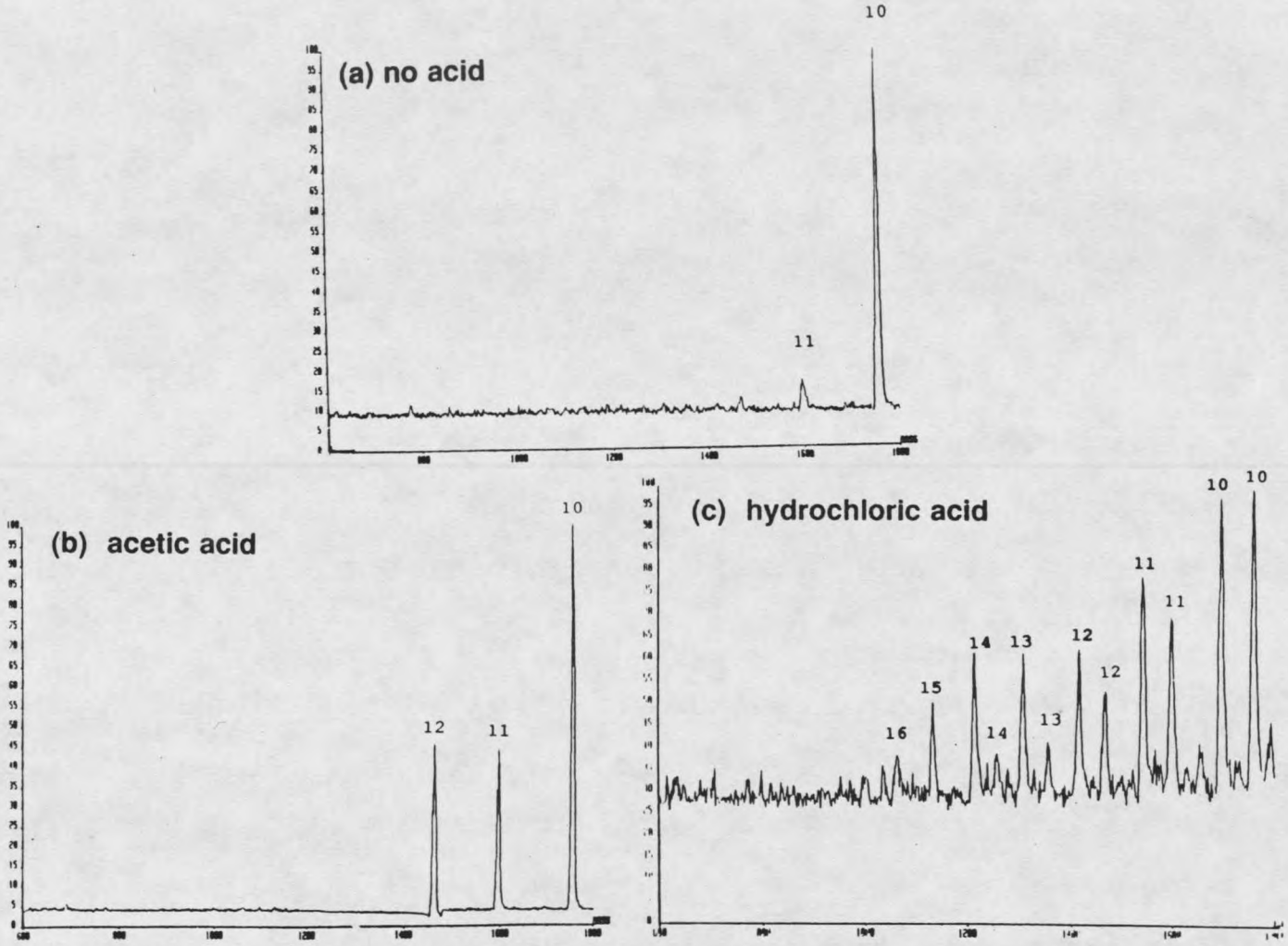

Figure 37. ESI mass spectra of myoglobin obtained from different acid addition to the spray region. Sample was dissolved in pure water. (a) No acid addition. (b) addition of acetic acid. (c) Addition of hydrochloric acid.

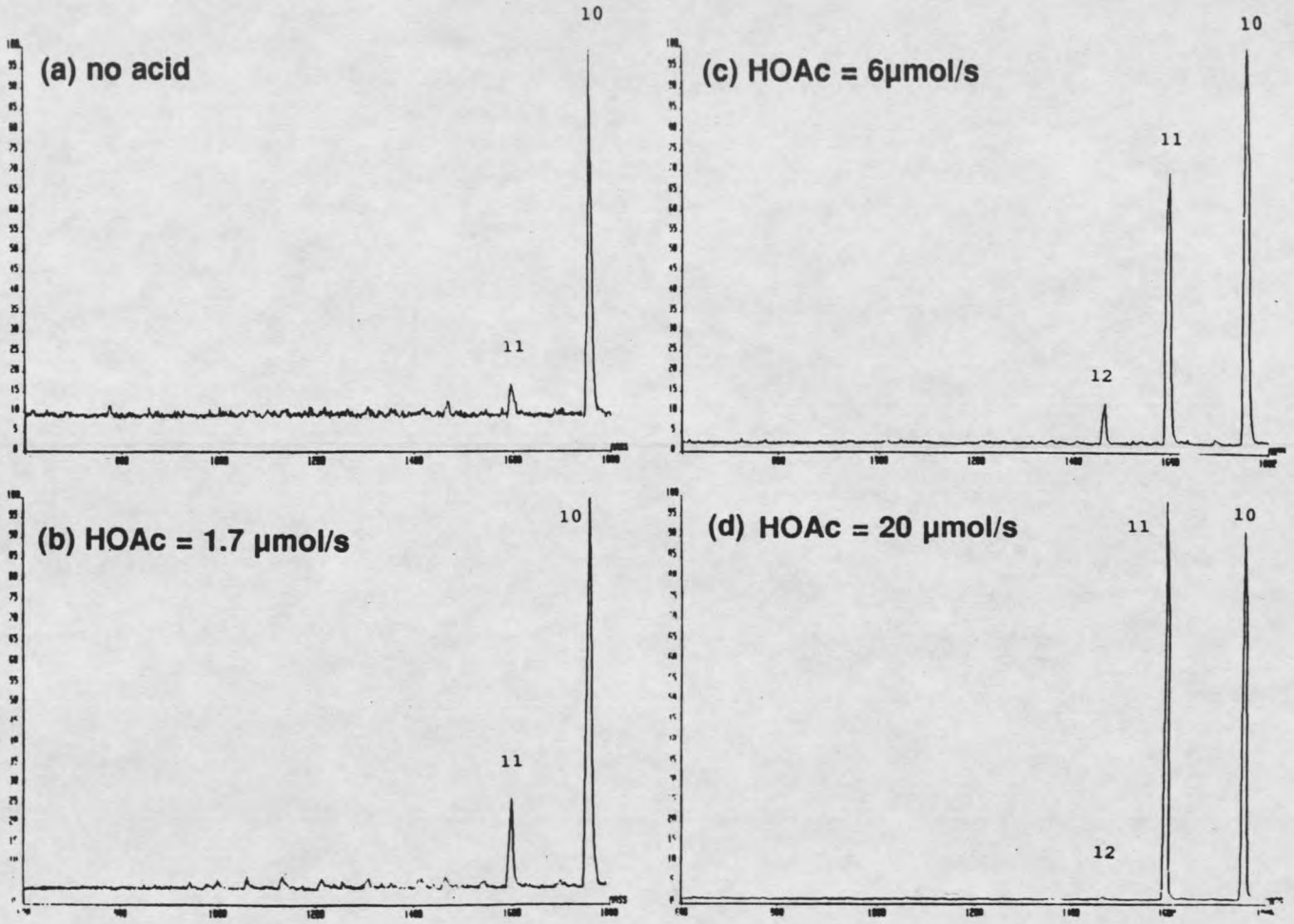

Figure 38. ESI mass spectra of myoglobin effected by the flow rate of acetic acid. Myoglobin was dissolved in water. (a) No acid addition. (b) Acid flow rate was 1.7 µmol/s. (c) Acid flow rate was 6 µmol/s. (d) Acid flow rate was 20 µmol/s.

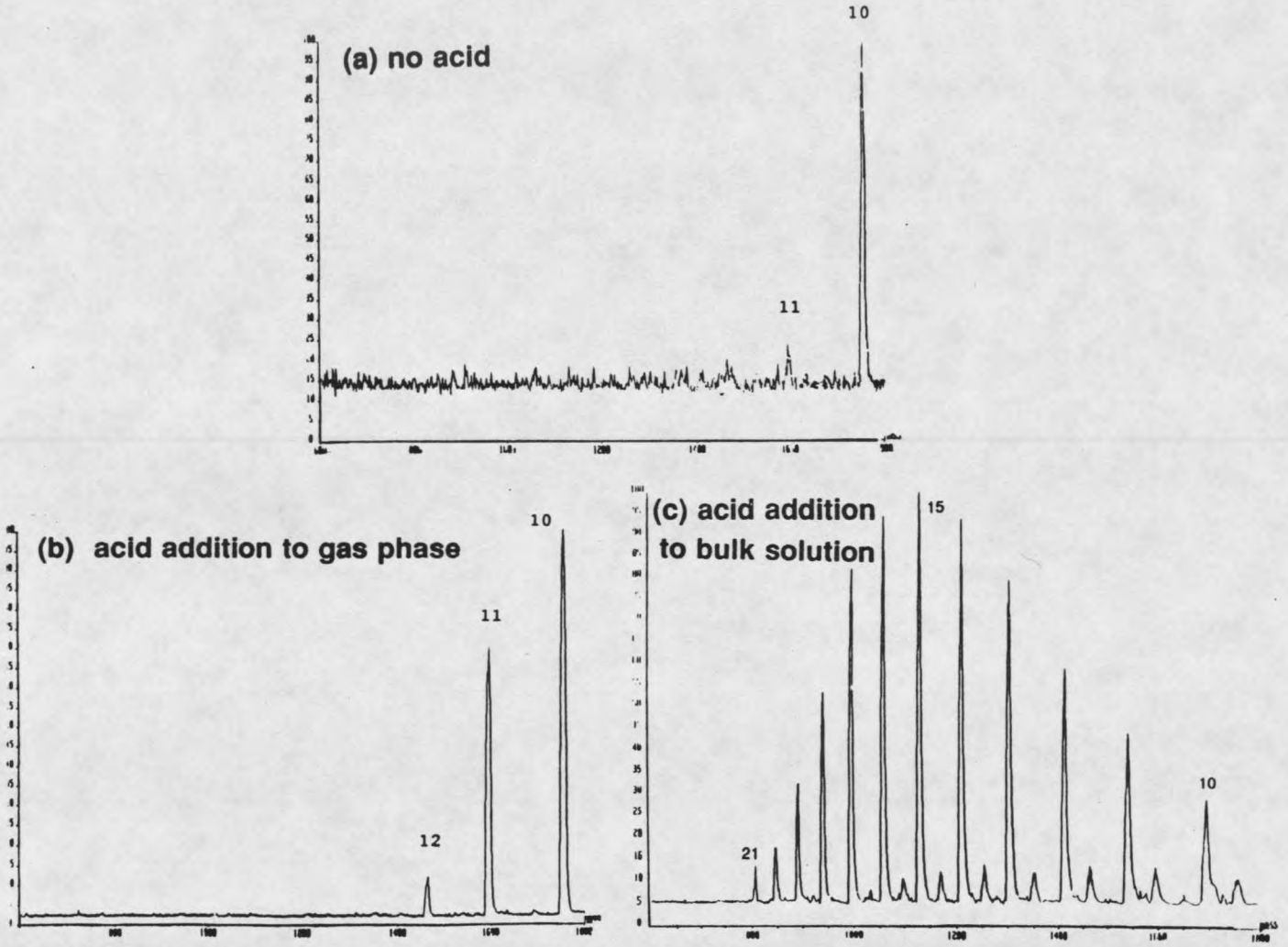

Figure 39. ESI mass spectra of myoglobin effected by conditions in bulk solution and in gas phase. (a) Sample was dissolved in pure water with pH of 5.5. (b) Sample was dissolved in pure water with pH of 5.5 and acetic acid was added to the spray region. (c) Sample was dissolved in acetic water solution with pH of 4.5.

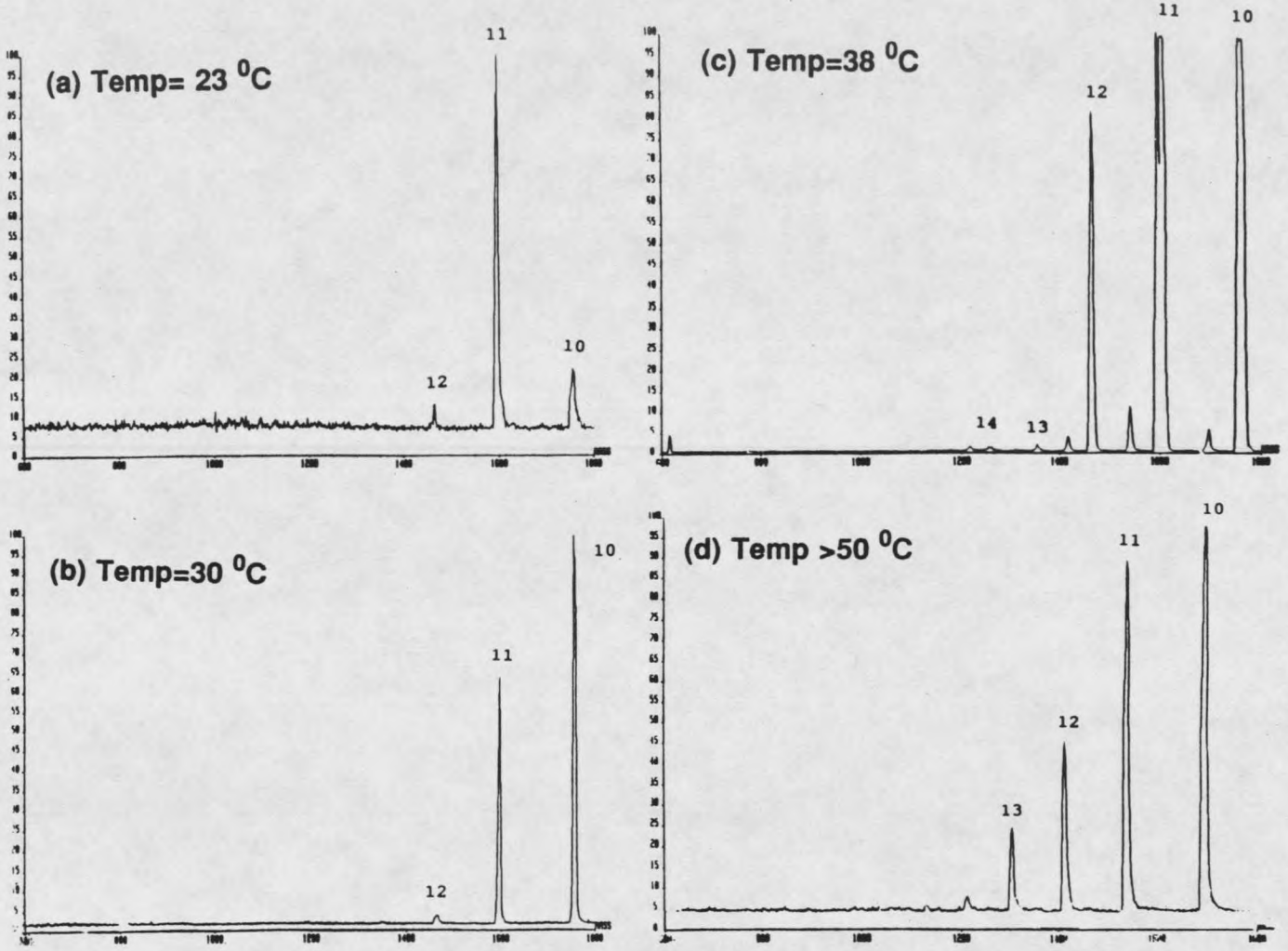

Figure 40. ESI mass spectra of myoglobin effected by the temperature at spray region. Myoglobin was dissolved in pure water. (a) Temperature was 23 ^{0}C. (b) Temperature was 30 ^{0}C. (c) Temperature was 38 ^{0}C. (d) Temperature was > 50 ^{0}C.

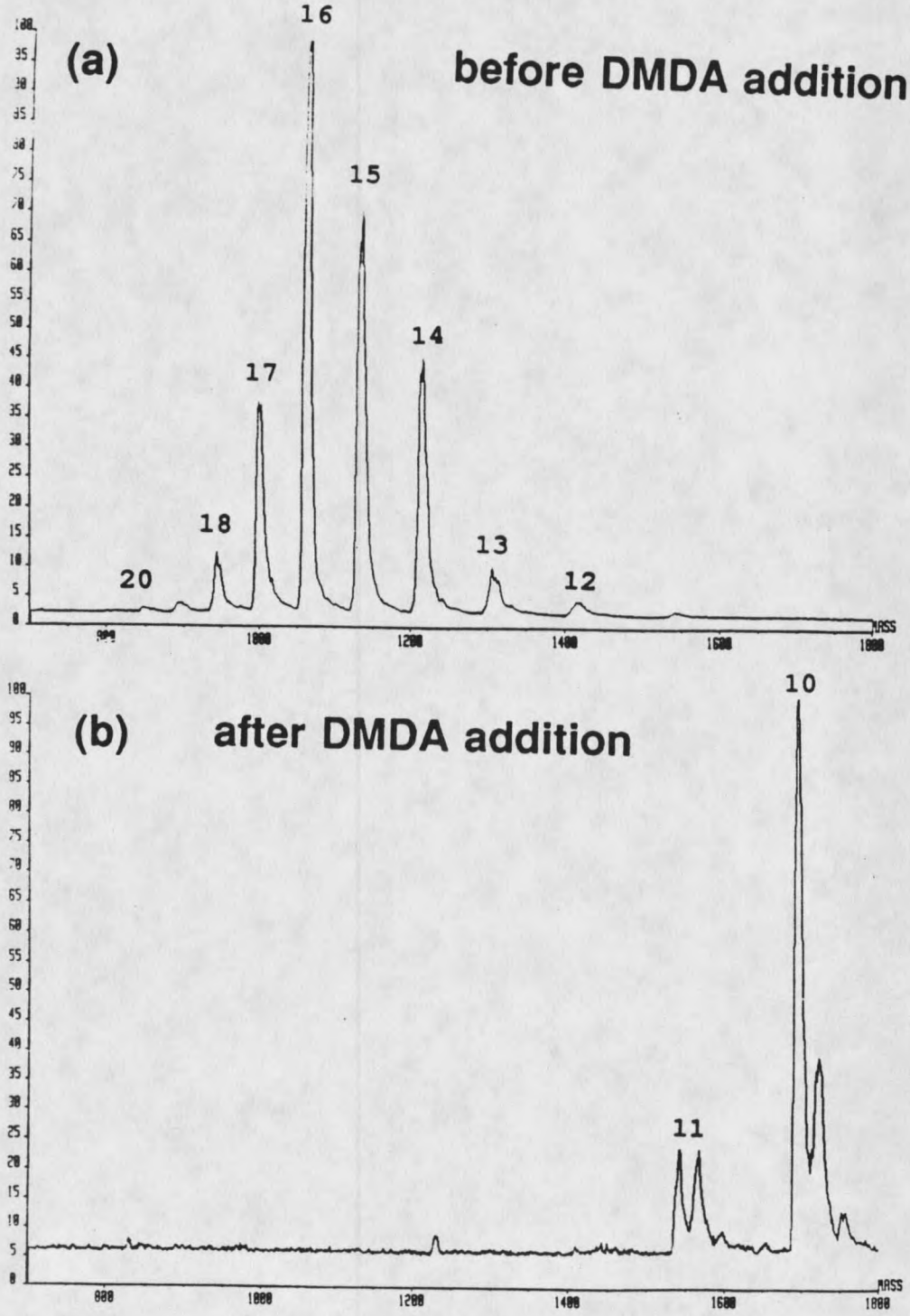

Figure 41. (a) ESI mass spectrum of myoglobin which was dissolved in water/methanol mixture with pH of 3. (b) ESI mass spectrum of same sample as in (a) but acquired after DMDA was added to spray region.

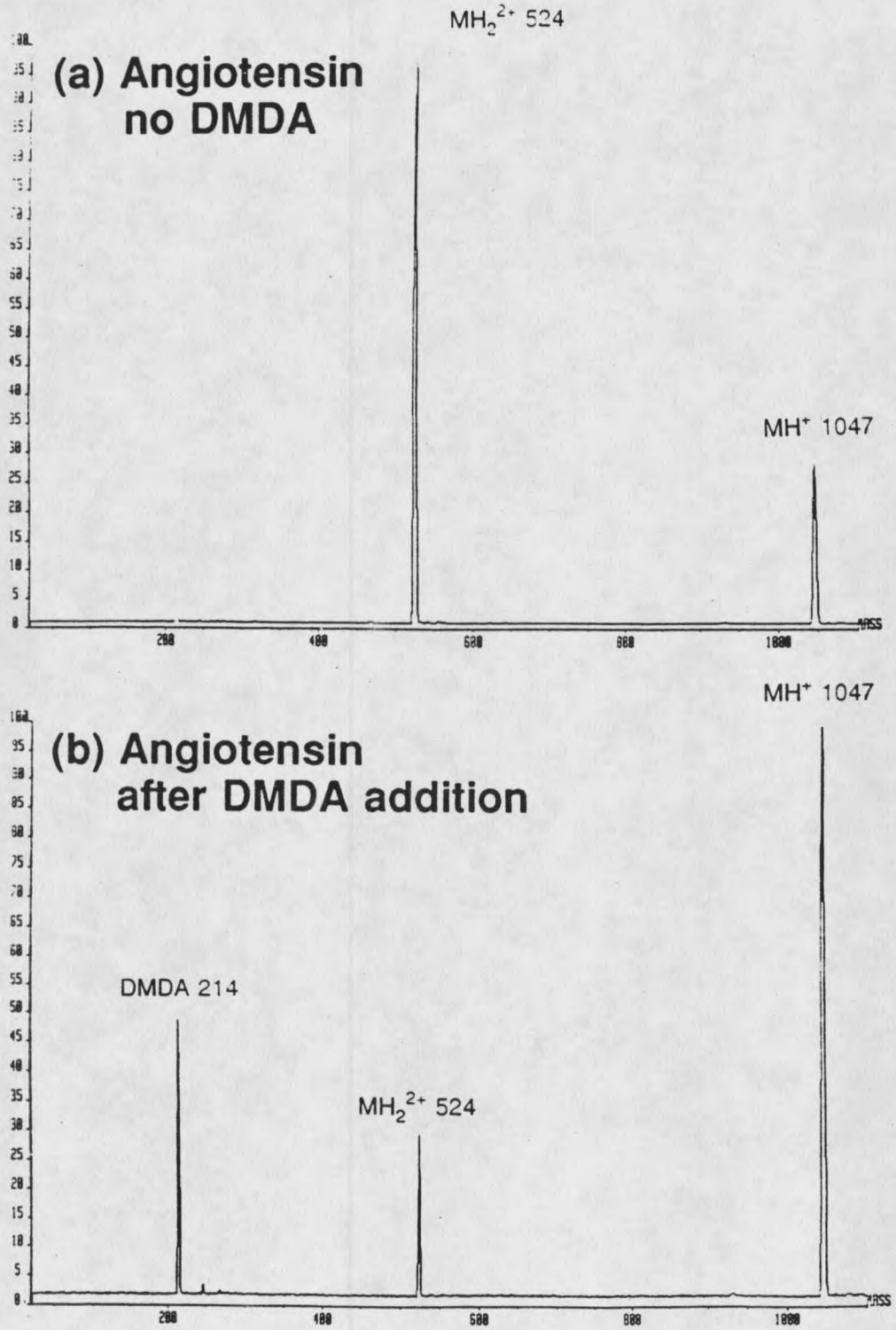

Figure 42. (a) ESI spectrum of angiotensin II which was dissolved in water/methanol mixture with pH of 3. (b) ESI mass spectrum of same sample as in (a) but acquired after DMDA was added to spray region.

Da. Figure 43 shows the activation process of chymotrypsinogen. The activation of the zymogen to an active chymotrypsin results from the specific cleavage of a peptide bond by trypsin. This process is complicated by the possibility of further proteolysis by chymotrypsin or by trypsin.

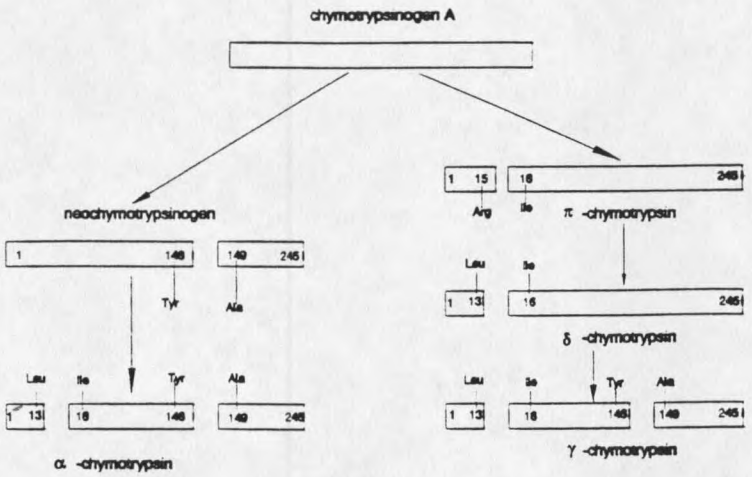

Figure 43. Activation of chymotrypsinogen

Northrop and Kunitz [133] activated chymotrypsinogen A under conditions giving a good yield of α-chymotrypsin crystals. Rapid activation, using larger quantities of trypsin, gives two different species of chymotrypsin, named π- and δ-chymotrypsin. Especially when activation is performed slowly, chymotryptic cleavage of chymotrypsinogen is possible, leading to degraded zymogens known as neochymotrypsinogen [122]. γ-chymotrypsin is identical to α-chymotrypsin but has quite distinct crystallization properties [123]. It has been shown by crystallographic studies that the transition between

shown by crystallographic studies that the transition between the α- and γ- forms of the enzyme is reversible [124]. On the basis of the crystallographic similarity of δ- and γ-chymotrypsin, it has been suggested that the "slow" activation which leads to α-chymotrypsin occurs via neochymotrypsinogen, while autolysis of δ-chymotrypsin leads directly to γ-chymotrypsin [122].

The molecular weights of each species resulting from the activation of chymotrypsinogen A are listed in Table 8.

Table 8: Derivatives from activation of chymotrypsinogen A.

form	cleavage	molecular weight
chymotrypsinogen A	none	25,656
π-chymotrypsin	Arg15 and Ile16	25,674
δ-chymotrypsin	loss Ser14-Arg15	25,430
neochymotrypsinogen	loss Thr147-Asn148	25,459
γ-chymotrypsin α-chymotrypsin	loss Ser14-Arg15 and Thr147-Asn148	25,233

Figure 44 displays electrospray mass spectra of differnt forms of chymotrypsin. Figure 44 (a) shows chymotrypsinogen A sprayed from a water solution. The charge state distribution ranges from 15^+ to 20^+, with 15^+ being the most intense. The observed molecular weight is 25,663. Figure 44 (b) shows neochymotrypsinogen from a mixture of water and methanol. The measured molecular weight is 25,444 and the charge distribution ranges from 15^+ to 20^+, with 17^+ being the

most intense. Figure 44 (c) shows a spectrum of α-chymotrypsin sprayed from water. The charge states, ranges from 14^+ to 22^+, with 19^+ being the most intense. The measured molecular weight is 25,230. These spectra demonstrate that ESI mass spectrometry is an very convenient method for distinguishing between closely related proteins such as neochymotrypsinogen and α-chymotrypsin by measuring protein molecular weights.

Mixtures of Chymotrypsinogen Derivatives

Commercially available active α-chymotrypsin is made by the activation of chymotrypsinogen A. Several derivatives can be generated during the activation processes which include tryptic catalysis followed by auto catalysis, as shown in Figure 43. In the case of the slow activation process, neochymotrypsinogen can be a major byproduct to the final α-chymotrypsin derivative. In the case of fast activation, δ- and π-chymotrypsin can be the major byproducts. Commercial α-chymotrypsin is prepared free of autolysis products and low molecular weight contaminants by the procedure of Yapel, et al. [125]. It will be demonstrated here that electrospray mass spectrometry is a superior method for the characterization of such reaction mixtures.

The electrospray ionization mass spectrum of a commercial sample of bovine α-chymotrypsin is shown in Figure 45. This sample (α-chymotrypsin, type 1-s) was obtained from Sigma Chemical Co., St.Louis, MO and was used without any further

purification. The sample was dissolved in high purity water without any acid addition. The charge distribution in this spectrum ranges from 15^+ to 19^+, with 15^+ being the most intense. Each charge state consists of three peaks, which indicates the presence of three different proteins (Table 9). The molecular mass obtained for the most intense peaks (2nd peak) is 25,466.0, that for the least intense peaks (1st peak) is 25,219.4, and that for the 3rd peak is 25,642.6.

Table 9: Observed molecular mass from Sigma's α-chymotrypsin.

protein	calculated molecular weight	observed molecular weight	MW error %
chymotrypsinogen A	25,656	25,642.6	-0.05
neochymotrypsinogen	25,458.5	25,466.0	+0.03
α-chymotrypsin	25,233.5	25,219.4	-0.05

The comparisons in Table 9 show that the experimental molecular weights agree closely (but not perfectly) with α-chymotrypsin, neochymotrypsinogen, and chymotrypsinogen A, respectively. In this "type 1-s" α-chymotrypsin sample, the major form of the enzyme is neochymotrypsinogen and not α-chymotrypsin as stated by Sigma. Indeed, the intensities of α-chymotrypsin are much lower and the amount of α-chymotrypsin in this sample is probably very low. Thus, the activation of chymotrypsinogen A in this "type 1-s" sample basically stopped at the neochymotrypsinogen step. In order to obtain α-chymotrypsin, further sample treatment would be required. It

is known that many proteins are not well dissolved in solutions that contains a high fraction of organic solvents. It is possible that the suppression of α-chymotrypsin and chymotrypsinogen A at high methanol concentrations is due to such solubility problems.

The "type 1-s" α-chymotrypsin sample was bought from the Sigma Company. As discussed above, this sample did not give a required α-chymotrypsin ions in electrospray mass spectrometry. Another α-chymotrypsin sample was then obtained from Worthington Biomedical Corporation (catalog # 1430). Also, this sample was prepared free of autolysis products and low molecular weight contaminants by the procedure of Yapel, et al. [125]. The Worthington sample was used without purification and was dissolved in pure water. Figure 47 (a) shows the electrospray mass spectrum of this sample. The observed molecular mass is 25,226.3 amu, which closely agrees to that calculated for α-chymotrypsin. The charge state distribution ranges from 15^+ to 22^+, with 19^+ being the most intense. This spectrum proves that the Worthington sample is indeed α-chymotrypsin. There is no detectable presence of byproducts. A comparison with the Sigma sample spectrum, Figure 47 (b), shows the dramatic difference. Clearly, in this case, Worthington offers a superior product.

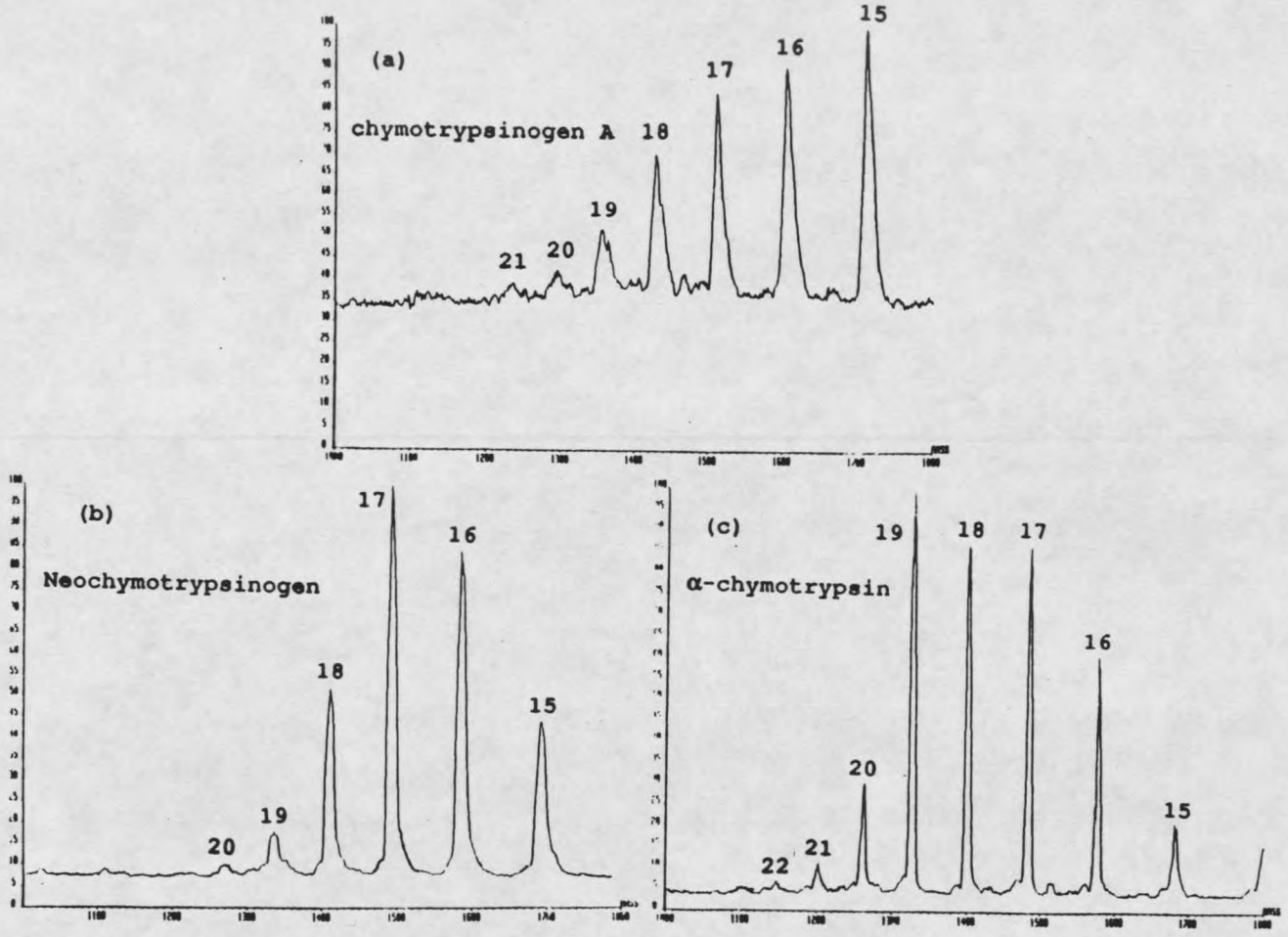

Figure 44. ESI mass spectra of (a) chymotrypsinogen A with MW = 25,656 Da; (b) neochymotrypsinogen with MW = 25,459 Da; (c) α-chymotrypsin with MW = 25,234 Da.

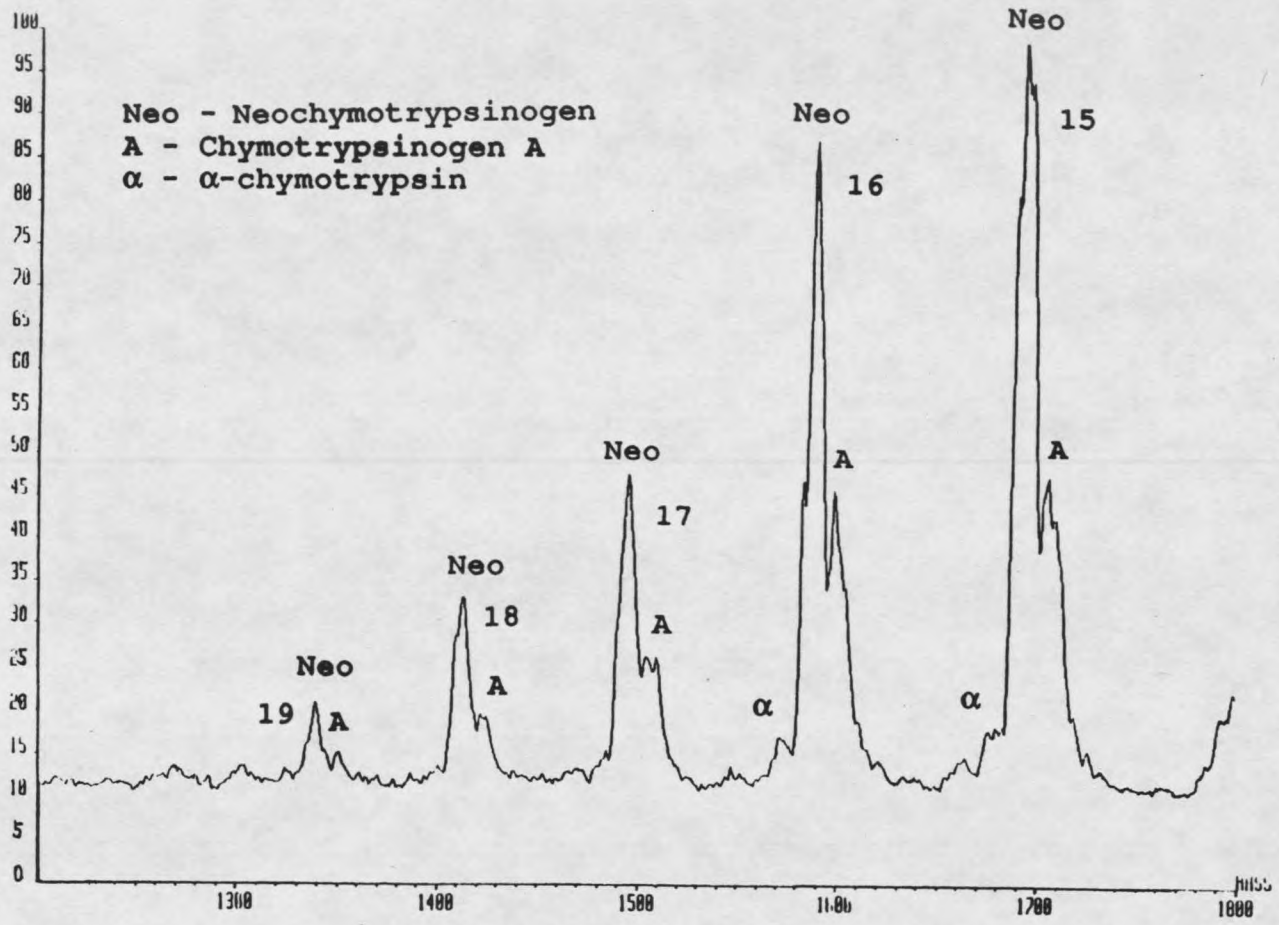

Figure 45. ESI mass spectrum of chymotrypsinogen derivatives dissolved in pure water. Of those, neochymotrypsinogen gave most intense peaks; α-chymotrypsin and chymotrypsinogen A presented weak intensities.

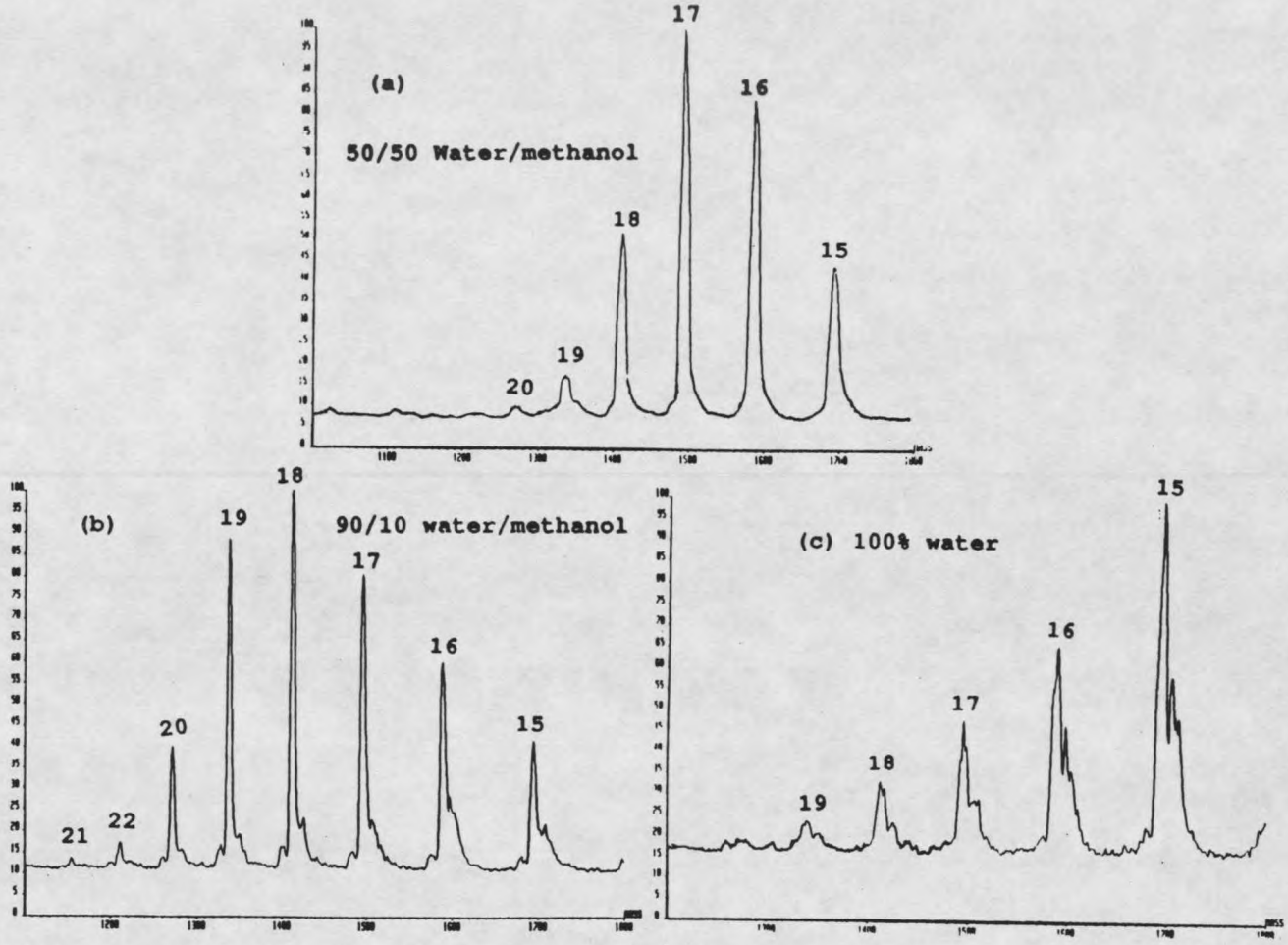

Figure 46. Effect of solution conditions to the presence of chymotrypsin derivatives. (a) Sample was dissolved in 50/50 water/methanol mixture with pH of 3. (b) Sample was dissolved in 90/10 water/methanol mixture with pH of 3. (c) Sample was dissolved in 100% water mixture with pH of 5.5.

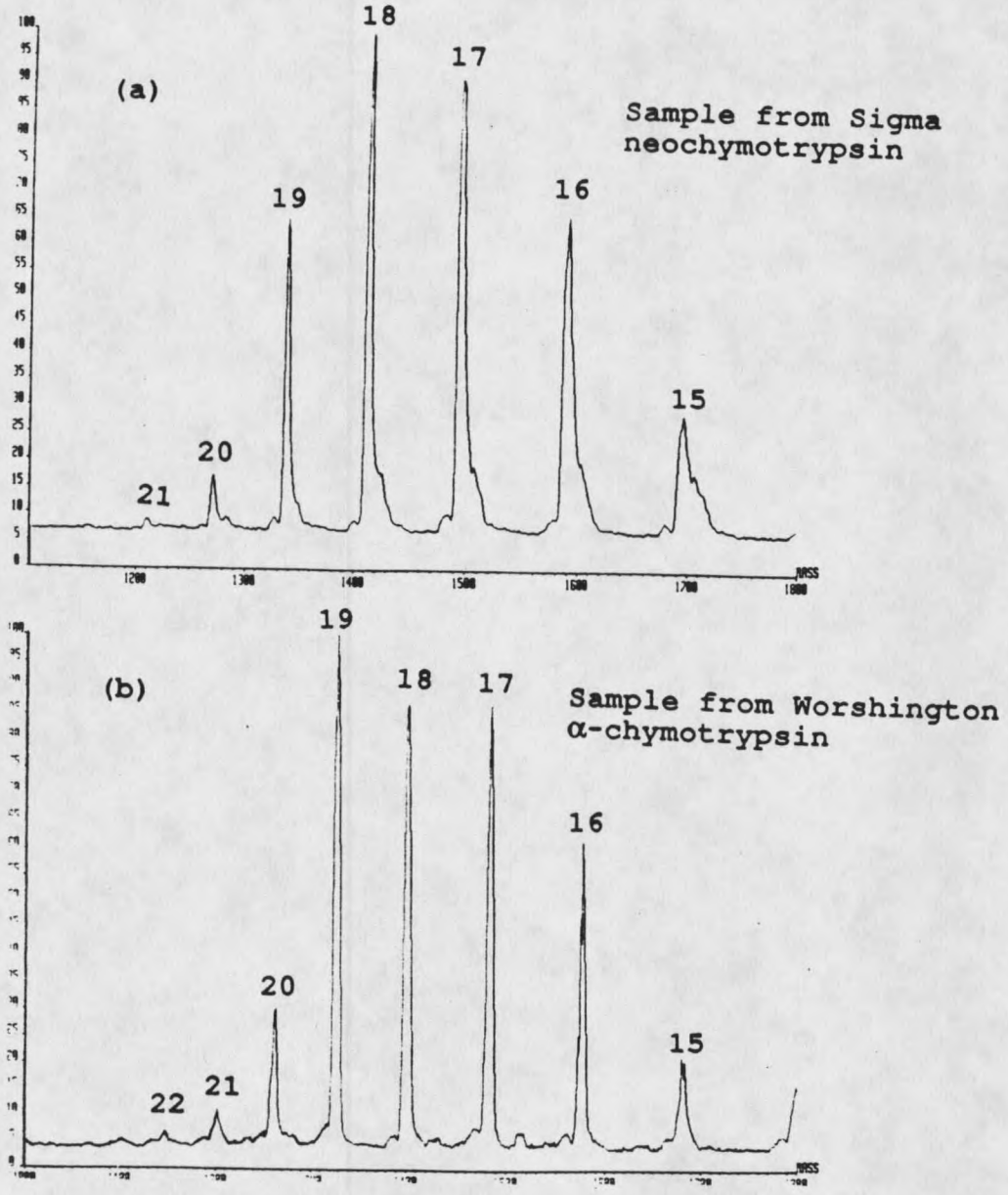

Figure 47. ESI mass spectra of α-chymotrypsin from different companies. (a) Sigma's sample contains only neochymotrypsinogen. (b) Worthington's sample contains only α-chymotrypsin.

HPLC/ESI/MS of Tryptic Digest of Modified Cytochrome c

The on-line coupling of HPLC with electrospray has proven to be an extremely powerful tool for the characterization of modified proteins. The protein is first tryptically digested and the resulting peptides are separated by HPLC (High Performance Liquid Chromatography) and mass determined by ESI/mass spectrometry. As an example, Hancoke and co-workers [83] obtained information on glycosylation sites in recombinant tissue plasminogen activator using this technique.

In the present study, horse heart cytochrome c was used as a model protein to develop the experimental procedure of combined HPLC/ESI/mass spectrometry for tryptic mapping. Subsequently, the sites of modification in a labeled cytochrome c was determined by the same procedure. The modified cytochrome c was obtained from Drs. Jesaitis and Quinn in the Department of Microbiology at Montana State University.

Cytochrome C

The cytochromes are iron-containing hemoprotein in which the iron atom oscillates between Fe^{3+} and Fe^{2+} during oxidation and reduction. Thus, these proteins rely on the redox potential of the iron atom to transfer electrons. Several different cytochromes occur in the respiratory chain, i.e., cytochromes b, c_1, c, a, and a_3. Of these, only cytochrome c

is soluble. The b and c cytochromes, like myoglobin, have iron-protoporphyrin IX as their heme group. In cytochrome c, the heme is covalently bound to polypeptide chain by thioether linkages to two cysteinyl residues, see Figure 48. In addition, a histidine coordinates to the iron atom much as His F8 does in myoglobin. Another side chain provides a sixth ligand, so that the iron atom is completely surrounded by an octahedral arrangement of ligands. Thus, the heme is firmly attached to polypeptide chain by means of residues Cys 14, Cys 17, and His 18 on the left, but its connection to the sixth ligand, on the right, seems more tenuous [126]. Horse heart cytochrome c is composed of 104 amino acids, yielding a molecular mass of 12,360 Da including the heme group.

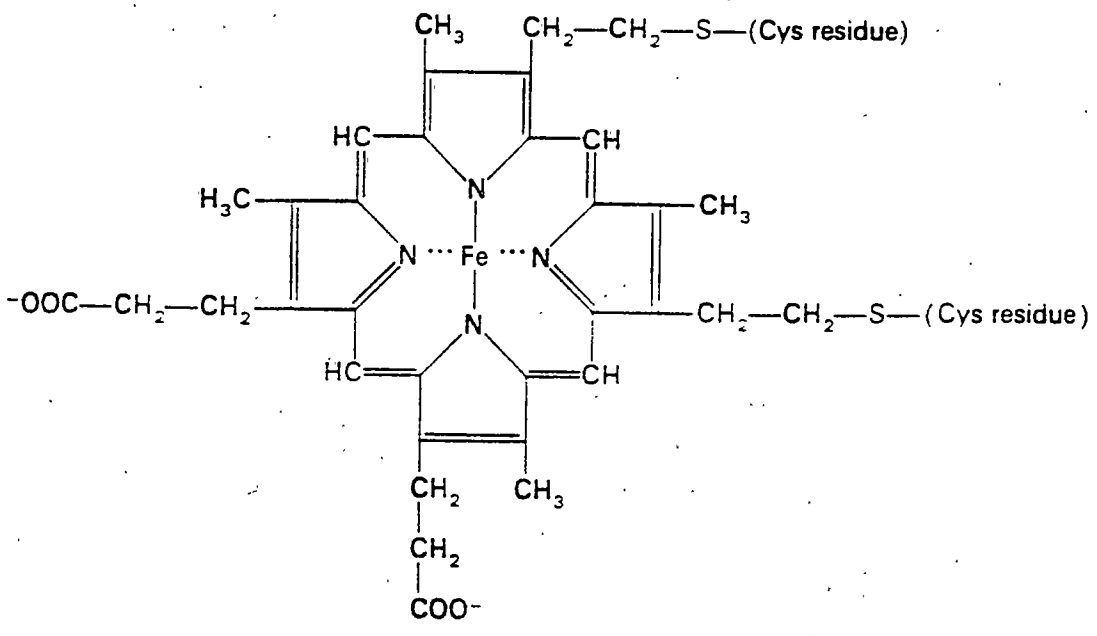

Figure 48. Heme of cytochrome c is covalently bonded to the sulfhydryl groups of two cysteines [102].

Modified cytochrome c

Electrospray/mass spectrometry was used to analyze both unmodified and modified cytochrome c. Figure 49 (a) shows the ESI mass spectrum of cytochrome c dissolved in a 50/50 water/methanol mixture. This spectrum has already been discussed in Figure 28. The measured molecular mass is 12,361, which closely agrees with the calculated mass of 12,360 Da. Figure 49 (b) shows the spectrum of modified cytochrome c. This sample was dissolved in pure water but otherwise electrosprayed under the same condition as cytochrome c in Figure 49 (a). There are two series of ion peaks. The most intense peaks have the same m/z values as unmodified cytochrome c and the charge distribution is similar. The extra series of peaks (marked black) between successive cytochrome c peaks yield a molecular weight of 12,860. The mass difference between labeled cytochrome c (12,860 Da) and the unlabeled cytochrome c (12,361 Da) is 499 Da. In this particular sample modification, a Cascade Blue derivative was covalently bonded to the cytochrome c. Cascade Blue derivatives are fluorescent dyes that are used as tracers and that chemically react with biological molecules [127]. The structure of the Cascade Blue derivative is shown in Figure 50. The molecular weight is calculated to be ca 500 Da. This matches the mass difference obtained between the two series of peaks in Figure 49 (b).

The low intensity of the modified cytochrome c probably

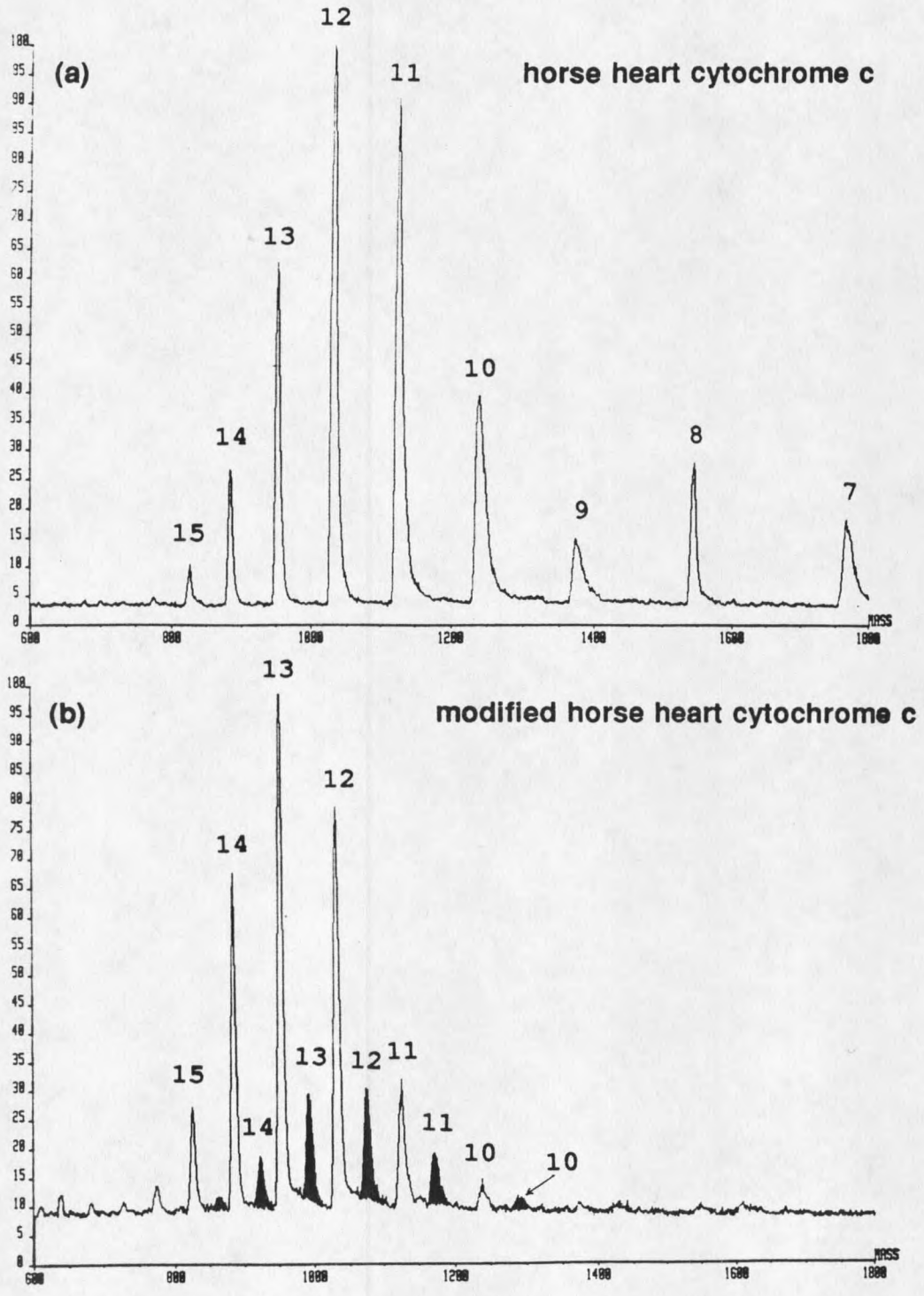

Figure 49. (a) ESI mass spectrum of horse heart cytochrome c. MW is 12,360 Da. (b) ESI mass spectrum of modified horse heart cytochrome c. Measured MW is 12,860 Da.

mean that only a small fraction of the cytochrome c had been modified while most of the protein was still intact.

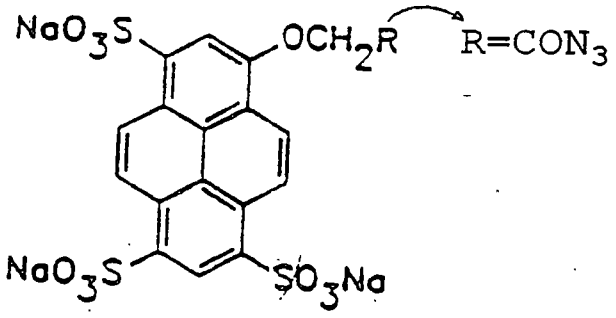

Figure 50. Structure of cascade blue derivative [127].

Figure 51 shows mass spectra of modified cytochrome c sprayed under different conditions. For Figure 51 (a), the solvent was pure water while for Figure 51 (b), it was (50/50) water/methanol mixture. The protein concentration was the same (40 μM). When comparing these two spectra, it is seen that the intensities of the cytochrome c ions are almost the same, but the modified cytochrome c peaks (marked black) are about three times higher in pure water than in the water/methanol mixture. It is expected that the sulfonate groups ($-SO_3Na$) is soluble in water but much less soluble in organic solvents, such as methanol. This might explain the intensity difference for the modified protein seen in Figure 51.

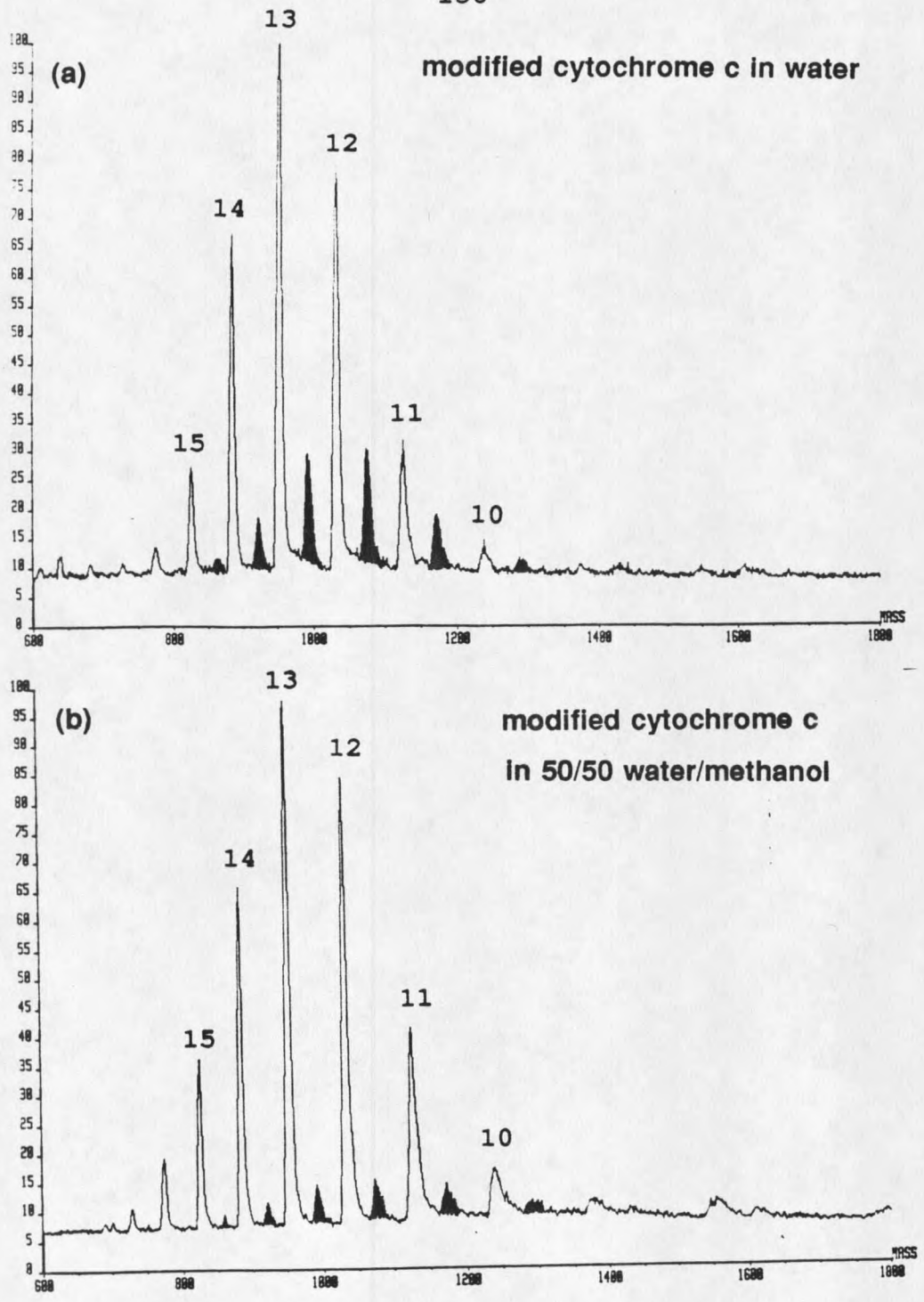

Figure 51. (a) ESI mass spectrum of modified cytochrome c that was dissolved in pure water. (b) ESI mass spectrum of modified cytochrome c that was dissolved in 50/50 water/methanol mixture.

Tryptic mapping of cytochrome c

The first step in this work was to tryptically digest cytochrome c with trypsin and to identify all the peptides produced. This information is needed as a comparison with results from modified cytochrome c using the same procedure.

The HPLC UV-absorbance chromatogram of horse heart cytochrome c tryptic digest is shown in Figure 52. Fractions of the column effluent from each absorbance peak were collected. Fraction numbers are indicated in the same figure. The approximate peptide concentration in a fraction collected from the HPLC is 0.5 μM. After evaporation of solvent under vacuum, the concentration was increased to 3 μM. Electrospray mass spectra of each fraction were then obtained. They are represented in Figure 53, with the fraction number given in the upper left corner. Most fractions gave high intensity spectra and good mass resolution. With a solution flow rate of 1 μL/min, about 3 pmol of peptides were consumed for each mass spectrum. It is seen that the peptides have higher sensitivities than the proteins. The reason is that the peptides are much smaller and have much lower charges. The spectrum from each fraction shows one or several prominent peaks.

The sequence of cytochrome c is shown in Figure 54 [128]. Trypsin breaks the polypeptide chain after the lysine and arginine amino acids. The peptide fragments anticipated to occur in this digest are indicated by broken lines in the

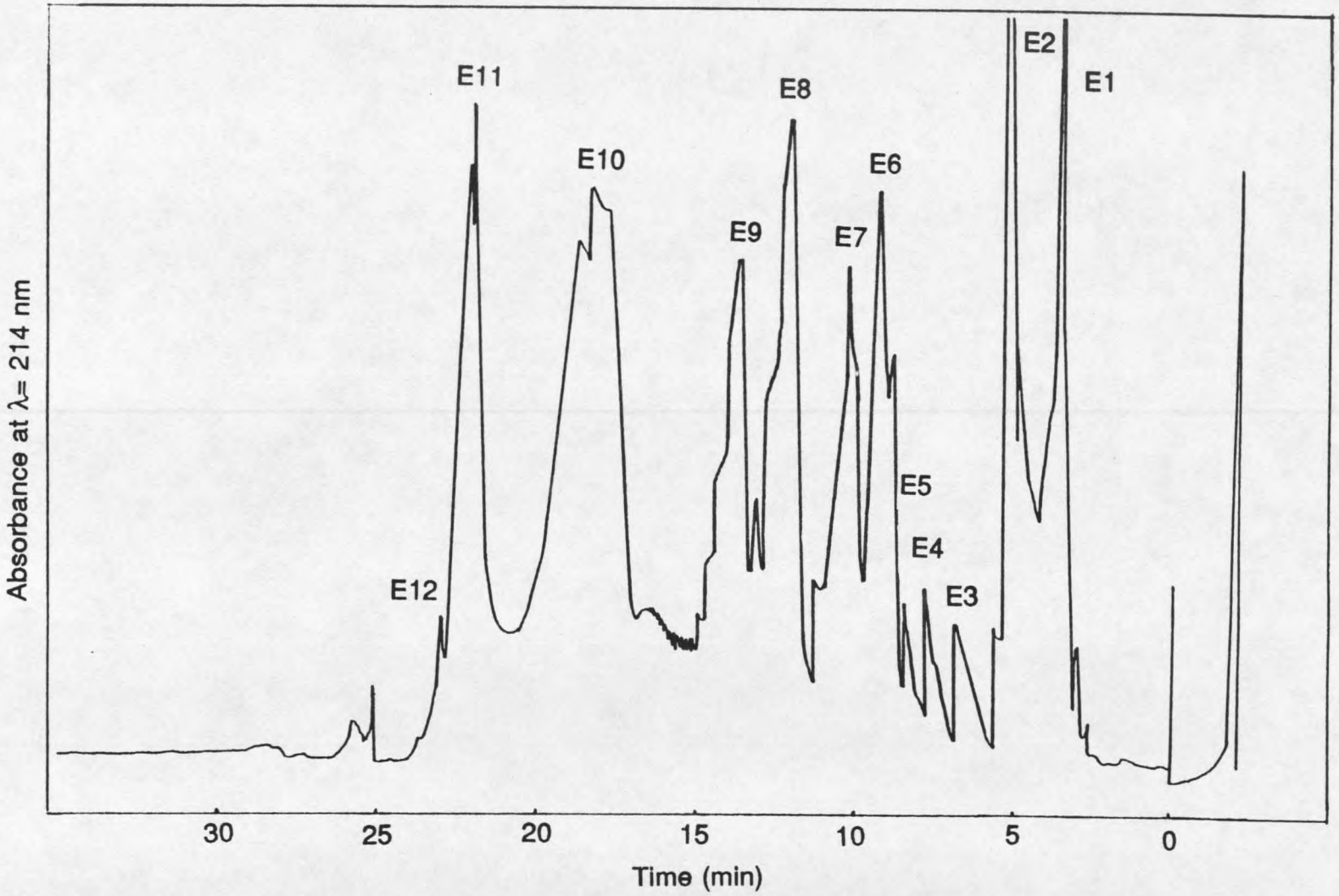

Figure 52. HPLC separation of tryptic digest mixture of horse heart cytochrome c. λ=214 nm. Solvent A: water with 1% HCl. Solvent B: acetonitrile with 1% HCl.

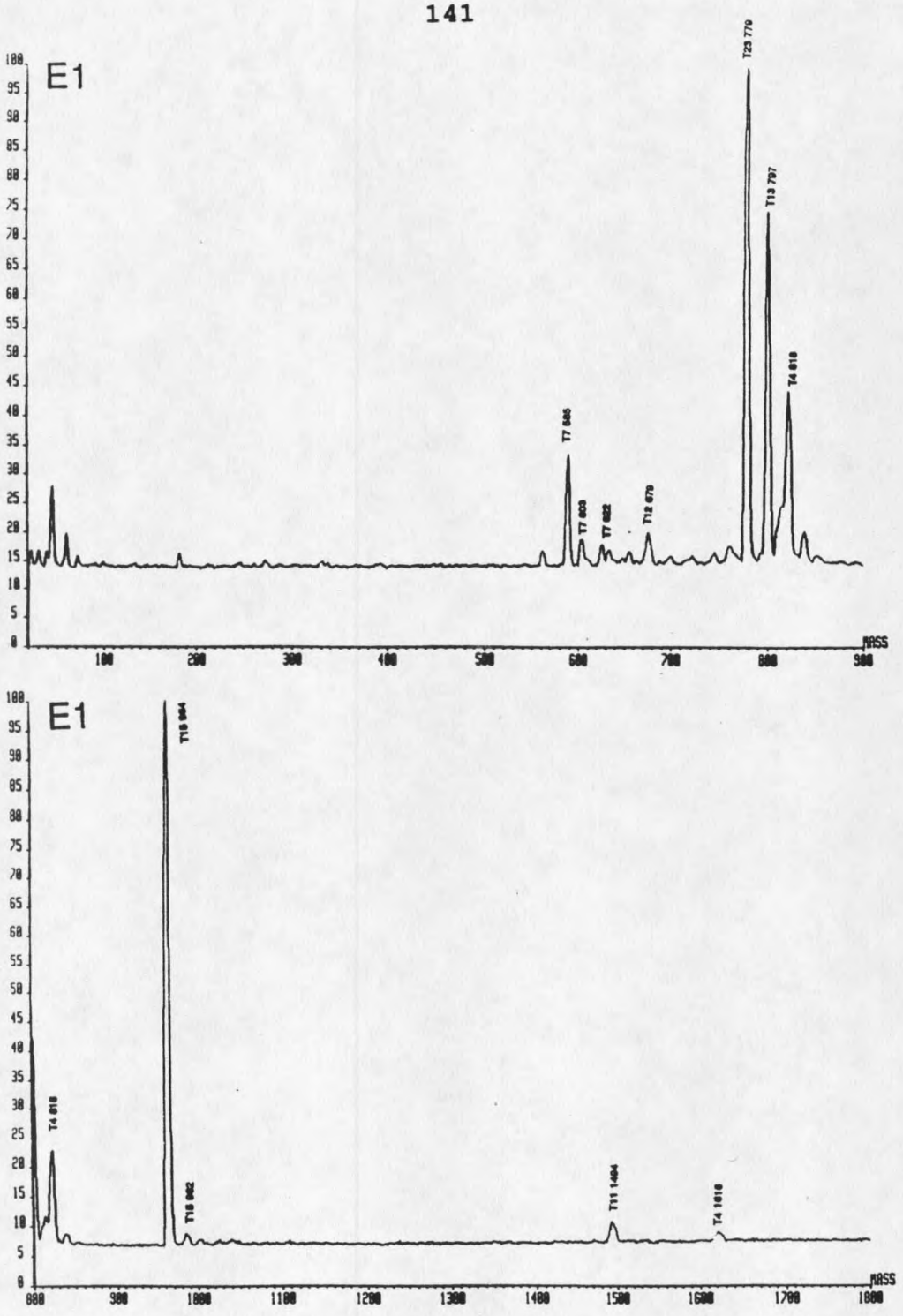

Figure 53 (E1). ESI mass spectra of HPLC effluents of tryptic digest cytochrome c.

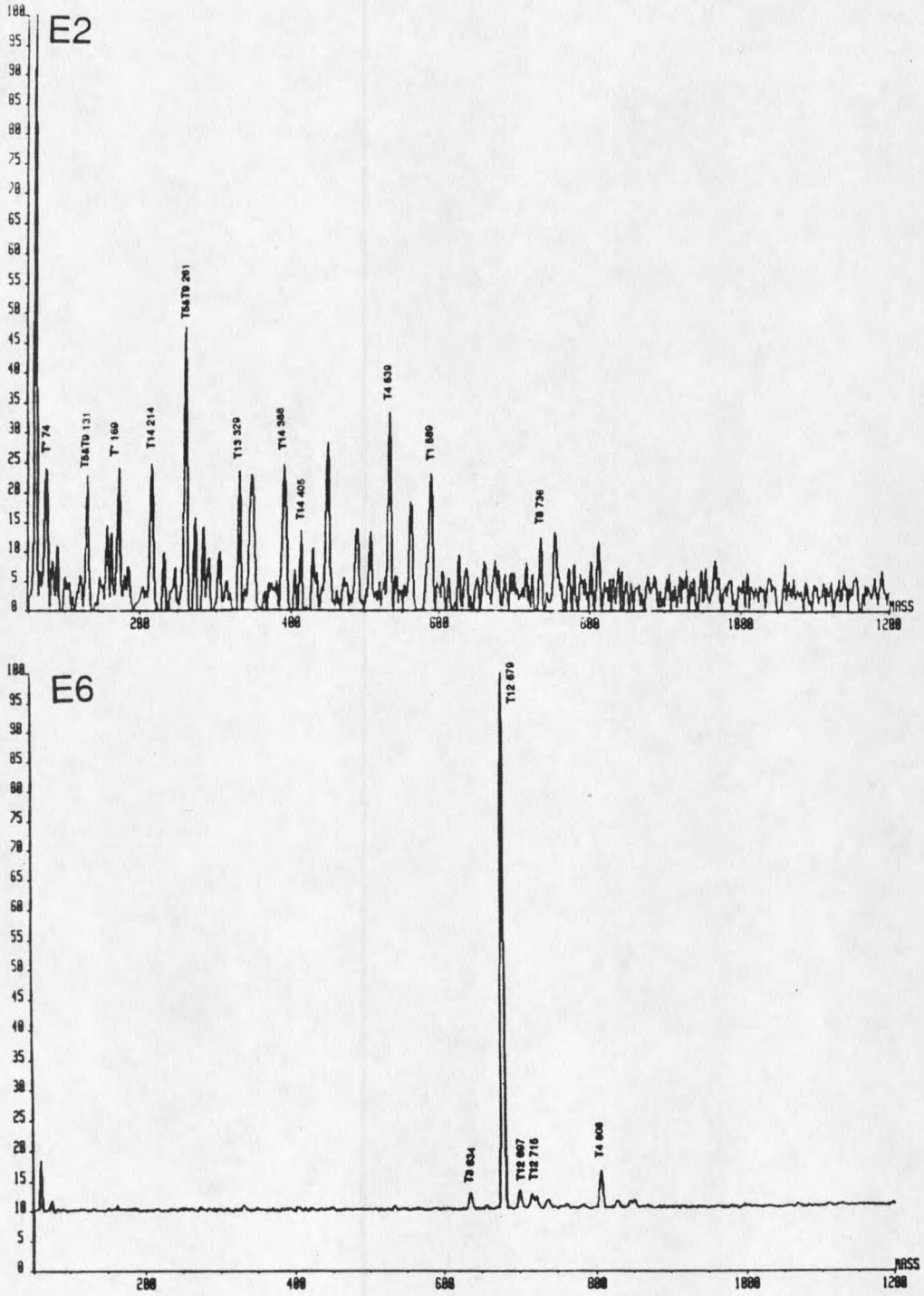

Figure 53 (E2,E6). ESI mass spectra of HPLC effluents of tryptic digest cytochrome c.

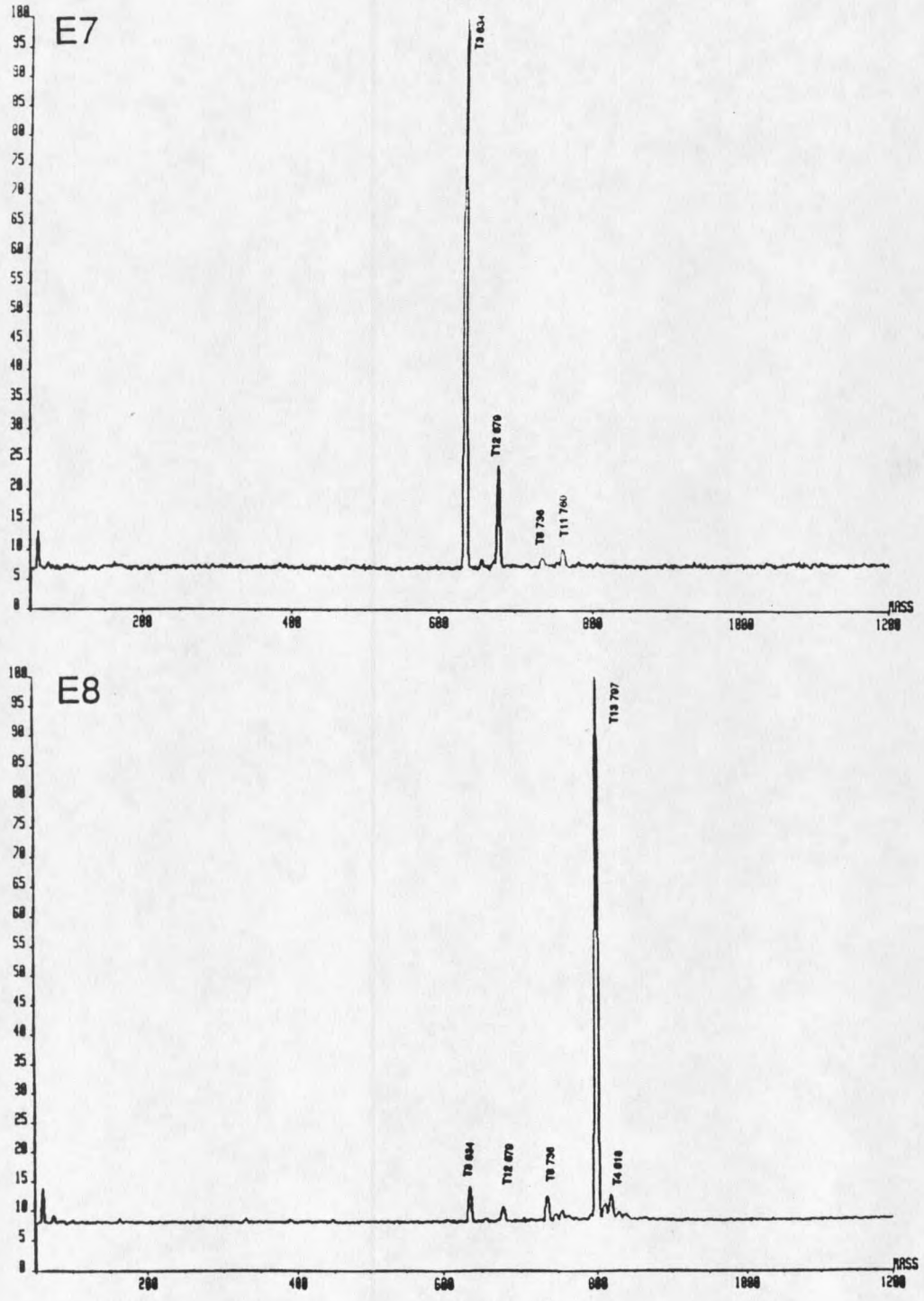

Figure 53 (E7,E8). ESI mass spectra of HPLC effluents of tryptic digest cytochrome c.

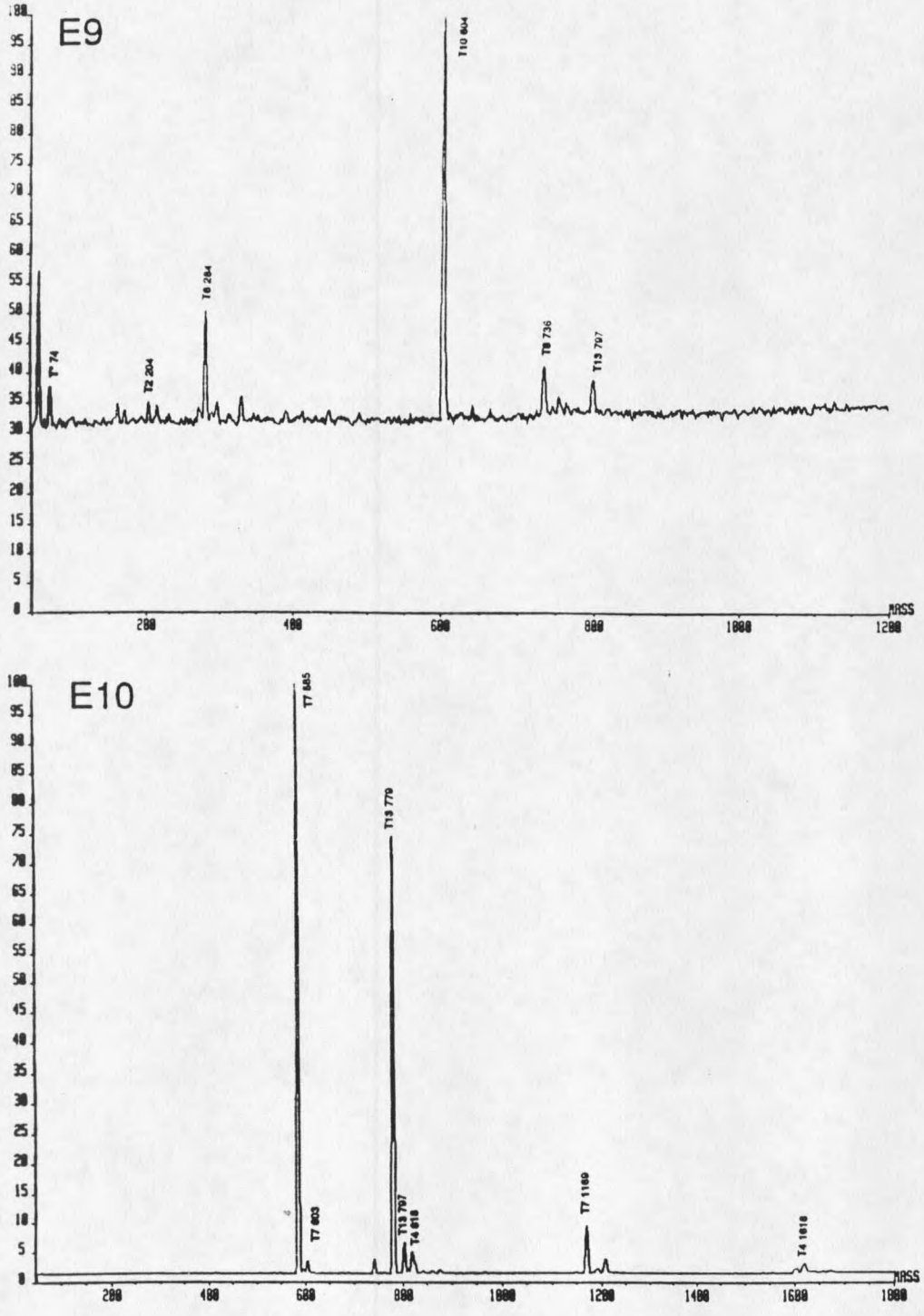

Figure 53 (E9,E10). ESI mass spectra of HPLC effluents of tryptic digest cytochrome c.

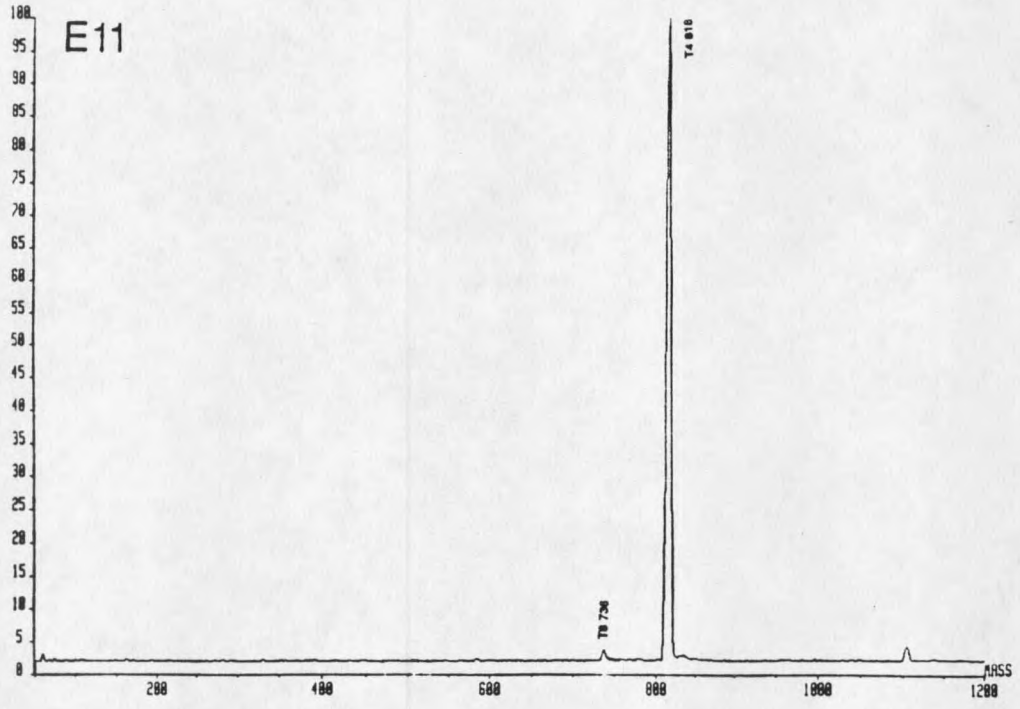

Figure 53 (E11). ESI mass spectra of HPLC effluents of tryptic digest cytochrome c.

figure. These fragments and their corresponding labels are listed in Table 10, together with their calculated masses.

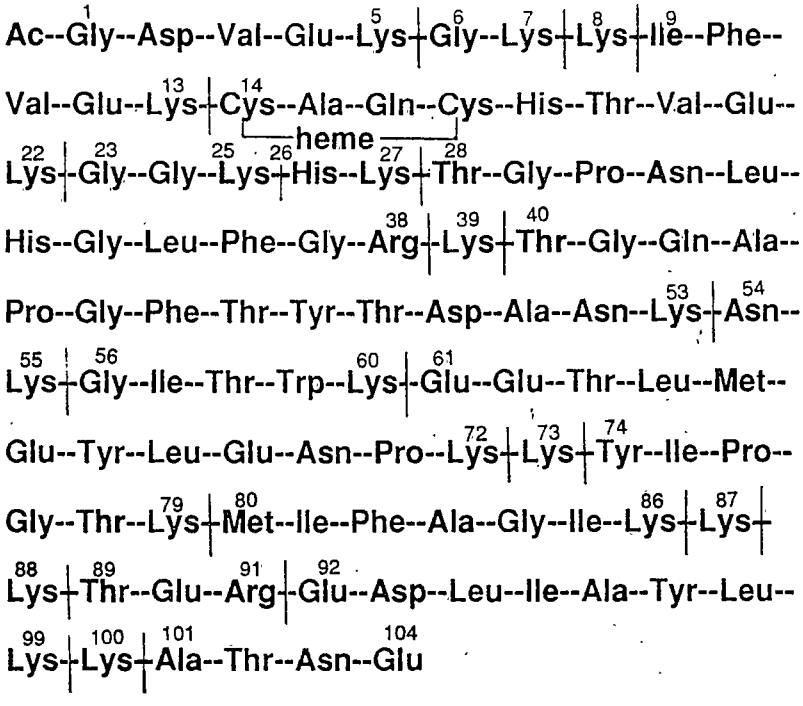

Figure 54. Sequence of cytochrome c and fgragments anticipated to occur in tryptic digest (indicated by vertical lines) [128].

Inspection of the ESI spectra in Figure 53 showed that all the expected peptides except one were indeed observed, within 1 - 2 Da of the expected mass. This was facilitated by the fact that each peptide has a distinct mass. All those fragments that were observed have "yes" signs and all those that were not observed have "no" signs in Table 10. The observed m/z and the identities of each ion are also given in the table. The reason that fragment T16 is missing in the ESI spectra is probably that this peptide (Ala-Thr-Asn-Glu) has only acidic sites.

Table 10: Peptide fragments from unmodified cytochrome c.

frag[a]	tryptic peptide	calc. mass	ion in ESI/MS	observed ions in ESI/MS	
				singly charged	doubly charged
Lys[b]	T*	146	yes	169 $(MNa)^+$	74 $(MH_2)^{+2}$
Ac1-5	T1	588	yes	589 $(MH)^+$	
6-7	T2	203	yes	204 $(MH)^+$	
9-13	T3	633	yes	634 $(MH)^+$	329 $(MHNa)^{+2}$
14-22	T4	1615	yes	1616 $(MH)^+$	809 $(MH_2)^{+2}$ 818 $(M \cdot H_2O)\,H_2^{+2}$
23-25	T5	260	yes	261 $(MH)^+$	131 $(MH_2)^{+2}$
26-27	T6	283	yes	284 $(MH)^+$	
28-38	T7	1168	yes	1169 $(MH)^+$	585 $(MH_2)^{+2}$ 603 $(M \cdot 2H_2O)\,H_2^{+2}$
40-53	T8	1470	yes		736 $(MH_2)^{+2}$
54-55	T9	260	yes	261 $(MH)^+$	131 $(MH_2)^{+2}$
56-60	T10	603	yes	604 $(MH)^+$	
61-72	T11	1495	yes	1496 $(MH)^+$	760 $(MHNa)^{+2}$
74-79	T12	678	yes	679 $(MH)^+$ 697 $(M \cdot H_2O)\,H^+$ 715 $(M \cdot 2H_2O)\,H^+$	
80-86	T13	778	yes	779 ($(MH)^+$ 797 $(M \cdot H_2O)\,H^+$	
89-91	T14	404	yes	405 $(MH)^+$	214 $(MH_2)^+$
92-99	T15	963	yes	964 $(MH)^+$ 982 $(M \cdot H_2O)\,H^+$	
101-104	T16	433	no		

[a] Fragments are derived from Figure 54. [b] Fragments that contain only one lysine.

Many of the cytochrome tryptic digests produce multiply charged ions, as seen in Table 10 and Figure 53 (E1-E11). All the heavier peptides, with molecular weight above 1000 Da, such as fragments T4, T7, T8, and T11, have doubly charged ions. Some smaller peptides, like T3, T5, T9, and T14, also give doubly charged ions. These peptides have at least two

basic sites including the N-terminus. Fragments T4 and T7 have very high doubly charge ion intensities since they have two basic amino acids, His & Lys, and His & Arg, respectively. Solvent attachment to the peptide ions is also seen in the ESI mass spectra. The HPLC solvent was originally composed of water, acetonitrile, and 1% hydrochloric acid. However, water is expected to remain as fractions evaporate under vacuum. Doubly charged as well as the singly charged peptides, fragments T4, T7, T12, T13, and T15, were observed with one water or two water molecules attached. In all cases, the bare ion was also observed and this can be seen from mass spectra where the intensity of MH^+ was significantly higher than that of $(M \cdot H_2O)H^+$. The solvent attachment is very common in electrospray ionization. Conditions of high temperature and high voltage bias between ion transport capillary and skimmer can eliminate solvation.

The tryptic peptide mixture of cytochrome c is not well separated in one HPLC experiment. In fact, each fraction contained at least two peptide fragments, fraction 2 (E2) contained as many as 8 peptides, see Figure 53. The extra dimension of information provided by ESI mass analysis allows for the easy identification of the unseparated components. FAB/MS has also been used to identify tryptic fragments of cytochrome c [128]. However, peptides of T2, T5, T6, T8, T9, T14, and T16 were not detectable by FAB. This was probably due to the wide range surface activities of the peptides. In

FAB, this results in sensitivity and suppression problems. In contrast, by using ESI, all the peptide fragments (except T16) were detected. Other advantages with electrospray are high sensitivity and low background noise.

Labelling Sites In Cytochrome c

Cytochrome c, covalently labeled with Cascade Blue, was first tryptically digested under the same condition as cytochrome c. The peptide mixture was then separated by HPLC and mass analyzed by ESI/MS in the same process as discussed above. Figure 55 shows the HPLC UV-absorbance chromatogram of the tryptic peptides. Again, fractions were collected as labeled in the figure. The fractions were then concentrated under vacuum and introduced to ESI mass spectrometer for mass determination. The concentration of the original modified cytochrome c was very low, only about 50 μM. After HPLC separation, the concentrations were about 3 nM. This was increased to about 20 nM (0.02 μM) by vacuum treatment. Figure 56 (E1-E12) show the ESI mass spectra of the fractions from Figure 55. Fraction numbers are also indicated for each mass spectrum. With solution flow rate of 1 μL/min, about 2×10^{-14} mole (20 fmole) of peptide were consumed in order to record the mass spectrum. With such low concentrations, the intensity in the mass spectra are seen to be low. However, there is still enough information for mass determination and peptide fragment identification.

Table 11: Peptide fragments from modified cytochrome c.

frag[a]	tryptic peptide	calc. mass	ion in ESI/MS	observed ions in ESI/MS	
				singly charged	doubly charged
Lys[b]	T*	146	yes	169 $(MNa)^+$	74 $(MH_2)^{+2}$ 85 $(MHNa)^{+2}$
Ac1-5	T1	588	yes	589 $(MH)^+$	
6-7	T2	203	yes		102 $(MH_2)^{+2}$ 120 $(M \bullet 2H_2O)\,H_2^{+2}$
9-13	T3	633	yes	634 $(MH)^+$	329 $(MHNa)^{+2}$
14-22	T4	1615	yes		809 $(MH_2)^{+2}$
23-25	T5	260	yes	261 $(MH)^+$	153 $(MNa_2)^{+2}$
26-27	T6	283	no		
28-38	T7	1168	yes	1169 $(MH)^+$	585 $(MH_2)^{+2}$
40-53	T8	1470	yes		736 $(MH_2)^{+2}$
54-55	T9	260	yes	261 $(MH)^+$	153 $(MNa_2)^{+2}$
56-60	T10	603	yes	604 $(MH)^+$	
61-72	T11	1495	yes		749 $(MH_2)^{+2}$
74-79	T12	678	yes	679 $(MH)^+$	340 $(MH_2)^{+2}$
80-86	T13	778	yes	779 $(MH)^+$ 797 $(M \bullet H_2O)\,H^+$	
89-91	T14	404	yes		214 $(MHNa)^{+2}$
92-99	T15	963	yes	964 ($(MH)^+$	483 $(MH_2)^{+2}$
101-104	T16	433	no		

[a] Fragments are derived from Figure 54. [b] Fragments that contain only one lysine.

Table 11 lists all the tryptic peptides of modified cytochrome c observed in the mass spectra. In general, the ions obtained from labeled cytochrome c (see Table 11) are very similar to those obtained from unlabeled cytochrome c (see Table 10). There are few differences, however: (1) The ion intensities for unmodified cytochrome c are much higher than for modified cytochrome c. This is because the

concentration of unmodified protein was 15 times higher than that of modified one. (2) Water attachment was more commonly observed for unmodified cytochrome c, i.e., for T4, T7, T12, T13, and T15. In contrast, sodium attachment was observed for the modified cytochrome c. Thus, T*, T3, T5, T9, and T14 were observed with one or two Na^+ ions. It is expected that the modified sample should have a relatively high Na^+ concentration since the label compound contains sodium (see Figure 50). The mass spectra also showed a very high intensity of Na^+ at m/z=23. (3) Peptide fragment T6 is present in the unmodified cytochrome c but not in the modified cytochrome c. Thus, fraction 9 (E9) of unmodified cytochrome c (see Figure 53) shows an intense ion peak at 284 due to peptide fragment T6. However, this peak was not found in any of the fractions from the modified cytochrome c.

The site of labeling in cytochrome c can not be determined from the present data. Ideally, a labeled peptide should be detected with a molecular weight of the peptide plus the label. It is sure that some additional ions are found in the fraction spectra in Figure 56. A polyethylene glycol impurity is seen in fraction E7. More noteworthy is the m/z=392 in fractions E10 - E12. This happens to equal the expected mass of the doubly protonated ion of peptide T6 (m/z=283) bound to the label (m/z=500±2). However, additional work is required to decide whether this is correct.

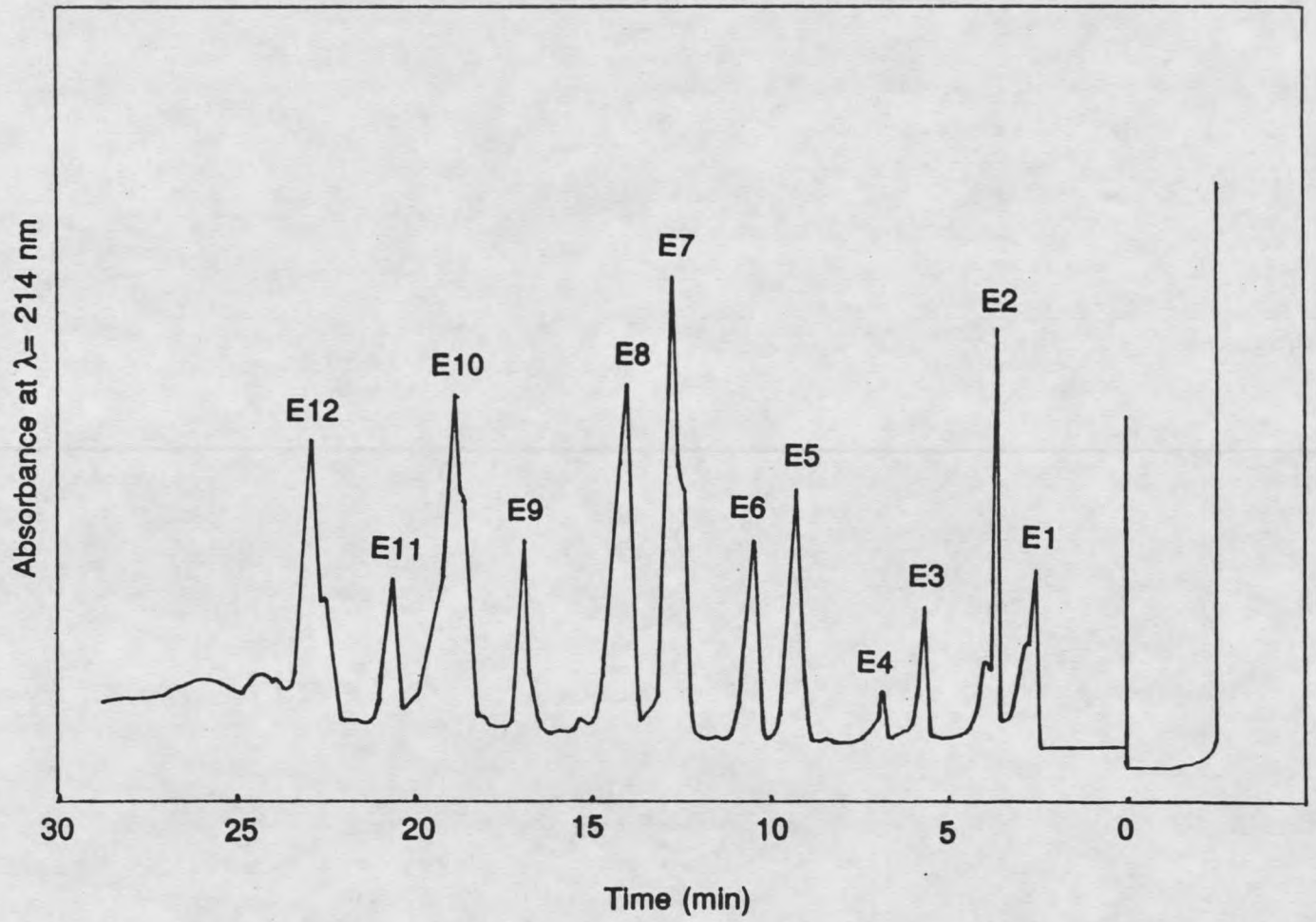

Figure 55. HPLC separation of tryptic digest mixture of modified horse heart cytochrome c. Experimental conditions were same as shown in Figure 52.

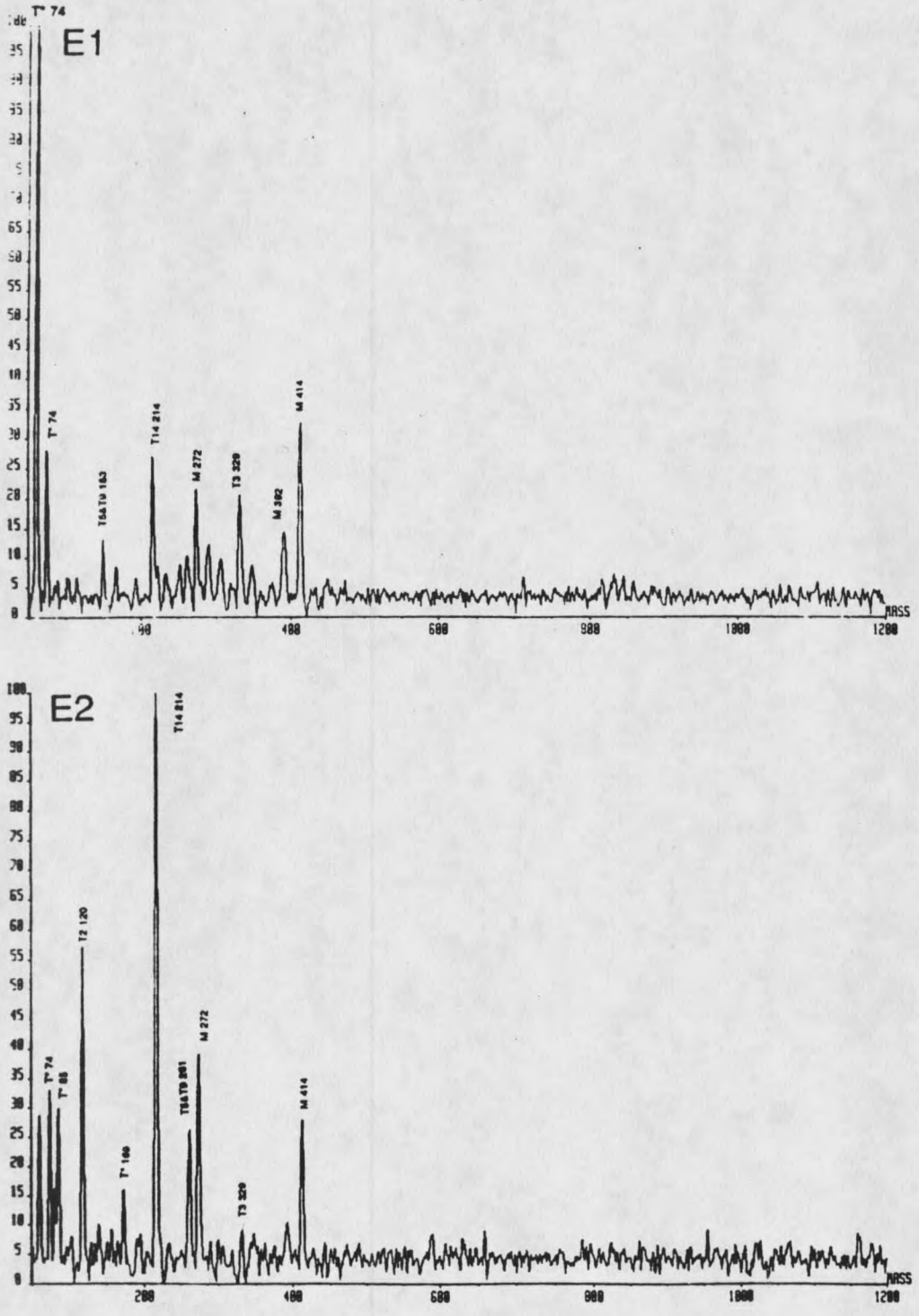

Figure 56(E1, E2). ESI mass spectra of HPLC effluents of tryptic digest cytochrome c.

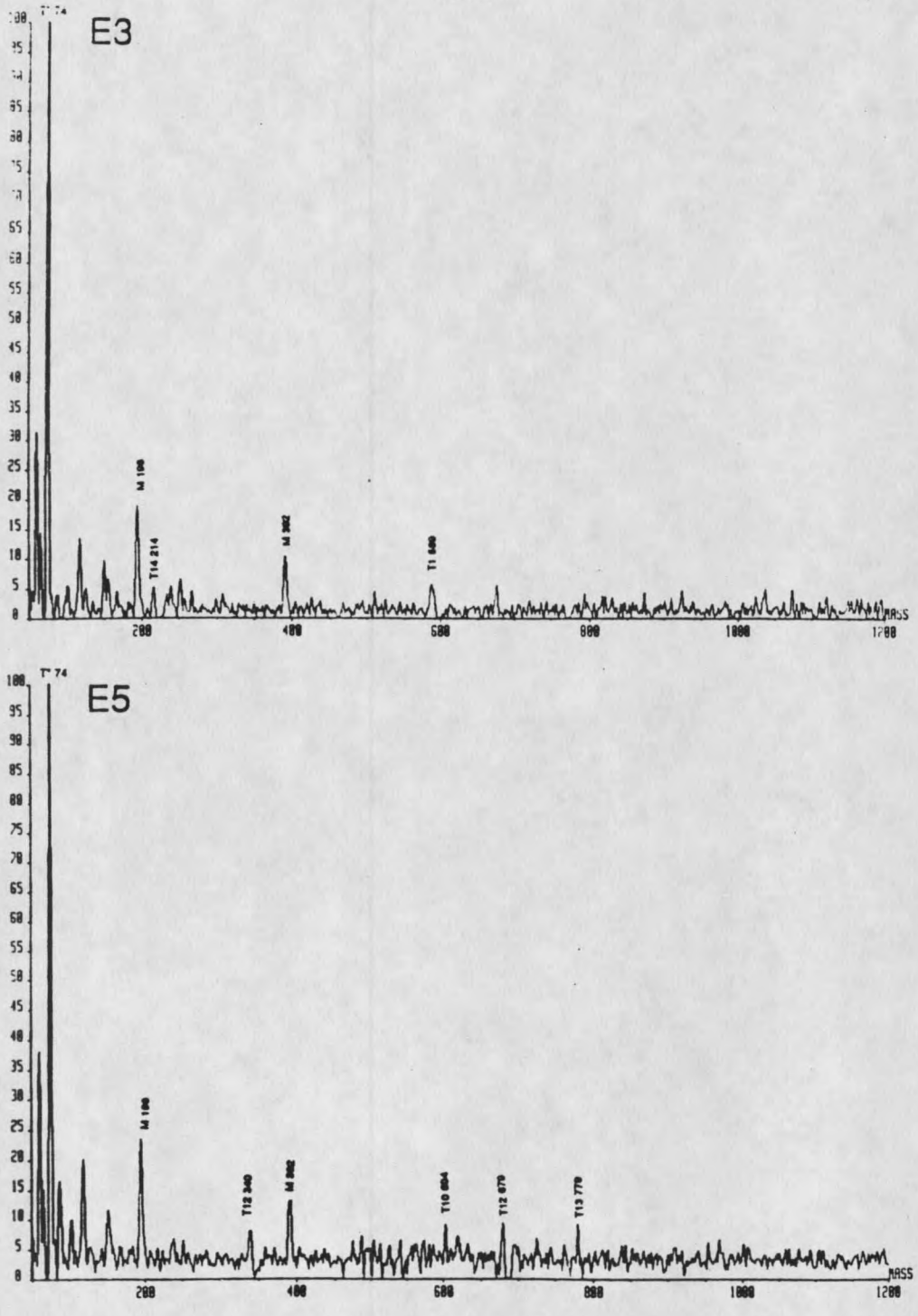

Figure 56(E3, E5). ESI mass spectra of HPLC effluents of tryptic digest cytochrome c.

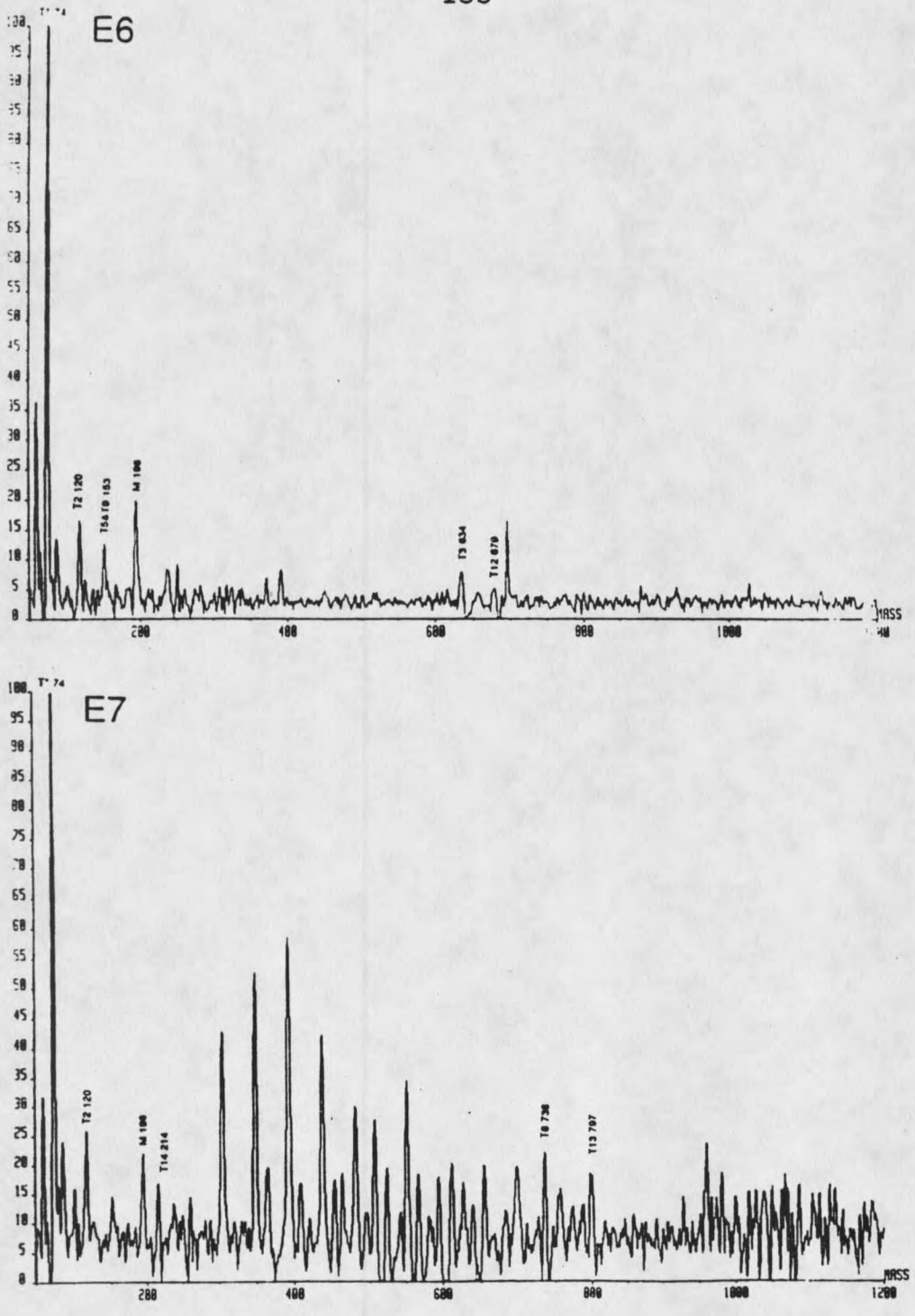

Figure 56(E6, E7). ESI mass spectra of HPLC effluents of tryptic digest cytochrome c.

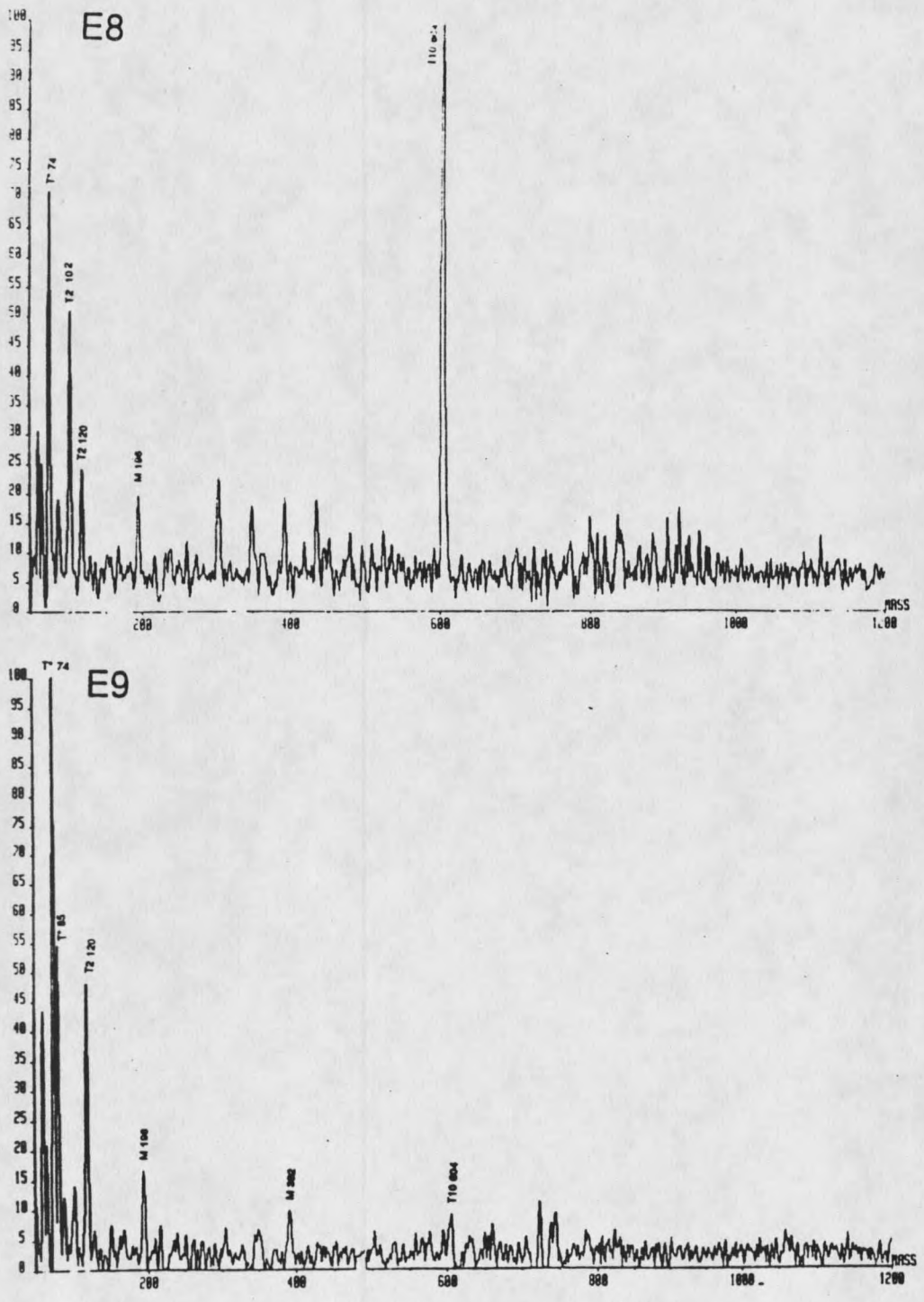

Figure 56(E8, E9). ESI mass spectra of HPLC effluents of tryptic digest cytochrome c.

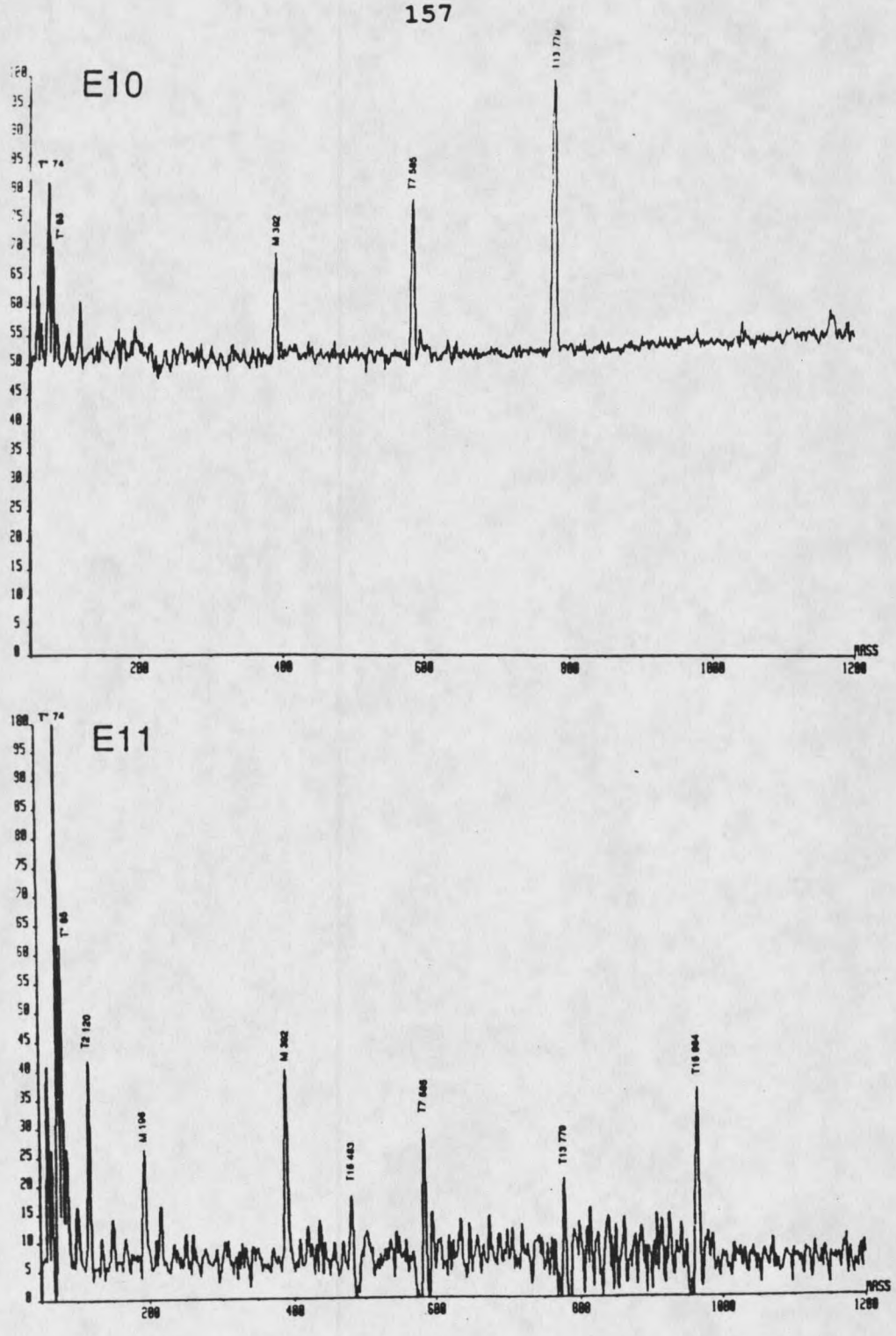

Figure 56(E10, E11). ESI mass spectra of HPLC effluents of tryptic digest cytochrome c.

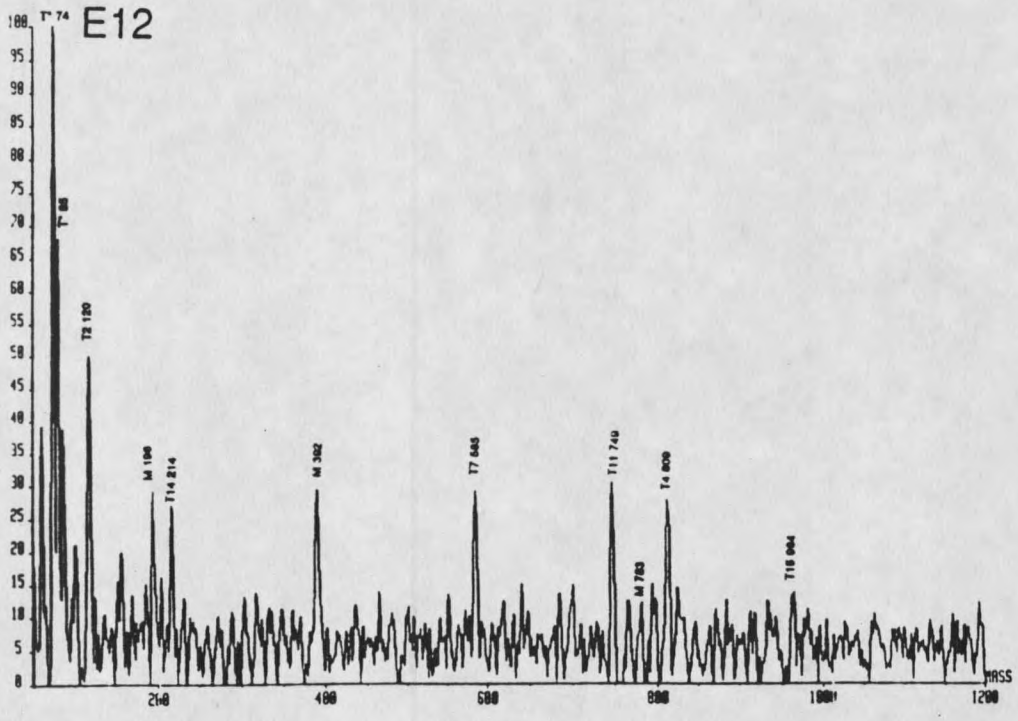

Figure 56(E12). ESI mass spectrum of HPLC effluent of tryptic digest cytochrome c.

CONCLUSIONS

1. Ion transport through capillaries follows a diffusion model. Thus, the loss of ion current is due to the ions diffusing to the capillary wall. The observed transmission efficiency is, however, often much larger than that calculated assuming a constant gas velocity profile over the capillary cross section. The effect of the actual parabolic flow profile is to decrease ion loss to the capillary wall and greatly increase the transmission efficiency.

2. A home built electrospray ion source was successfully installed and optimized. With this source, excellent spectra of very large proteins, up to 40,000 Da, were obtained. Accurate molecular weights were calculated from the spectra.

3. The conformation of myoglobin, as studied by the dissociation of the heme-myoglobin complex, is affected by the presence of acids, organic compounds, and by the temperature of the electrospray solution as well as of the gas phase. Acetic acid addition to the ion source gas phase can give high ion intensities and higher charge states without disruption of the non-covalent heme-myoglobin complex. This is important for future studies of non-covalently bonded protein-ligand complexes. In contrast, acid addition to the liquid phase tends to denature the protein.

4. An experimental protocol for the analysis of modified proteins through tryptic digestion followed by HPLC and electrospray mass spectrometry was developed. Cytochrome c, unlabeled as well as labeled with a fluorescent ligand was analyzed with this technique.

REFERENCES

[1] J.B. Fenn, M.Mann, C.K. Meng, S.F. Wong, Mass Spec. Rev., Vol. 9, 37 (1990).

[2] M. Dole, L.L. Mack, R.L. Hines, R.C. Mobley, L.D. Ferguson, M.B. Alice, H. Chem. Phys., Vol. 49, 2240 (1968).

[3] S.F. Wong, C.K.Meng, J.B. Fenn, J. Phys. Chem., Vol. 92, 546 (1988).

[4] C.K. Meng, M. Mann, J.B. Fenn, Phys. D. Atoms. Mol. Clusters, Vol. 10, 361 (1988).

[5] L.L. Mach, P. Kralik, A. Rheude, M. Dole, J. Chem. Phys., Vol. 52, 4977 (1970).

[6] G.A Clegg, M. Dole, Biopolymers, Vol. 10, 821 (1971).

[7] D. Teer, M Dole, J. Polym. Sci., Vol. 13, 985 (1975)

[8] C. M. Whitehouse, R. N. Dryer, M Yamashita, J. B. Fenn, Anal. Chem., Vol. 57, 675 (1985).

[9] C. M. Whitehouse, R. N. Dryyer, M. Yamashita, J. B. Fenn, Anal. Chem., Vol. 57, 675 (1985).

[10] J. B. Fenn, M. Mann, C. K. Meng, S. F. Wang, C. M. Whitehouse, J. Science, Vol. 246, 64 (1989).

[11] R. J. Beuhler, E. Flanigan, L. J. Green, L. J. Friedman, J. Am. Chem. Soc., Vol. 96, 3990 (1974).

[12] M. Karas, F. Killenkamp, Anal. Chem. Vol. 60, 2299 (1988).

[13] M. Barber, B. N. Green, Rapid Commun. Mass Spectrom., Vol. 1, 80 (1987).

[14] G. Jonsson, A. Hedin, P. Hakansson, B. U. R. Sundquist, H. Bennich, P. Roepstorff, Rapid Commun. Mass Spectrom., Vol. 3, 190 (1989).

[15] J. A. Loo, H. R. Udseth, R. D. Smith, Rapid Commun. Mass Spectrom., Vol. 2, 207 (1988).

[16] J. A. Loo, J. R. Udseth, R. D. Smith, Biomed. Environ, Mass Spectrom., Vol. 17, 411 (1988).

[17] J. A. Loo, H. R. Udseth, R. D. Smith, Anal. Biochem., Vol 176, 404 (1989).

[18] R. D. Smith, D. J. Barinaga, J. R. Udseth, J. Phys. Chem., Vol. 93, 5019 (1989).

[19] T. R. Covey, R. F. Bonner, B. I. Shushan, J. Henion, Rapid Commun. Mass Spectrom. Vol. 2, 249 (1988).

[20] Marcia Barinaga, Science, Vol. 246, 32 (1989).

[21] E. D. Lee, J. D. Henion, T. R. Covey, J. Microcolumn Spec. Vol. 1, 14 (1989).

[22] R. D. Smith, J. A. Loo, C. J. Barinaga, C. G. Edmonds, H. R. Udseth, J. Am. Soc. Mass Spectrom. Vol. 1, 53 (1990).

[23] R. D. Smith, J. A. Loo, C. G. Ednomds, C. J. Barinaga, H. R. Udseth, Anal. Chem., Vol. 62, 883 (1990).

[24] M. Yamashita, J. B. Fenn, J. Phys. Chem., Vol. 88, 4671

(1984).
[25] D. Michelson, J. D. Shorey, Nucl. Instrum. Methods, Vol. 82, 295 (1970).
[26] G. I. Taylor, Proc. R. Soc. London, A 280, 383 (1964)
[27] V. E. Krohn, J. Appl. Phys., Vol. 45, 1144 (1974).
[28] A. P. Bruins, T. R. Covey, J. D. Henion, Anal. Chem., Vol. 98, 2642 (1987).
[29] J. W. S. Rayleigh, Philos. Mag., Vol. 14, 184 (1882).
[30] E. W. Muller, Phys. Rev., Vol. 102, 618 (19560.
[31] F. W. Rollgen, E. Bramer-Wegner, L. Buffering, J. Phys., Vol. 48, C6-253 (1987).
[32] G. Schmelzeisen-Redeker, L. Buffering, F. W. Rollgen, Int. J. Mass Spectrom. Ion Processes, Vol. 90, 139 (1989).
[33] N.B. Zolotoi, G. V. Karpov, V. E. Skurat, Sov. Phys. - Tech. Phys., Vol. 33, 193 (1988).
[34] J. V. Iribarn, B.A. Thomson, J. Chem. Phys., Vol. 64, 2287 (1976).
[35] J. V. Iribarn, P. J. Dziedzic, B.A. Thomson, Int. J. Mass Spctrom. Ion Phys., Vol. 50, 331 (1983).
[36] M. Yamashita, J. B. Fenn, J. Phys. Chem., Vol. 88, 4451 (1984).
[37] S. K. Chowdhury, V. Katta, R.C. Beavis, B. T. Chait, J. Am. Soc. Mass Spectrom., Vol. 1, 382 (1990).
[38] R. Katta, S. K. Chowdhury, B. T. Chait, J. Am. Chem. Soc., Vol. 112, 5348 (1990).
[39] E. W. McDaniel, E. A. Mason, The Mobility and Diffusion of Ions in Gases, John Wiley & Sons, Inc. (1973).
[40] W. L. McCabe, J. C. Smith, P. Harriott, Unit Operation of Chemical Engineering, 4th Edition, McGraw-Hill Inc. (1985).
[41] C. K. Meng, J. B. Fenn, Organic Mass Spectrom., Vol. 26, 542 (1991).
[42] J. A. Loo, R. R. Ogorzalek Loo, K. J. Light, C. G. Edmonds, R. D. Smith, Anal. Chem., Vol. 64, 81 (1992).
[43] J. A. Loo, R. R. Ogorzalek Loo, H. R. Udseth, C. G. Edmonds, R.D. Smith, Rapid Commun. Mass Spectrom., Vol. 5, 101 (1991).
[44] J. A. Loo, C. G. Edmonds, H. R. Udseth, R.D. Smith, Anal. Chem., Vol. 62, 693 (1990).
[45] C. G. Edmonds, J. A. Loo, R. R. Ogorzalek Loo, H. R. Udseth, C. J. Barinaga, R.D. Smith, Biological Mass Spectrom., Vol 19, 943 (1991).
[46] J. A. Loo, C. G. Edmonds, R. D. Smith, Anal. Chem., 63, 2488 (1991).
[47] R. D. Smith, J. A. Loo, C. G. Edmonds, C. J. Barinaga, J. R. Udseth, J. Chromatography, Vol 516, 157 (1990).
[48] S.K. Chowdhury, B. T. Chait, Biomed. Biophys. Reas. Commun., Vol 173, 927 (1990).
[49] K. L. Duffin, J. D. Henion, J. J. Shieh, Anal. Chem., 63, 1781 (1991).
[50] A. P. Bruins, J. Chromatography, Vol. 554, 39 (1991).

[51] S. A. Carr, M. E. Hemling, M. F. Bean, G.D. Roberts, Anal. Chem., Vol. 63, 2802 (1991).
[52] K. D. Henry, J. P. Quinn, F.W. McLafferty, J. Am. Chem. Soc., Vol. 113, 5447 (1991).
[53] C. K. Meng, C. N. McEwen, B. S. Larsen, Rapid Commun. Mass Spectrom., Vol. 4, 147 (1990).
[54] B.S. Larsen, C. n. McEwen, J. Am. Soc. Mass Spectrom., Vol. 2, 205 (1991).
[55] J. F. J. Todd, A. D. Penman, Int. J. Mass Spectrom. Ion Processes, Vol. 106, 1 (1991).
[56] M. Sakairi, A. L. Yergey, K. W. Michael Sui, J. C. Y. L. Blanc, R. Guevremont, S.S. Berman, Anal. Chem., Vol 63, 1488 (1991).
[57] M. Hamdan, O. Curcuruto, Int. J. Mass Spectrom. Ion Processes, Vol. 108, 93 (1991).
[58] J. A. Loo, H. R. Udseth, R.D. Smith, Anal Biochem., Vol. 179, 404 (1989).
[59] D. K. Meng, M.Mann, J. B. Fenn, I. Phys. D., Vol. 10, 361 (1988).
[60] T. R. Covey, R. F. Bonner, B. I. Shushan, J. D. Henion, Rapid Commun. Mass Spectrom., Vol. 2, 249 (1988).
[61] I. Hayati, A. I. Bailey, T. F. Tadros, J. Colloid Interface Sci., Vol. 117, 222 (1987).
[62] Y. Konishi, R. Feng, The 40th ASMS Conference on Mass Spectrometry and Allied Topics, (1992).
[63] P. R. Griffin, J. A. Coffman, L. E. Hood, J. R. Yates III, Int. J. Mass Spectrom. Ion Processes, Vol. 111, 131 (1991).
[64] J. M. Meek, J. D. Craggs, Electrical Breakdown of Gases, Clarendon Press Oxford (1953).
[65] L. G. Christophorou, Adv. Electronics and Electron. Physics, Vol. 46, 55 (1987).
[66] M. G. Ikonomou, A. T. Blades, P. Kebarle, Anal. Chem., Vol. 63, 1989 (1991).
[67] A. T. Blades, P. Jayaweera, M. G. Ikonomou, P. Kebarle, J. Chem. Phys., Vol. 92, 5900 (1990).
[68] S. K. Chowdhury, B. Chait, Anal. Chem., Vol 63, 1660 (1991).
[69] T. E. Creighton, Proteins: Structures and Molecular Principles, W. H. Freeman, New York (1984).
[70] S. Lapanje, Physicochemical Aspects of Protein Denaturation, Wiley-Interscience, New York (1978).
[71] J. A Loo, C. G. Edmonds, R. D. Smith, Science (Washington D. C.), Vol. 248, 201 (1990).
[72] V. Katta, B. T. Chait, Rapid Commun. Mass Spectrom., Vol. 5, 214 (1991).
[73] R. Feng, Y. Konishi, The 40th ASMS Conference on Mass Spectrom. and Allied Topics, (1992).
[74] C. Ghelis and J. Yon, Protein Folding, pp. 225-239, Academic Press, New York (1982).
[75] M. A. Flanagan, E. B. Garcia-Moreno, S. H. Friend, R. J. Feldman, J. Scoulond, F. R. N. Gurd, Biochemistry, Vol.

22, 6027 (1983).
[76] S. H. Friend, F. R. N. Gurd, Biochemistry, Vol. 18, 4612 (1979).
[77] E. Antonini, M Brunori, Hemoglobin and Myoglobin In Their Reactions With Ligands, North-Holland Publishing Company, Amsterdam, pp 55-134, (1971).
[78] S. K. Chowdhury, V. Katta, B. T. Chait, J. Am. Chem. Soc., Vol 112, 9012 (1990)
[79] T. T. Herskovits, B. Gadegbeku, H. Jaillet, J. Biol. Chem., Vol. 245, 2599 (1970)
[80] K. D. Wilkinson, A. N. Mayer, Arch. Biochem. Biophys., Vol. 250, 390 (1986).
[81] N. M. Reid, J. A. Buckley, J. B. French, C. C. Poon, Adv. Mass Spectrom., Vol. 8b, 1843 (1979).
[82] Sciex Inc., 55 Glencameron Road, Thornhill, Ontario, Canada.
[83] V. Ling, A. W. Guzzetta, E. C. Davis, J. T. Stults, W. S. Hancock, Anal. Chem., Col. 63, 2909 (1991).
[84] S. A. Carr, M. E. Hemling, M. F. Bean, G. D. Roberts, Anal. Chem., Vol. 63, 2802 (1991).
[85] P. A. Hartman, J. D. Stodola, G. C. Harbour, J. G. Hoogerheide, J. Chromatogr., Vol. 463, 375 (1989).
[86] R. J. Hamilton, P. A. Sewell, Introduction to HPLC, 2nd Ed., Chapman and Hall (1982).
[87] K. E. Bij, C. Horvath, W. R. Melander, A. Nahum, J. Chromatogr., Vol. 203, 65 (1981).
[88] C. Horvath, High Performance Liquid Chromatography, Vol. 3, Academic Press (1983).
[89] M. T. Gilbert, High Performance Liquid Chromatography, Wright, Bristol (1987).
[90] M. T. W. Hearn, F. E. Regnier, C. T. Wehr, High-Performance Liquid Chromatography of Proteins and Peptides, Academic Press (1983).
[91] R. J. Pfeiffer, C. D. Hendricks, AIAA J., Vol. 6, 496 (1968).
[92] M. G. Ikonomou, A. T. Blades, P. Kebarle, Anal. Chem., Vol. 62, 957 (1990).
[93] A. T. Blades, M. H. Ikonomou, P. Kebarle, Anal. Chem., Vol 63, 2109 (1991).
[94] D. P. H. Smith, IEEE Trans. Ind. Appl., 1A-22, 527 (1986).
[95] G. I. Taylor, Proc. Roy, Soc. A, A280, 383 (1964).
[96] M. H. Ikonomou, A. T. Blades, P. Kebarle, Unpublished result, (1990).
[97] L. Tang, P. Kebarle, Anal. Chem., Vol. 63, 2709 (1991).
[98] Prof. A. Jesaitis and M. Quinn, Department of Microbiology, Montana State University.
[99] D. A. Dahl, J. E. Delmore, SIMION PC/PS2 (computer software), Idaho National Engineering Laboratory, EG&G Idaho Inc., 1987.
[100] M. Mann, C. K. Meng, J. B. Fenn, Anal. Chem., Vol 61, 1702 (1989).

[101] R. Guevremont, K. W. M. Siu, J. C. Y. Le Blanc, S. S. Berman, J. Am. Soc. Mass Spectrom., Vol. 3, 216 (1992).
[102] F. B. Armstrong, Biochemistry, 2nd edition, Oxford University Press, Inc. (1983).
[103] R. E. Dickerson, I. Geis, Hemoglobin:Structure, Function, Evolution, and Pathology, The Benjamin/Cummings Publishing Company, Inc. (1983).
[104] R. Katta, B. T. Chait, J. Am. Chem. Soc., Vol. 113, 8534 (1991).
[105] S. H. Friend, F. R. N. Gurd, Biochemistry, Vol 18, 4612 (1979).
[106] K. W. M. Siu, R. Guevremont, S. S. Berman, Organic Mass Spec., Vol. 26, 831 (1991).
[107] M. Mann, Organic Mass Spectrom,, Vol. 25, 575 (1990)
[108] S. K. Chowdhury, V. Katta, B. T. Chait, Rapid Commun. Mass Spectrom., Vol 4, 81 (1990).
[109] J. A. Loo, H. R. Udseth, R. D. Smith, Rapid Commun. Mass Spectrom., Vol. 2, 207 (1988).
[110] V. Katta, S. K. Chowdhury, B. T. Chart, Anal. Chem., Vol. 63, 174 (1991).
[111] A. L. Rockwood, M. Busman, H. R. Udseth, R. D. Smith, Rapid Commun. Mass Spectrom., Vol. 5, 582 (1991).
[112] R.D. Smith, J. A. Loo, R. R. Ogorzalek, M. Busman, H.R. Udseth, Mass Spectrom. Reviews, Vol. 10, 359 (1991).
[113] R. D. Voyksner, T. Pack, Rapid Commun. Mass Spectrom., Vol. 5, 263 (1991).
[114] R. R. Ogorzalek Loo, J. A. Loo, R. D. Smith, The 40th ASMS Conference on Mass Spectrom. and Allied Topics, (1992).
[115] G. D. Fasman, Ed.; Hand Book of Biochemistry and Molecular Biology, 3rd Ed., Vol. III; CRC Press, Cleveland (1975).
[116] M. O. Dayhoff, Ed.; Atlas of Protein Sequence and Structure, Vol. 5, Supplement 3, CRC Press, Cleveland (1978).
[117] E. L. Smith, R. L. Hill, I. R. Lehman, R.J. Lefkowitz, P. Handler, A. White, Principles of Biochemistry: Mammalian Biochemistry, 7th ed., McGraw-Hill Book Company (1983).
[118] M. O. Dayhoff, ed.; Atlas of Protein Sequence and Structure, Vol. 5, CRC Press, Cleveland (1975).
[119] N. V. Bhagavan, Biochemistry, 2nd ed., J. B. Lippincott Company (1978).
[120] A. White, P. Handler, E. L. Smith, Principles of Biochemistry, 4th ed., McGraw-Hill Book Company (1968).
[121] J. A. Loo, C. G. Edmonds, R. D. Smith, Biomed. Envoron. Mass Spectrom., Vol. 19, 286 (1990).
[122] D. M. Blow, The Enzymes, Vol 3, ed by P. D. Boyer, Academic Press, New York (1971).
[123] J. H. Northorp, M. Kunitz, R. Herriott. Crystalline Enzymes, Columbia Univ. Press, New York (1939).
[124] R. B. Corey, O. Battfay, D. A. Brueckner, F. G. Mark,

BBA,m Vol. 94, 535 (1965).
[125] A. Yapel, M. Han, R. Lumry, A. Rosenberg, D. F. Shiao, J. Am. Chem. Soc., Vol. 88, 2573 (1966).
[126] R. E. Dickerson, I. Geis, The Structure and Action of Proteins, Harper & Row, Publishers (1969).
[127] J. E. Whitaker, R. P. Haugland, P. L. Moore, P. C. Hewitt, M. Reese, Anal. Biochem., Vol. 198, 119 (1991).
[128] S. Naylor, A. F. Findeis, B. W. Gibson, D. H. Williams, J. Am. Chem. Soc., Vol. 108, 6359 (1986).
[129] Prof. K. Hapner, Department of Biochemistry, Montana State University.
[130] R. M. Caprioli, W. T. Moor, M. Martin, B. B. DaGue, J. Chromatogr., Vol. 480, 247 (1989).
[131] B. E. Winger, K. Light-Wahl, R. D. Smith, J. Am. Soc. Mass Spectrom., Vol. 3, 624 (1992).
[132] Jan Sunner, Chemistry Department, Montana State University.
[133] J. H. Northrop, M. Kunitz, R. Herriott, Crystalline Enzymes Columbia Univ. Press, New York, 1939.